Lossy Filter Synthesis

by

Saman Nasirahmadi

A thesis
presented to the University of Waterloo
in fulfillment of the
thesis requirement for the degree of
Master of Applied Science
in
Electrical and Computer Engineering

Waterloo, Ontario, Canada, 2013

I hereby declare that I am the sole author of this thesis. This is a true copy of the thesis, including any required final revisions, as accepted by my examiners.

I understand that my thesis may be made electronically available to the public.

Abstract

All telecommunication systems, such as cellular mobile networks (cellphones), object-detection systems (radars), and navigation systems that include satellite positioning systems (GPS), base their functioning on radio wave radiation with pre-defined frequencies and thus require a microwave filter to select the most appropriate frequencies. Generally speaking, the more highly-selective a filter is, the less non-useful frequencies and interference it picks up. Recent advances in microwave instruments, semiconductors, fabrication technologies and microwave filters applications have ushered in a new era in performance but have also brought significant challenges, such as keeping fabrication costs low, miniaturizing, and making low-profile devices. These challenges must be met while at the same time maintaining the performance of conventional devices. The thesis proposes use of lossy filter concepts to maintain high quality filtering frequency response flatness and selectivity regardless of the filter's physical size. The method is applied to lumped element filters. It introduces resistances to the physical structure of the filter and hence a certain amount of loss to the frequency response of the filter. The lossy filter synthesis is based on the coupling matrix mode. The thesis also proposes modifications to the traditional lossy filter design techniques, to improve the filter performance in the stopband.

Acknowledgements

I would like to express the deepest appreciation to my supervisor Professor Raafat Mansour, who has shown the attitude and the substance of a genius: he continually and persuasively conveyed a spirit of adventure in regard to research. Without his supervision and constant help this dissertation would not have been possible.

I would like to thank my committee members, Professor Safieddin Safavi Naeini and Professor Simarjeet Saini for graduate study advice and mentorship.

Special thanks to my friends and family for supporting me through my education.

Table of Contents

List of Figures vii

List of Tables xi

Chapter 1 1

1.1 Motivation 1

1.2 Objectives 2

1.2.1 Lumped element lossy filter synthesis and fabrication 2

1.2.2 Improving the reflection loss in the stopband of lossy filters 2

1.3 Outline 3

Chapter 2 4

2.1 Introduction 4

2.2 Predistorted Filters: Concept and history 4

2.3 Lossy Filters: Concept and history 14

Chapter 3 21

3.1 Introduction 21

3.2 Coupling matrix synthesis methods 21

3.2.1 Direct Method: Multi-coupled sequential network 22

3.2.2 Transversal network model 24

3.3 Lossy Filter 27

3.3.1 Lossy Coupling Matrix Synthesis 27

3.3.2 Lossy Filter Synthesis Using an Attenuator 30

3.3.3 Coupling Matrix Rotation (reduction) 32

3.3.4 Loss Distribution Technique 35

3.3.5 Simulation and Results 36

3.3.6 Actual Physical Q vs. Achievable Equivalent Q 42

3.4 Predistorted Filter 50

3.4.1 Concept and Formulation 50

3.4.2 Illustrative Example 51
Chapter 4 55
4.1 Introduction 55
4.2 Four-pole lossy filter 55
4.3 Two-pole cascade lossy filters vs. six-pole ideal filter 69
4.3.1 EM Design and simulation results 77
Chapter 5 81
5.1 Summary 81
5.2 Future work 82
Bibliography 85

List of Figures

Figure 2.1. The ideal response and predistorted response of the waveguide filter [3]. 5
Figure 2.2. Typical location of poles and zeros for a 6-pole elliptic-function bandpass filter [5]. 6
Figure 2.3. ***a***) 3.986 GHz 6-pole C-band dual-mode dielectric-function filter and 3.986 GHz 6pole C-band air-filled dual-mode filter. ***b***) 12-GHz 4-pole predistorted elliptic-function filter [5]. 6
Figure 2.4. Transmission and return loss response of a predistorted, 12-GHz 20-MHz bandwidth 4-pole elliptic-function filter [5]. 7
Figure 2.5. Transmission response of low Q and predistorted 6-pole C-band elliptic function filters [5]. 8
Figure 2.6. Adaptive values used to shift the transfer function poles [7]. 9
Figure 2.7. Comparison between adaptive and conventional predistortion [7]. 9
Figure 2.8. ***a***) Predistorted dielectric-resonator filter at Ku-band; ***b***) size comparison between coaxial resonator predistorted and conventional dielectric resonator filter [7]. 10
Figure 2.9. Measured insertion loss performance of 10-4-4 C-band filter (normalized to 5.9 dB) [7]. 10
Figure 2.10. Measured loss versus simulated with ideal Q of 10-4-4 C-band filter [7]. 10
Figure 2.11. Measured insertion loss performance of 10-4-4 Ku-band filter [7]. 11
Figure 2.12. Possible arrangements for the reflection zeros for the symmetric 6-2 quasi-elliptic characteristic. Left is asymmetrical synchronous design; middle and right are symmetrical asynchronous designs [8]. 11
Figure 2.13. SIW K-band filter: up, non-predistorted; down, predistorted [9]. 12
Figure 2.14. ***a***) Synthesized predistorted prototype. ***b***) Ideal circuit responses of non-predistorted and predistorted filters [9]. 12
Figure 2.15. ***a***) Simulated results of non-predistorted and predistorted filters. ***b***) Measured results of non-predistorted and predistorted filters [9]. 13
Figure 2.16. Schematic of a six-pole elliptic micro-ring filter with four transmission zeros (μs are coupling values). 13
Figure 2.17. Dashed and solid gray lines are the responses of the lossless non-predistorted filter design and when the Q factor is degraded, respectively. Dashed and solid black lines are the responses of the predistorted filter with no loss and when the Q factor is degraded, respectively [10]. 14
Figure 2.18. Measured performance [12]. 15
Figure 2.19. ***a***) Effect of loss factor on S11 for lossy 5^{th} degree Butterworth. ***b***) 3^{rd} Degree Butterworth networks [14]. 15

Figure 2.20. ***a***) Lossy third-order Butterworth with resonant resistive cross coupling. ***b***) Non-resonant approximation of the resistive cross coupling [15]. 16
Figure 2.21. Responses of lossy third-order Butterworth filters with resonant and non-resonant resistive cross couplings: ***a***) before multiplying the reflection function by attenuation factor of K; ***b***) after attenuation K multiplication [15] 16
Figure 2.22. ***a***) fabricated filter. ***b***) The proposed physical layout [17]. 17
Figure 2.23. Generalized coupled cavity model [18]. 18
Figure 2.24. ***a***) HFSS model of lossy filter and its node diagram. ***b***) Fabricated filter [18]. 18
Figure 2.25. Measurement versus synthesis results at 11.18 GHz (tuned due to the fabrication tolerance) [18]. 18
Figure 2.26. ***a***) Equivalent lossy circuit for the K^{th} resonator in the array. ***b***) Equally distributed Q configuration after hyperbolic rotation [21]. 19
Figure 2.27. *N* resonator transversal array including direct source-to-load complex coupling J_{SL} [21]. 20
Figure 2.28. ***a***) Lossy 10–4–4 pseudoelliptic bandpass filter function with equal return loss levels of -30 dB. ***b***) Lossy asymmetrical three-pole pseudoelliptic filter response with different return loss levels of -3dB and -9 dB, respectively [21] 20
Figure 3.1. Sequential low-pass prototype multi-coupled filter. 22
Figure 3.2. A general 2-port composed of synchronously tuned coupled cavities [26]. 23
Figure 3.3. ***a***) N-resonator transversal model, ***b***) equivalent lossy circuit for the Nth resonator [30]. 25
Figure 3.4. N+2 fully canonical complex coupling matrix for the lossy transversal array [30]. 25
Figure 3.5. Admittance inverter model of low-pass prototype filter. 25
Figure 3.6. Possible representation of a lossy filter [31] 30
Figure 3.7. Attenuator network attached to the first (last) resonator [31] 30
Figure 3.8. Equivalent model for attenuator attached to the first (last) resonator [31]. 30
Figure 3.9. Lossless N+2 coupling matrix [31]. 31
Figure 3.10. Lossy N+2 coupling matrix [31]. 31
Figure 3.11. N=7 degree folded representation of the coupling matrix. 32
Figure 3.12. Folded coupling matrix representation of N=7: *x*, cross couplings; *m*, main-line couplings; and *s*, self-couplings. 33
Figure 3.13. A 6-by-6 rotation matrix with pivot =[3, 4] 33
Figure 3.14. Elements of coupling matrix to be annihilated. 34
Figure 3.15. Lossless canonical pseudoelliptic filter. 38
Figure 3.16. S-parameter of folded coupling matrix with different loss level 41

Figure 3.17. Lossless 4-pole Chebyshev filter response. 43
Figure 3.18. Lossless circuit model of a 4-pole Chebyshev filter. 43
Figure 3.19. ADS simulation result of a lossless 4-pole Chebyshev filter. 44
Figure 3.20. Q=400 Chebyshev prototype circuit model. 45
Figure 3.21. S-par simulation results of 4-pole Chebyshev filter with Q=400. 45
Figure 3.22. MATLAB plot of a 4-pole lossy Chebyshev filter. 47
Figure 3.23 ADS plot of a 4-pole lossy Chebyshev filter. 48
Figure 3.24. Actual Q vs. loss level, equivalent Q=1000, FBW =1%. 48
Figure 3.25. Actual Q vs. loss level, equivalent Q=1000, FBW =5%. 49
Figure 3.26. Actual Q vs. loss level, equivalent Q=1000, FBW =10%. 49
Figure 3.27. Original and shifted roots of polynomial E(s) towards the right-half s-plane. 52
Figure 3.28. New roots of F(s) polynomial. 52
Figure 3.29. Predistorted filter frequency response (MATLAB simulation). 53
Figure 3.30. Predistorted filter frequency response after adding Q=1000 (MATLAB simulation). 53
Figure 3.31. Predistorted filter frequency response after adding Q=1000 (MATLAB simulation). 54
Figure 3.32 Predistorted filter frequency response after adding Q=1000 vs. before adding Q=1000 (MATLAB simulation) 54
Figure 4.1. Frequency response (S-par) of lossy filter based on the coupling matrix 56
Figure 4.2. ADS simulation of S-parameters using ideal coupling elements 57
Figure 4.3 Manipulated circuit model in ADS 58
Figure 4.4. ***a***: Lumped element coupling and ABCD model of TL, ***b***: lumped element coupling and TL 59
Figure 4.5. *a*: ABCD model coupling and TL, ***b***: ideal circuit based on ABCD model 59
Figure 4.6. ***a***: FBW=1%, ***b***: FBW=2%, ***c***: FBW=3%, ***d***: FBW=4% 60
Figure 4.7. ADS simulated S-par results for low pass filter, ***a***: Circuit model, ***b***: Amplitude and phase frequency response, ***c***: zoomed-in Amplitude frequency response 61
Figure 4.8. Circuit model and simulated S-par of *a*: Proposed inductive-capacitive impedance inverter, ***b***: ideal ABCD impedance inverter model, ***c***: Conventional capacitive impedance inverter with negative capacitor 63
Figure 4.9. The phase characteristic of proposed pi impedance inverter circuit at 2GHz. 63
Figure 4.10. Circuit model simulation of ***a***: s-parameter of 4-pole lossy filter with FBW=4%, ***b***: s-parameter of 4-pole lossy filter with FBW=1% 64
Figure 4.11. ***a***) Frequency response of 4-pole lossy filter, ***b***) MATLAB simulation of 4-pole Chebyshev filter with Q=100 64

Figure 4.12. ***a***: initial resonator, ***b***: modified Resonator using scaling factor *a* 65
Figure 4.13. Frequency response of the tuned and reduced element circuit 67
Figure 4.14. Lumped element circuit schematic of 4-pole lossy filter..... 68
Figure 4.15. Cascaded circuit model..... 70
Figure 4.16. Frequency response of three 2-pole filters (ADS simulation) 71
Figure 4.17. Inductance EM simulation in SONNET 71
Figure 4.18. Circuit model and frequency response of the modified filter 72
Figure 4.19. Lumped element ccircuit model (capacitive coupling) and frequency response of the modified filter 73
Figure 4.20. Lumped element ccircuit model (inductive coupling) and frequency response of the modified filter 73
Figure 4.21. ***a***) *a*=1, ***b***) *a*=5, ***c***) *a*=10, ***d***) *a*=20 74
Figure 4.22. Frequency response of 2-pole lossy filter (ADS simulation) 75
Figure 4.23. Frequency response of 2-pole lossy filter (ADS simulation) 75
Figure 4.24. Two-pole lossy filter, top: circuit model, bottom: s-par 76
Figure 4.25. Frequency response of cascaded 2-pole filters (ADS simulation)..... 76
Figure 4.26. Physical layout of 2-pole filter (SONNET) 77
Figure 4.27. Frequency response of 2-pole filter (SONNET simulation)..... 77
Figure 4.28. Optimized frequency response of 2-pole filter (SONNET simulation) 78
Figure 4.29. Physical layout of 2-pole lossy filters (SONNET) 78
Figure 4.30. Physical layout of the cascaded 2-pole lossy filters (SONNET) 79
Figure 4.31. EM simulation results for 3x2-pole cascade filter (Q=30) 79
Figure 4.32. Circuit model simulation of 6-pole ideal filter with Q=30 80

List of Tables

Table 3.1. Roots of filter polynomials. 36
Table 3.2. Coefficients of filter polynomials. 36
Table 3.3. Coefficients of Y-parameters. 36
Table 3.4. Coupling matrix elements. 37
Table 3.5. Transversal coupling matrix, lossless network. 37
Table 3.6. Feasible folded form of the coupling matrix after the rotation. 38
Table 3.7. Lossy elements and modified admittance inverter values. 39
Table 3.8. Coefficient of Y-parameters. 39
Table 3.9. Elements of the initial coupling matrix 40
Table 3.10. N+2 transversal coupling matrix. 40
Table 3.11. Folded coupling matrix. 41
Table 3.12. Lossless coupling matrix of 4-pole Chebyshev filter with RL=22 dB. 42
Table 3.13. The *N*+2 lossy coupling matrix. 46
Table 3.14 *N*+4 coupling matrix 46
Table 3.15. Lossless polynomials coefficients and roots. 51
Table 4.1. Coupling matrix of the 4-pole lossy filter with 18 dB insertion loss 56
Table 4.2. Element values after impedance scaling to Z0=50 ohm 65
Table 4.3. Modified values of the 4-pole lossy filter 66
Table 4.4. Impedance Scaled values 69
Table 4.5. Modified values of elements of 2-pole filter 74
Table 4.6. Modified elements of 2-pole lossy filter 76

Chapter 1

1.1 Motivation

Radio wave radiation is an integral part of the functioning of modern technology, including telecommunication systems (cell phones), navigation systems (GPS), object detection systems (radars), TV broadcasting, and so on. Wave radiation occurs in allocated ranges from low to high frequencies that are typically between hundreds of MHz to several tens of GHz. For this to occur, a device is needed to select the correct frequencies to carry the requisite information. Frequency selectivity is made possible by a device known as a "microwave filter".

The theory and design of microwave filters have been subjects of intense research and development over the past few decades. Employing highly selective filters helps to enhance the rejection of unwanted signals and leads to overall better communication quality. However, recent advances in microwave instruments, semi-conductor and micro-fabrication technologies, along with the applications of microwave filters, have ushered in several new challenges. The main ones can be categorized as lowering the cost of fabrication and miniaturizing and realizing low profile (small size) devices while maintaining optimal performance levels.

Advances in technology have introduced several applications for microwave filters, and each application demands its own filtering specification. For instance, radar technology requires wide-band and tunable filters, which has led to high performance waveguide and coaxial resonator filters. Satellite communication and other space applications demand low-loss, small-size, narrow-band filters with highly selective amplitude response and linear phase response. These specifications have led to the development of dual-mode waveguide and dielectric resonator filters. Cellular communication also brought a demand for low-loss, low-cost, high-power, small-size and selective filters for base stations. This has led to improvements in coaxial, dielectric resonators and superconducting filters. For mobile handsets, there is a need for very small-size, low-cost, low-loss and selective filters for mass production, which has led to advances in integrated active filters, micro-electromechanical system base filters (MEMS), and surface acoustic wave filters.

In all types of the applications mentioned above, there is a common demand: high selectivity and flat response. In other words, having a sharp and highly selective filter with a flat frequency response in the passband is the main requirement of a microwave filter, regardless of its application.

In circuit theory analysis and synthesis, this effect is dealt with using the "quality factor", or "Q factor" for short. Loss seems to be inevitable in microwave filters due to the material properties used in the realization of the filter. Therefore, in order to have a high performance filter, the Q factor of the resonator should be maximized, which is achievable either by maximizing the amount of stored energy and/or minimizing the loss. The former approach usually results in filters that are large in size, which can be tolerated in some applications, but the latter approach can be achieved in different ways depending on the type of the filter.

In some resonator filter structures, it is possible to make the filter physically large. As such, it can be tolerated as dielectric resonator filters and waveguide filters. Others can be made using low-loss superconductive filter materials and thus have a high Q in spite of their small size. However, in some structures like MMIC and on chip filters (which are mostly used for mobile communication handsets), it is not possible to have a small-size filter while retaining optimal filtering function in terms of passband flatness and selectivity.

A recent area of research on "lossy filters" has been developed in order to obtain a highly selective filter using low Q resonators at the cost of a significant increase in the absolute insertion loss. In this type of filter, losses are intentionally added according to the design specifications, which introduce a certain insertion loss to the frequency response of the filter. In other words, it is possible to achieve a high Q filter shape using low Q resonators. The prescribed insertion loss can be potentially compensated by an amplifier right before the filter.

1.2 Objectives

1.2.1 Lumped element lossy filter synthesis and fabrication

The first objective is to study lossy filter synthesis and to design and test lumped-element lossy filters with as low a Q as possible. Different types of lumped-element lossy filters would be synthesized (e.g., bandpass, band-stop and low-pass) with different bandwidths aimed at various applications.

1.2.2 Improving the reflection loss in the stopband of lossy filters

The introduced loss to the frequency response makes the filter less applicable for a number of applications. Therefore, the second objective of this thesis is to devise a technique to improve the stopband reflection loss of a lossy filter. One method is to cascade to ideal filters at the input and

output of the lossy filter. As such, the lossy filter would be sandwiched between two ideal filters to achieve the objective.

1.3 Outline

In Chapter 2, various techniques in the literature related to loss compensation are discussed. The survey covers predistortion techniques, the lossy filter concept and active compensation methods. In Chapter 3, the lossy filter synthesis technique based on coupling matrix and predistortion techniques is explained in detail and accompanied by several examples and simulation results. Chapter 4 discusses two different lossy filter design and simulation results. Specifically, one 4-pole lumped-element lossy filter with an actual quality factor of 100 and a six-pole cascade lossy filter with an actual quality factor of 30 are designed.

Chapter 2

2.1 Introduction

Having a sharp and highly selective filter with a flat frequency response in the passband is the main requirement of a microwave filter, and achieving these filtering properties has been an intensive subject of study over the past several decades. In microwave filter design, it is possible to achieve a reasonable frequency response in theory; however, in practice, obtaining these characteristics is limited by physical constraints such as dissipation of electromagnetic energy.

Filter theory has been developed based on pure reactive elements, i.e., capacitors and inductors. In other words, microwave filters are usually designed using lossless prototype networks as a starting point. However, in practice, such networks retain a certain amount of loss due to the material properties used in their fabrication, and the filter's performance is thereby detrimentally affected by the presence of loss. By definition, loss would degrade the quality factor of the reactive elements (the resonators) and a low Q factor would affect the band-edge sharpness, meaning it rounds the band-edges in the passband and also degrades the insertion loss at the center frequency.

Compensating for the loss effect has served as a research focus of late, and vast efforts have been expended to restore the selectivity and flatness of the filter response in the presence of the loss or even to compensate for the loss effect. In this chapter, three of these concepts are reviewed.

2.2 Predistorted Filters: Concept and history

The concept of the predistortion technique was first introduced by Darlington in 1939 [1] and later verified by Dishal in 1949 [2]. It was shown that the lossless insertion loss frequency response of a filter network can be recovered by shifting the poles of the transfer function of the filter towards the imaginary axis by a certain amount (based on the unloaded Q factor of the resonators) to compensate for network loss. In other words, a lossless prototype network is synthesized in such a way that, in the presence of the intrinsic loss of the reactive elements in a resonator, the original lossless flat insertion loss response is recovered but shifted downwards by a finite amount of loss. Predistortion techniques can improve system efficiency for applications such as a transponder input multiplexer in satellite communication, where insertion loss can be tolerated to obtain passband flatness.

The insertion loss response of a predistorted filter before the presence of loss has finite mid-band loss and peaks to zero loss at the band edges. Moreover, in the predistortion method, the loss introduced in the insertion loss response would cause a finite in-band return loss response.

The predistortion technique was applied to an all-pole waveguide filter first by Livingston [3] in 1969 and then by Chen in 1975 [4]. The design characteristics of the waveguide filter are as follows. The filter function is chosen to be maximally flat, with a frequency of 6450 MHz and a 3-db Bandwidth of 44 MHz.

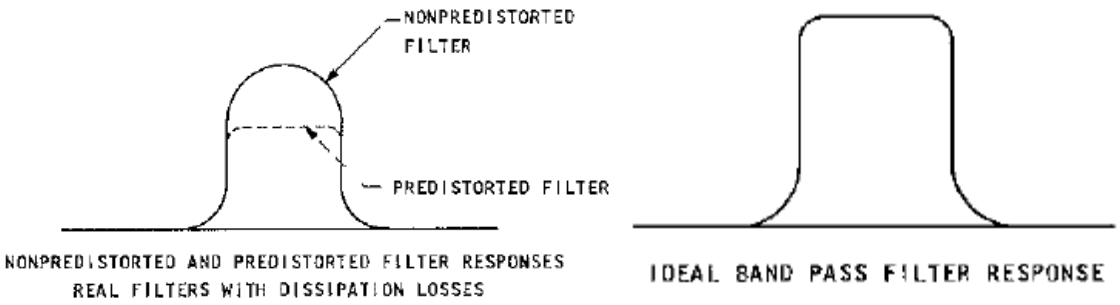

Figure 2.1. The ideal response and predistorted response of the waveguide filter [3].

One of the disadvantages of the predistorted technique reported in [3] is the sensitivity of the element values to even small perturbations. As reported, "[t]he filter appears to be more sensitive to incorrect element values than conventional, maximally-flat filters."

In 1985, Williams used the predistortion technique to design a multi-coupled cavity resonator filter with finite transmission zeros [5]. Three different cavity filters were designed and tested. A 20-MHz bandwidth, 4-pole, elliptic-function, predistorted filter with a center frequency of 12 GHz was designed with aluminum cavities and an unloaded Q factor of 8000. For a Q of 8000, the pole predistorted design factor was $r = 1/(Q_U \times FBW) = 0.075$, meaning that all of the poles of the transfer function were shifted towards the imaginary axis by 0.075.

Two 6-pole elliptic filters were designed with the dual HE_{11} dielectric-loaded cavity mode. The initial filter was designed by using conventional lossy techniques [6], and the second filter design was based on the predistortion technique. Both designs had a center frequency of 3.986 GHz, a bandwidth of 29 MHz, and an unloaded Q of 8000. Figure 2.4 and Figure 2.5 shows the frequency response of

the predistorted filter. The flattening effect of predistortion is obvious in the cost of in-band 4 dB insertion loss.

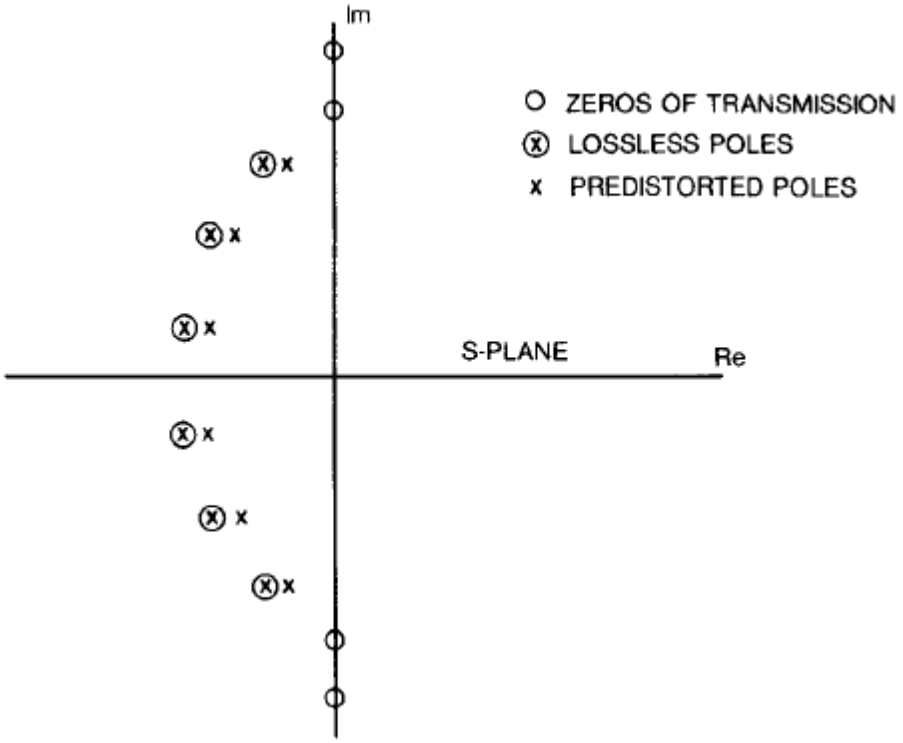

Figure 2.2. Typical location of poles and zeros for a 6-pole elliptic-function bandpass filter [5].

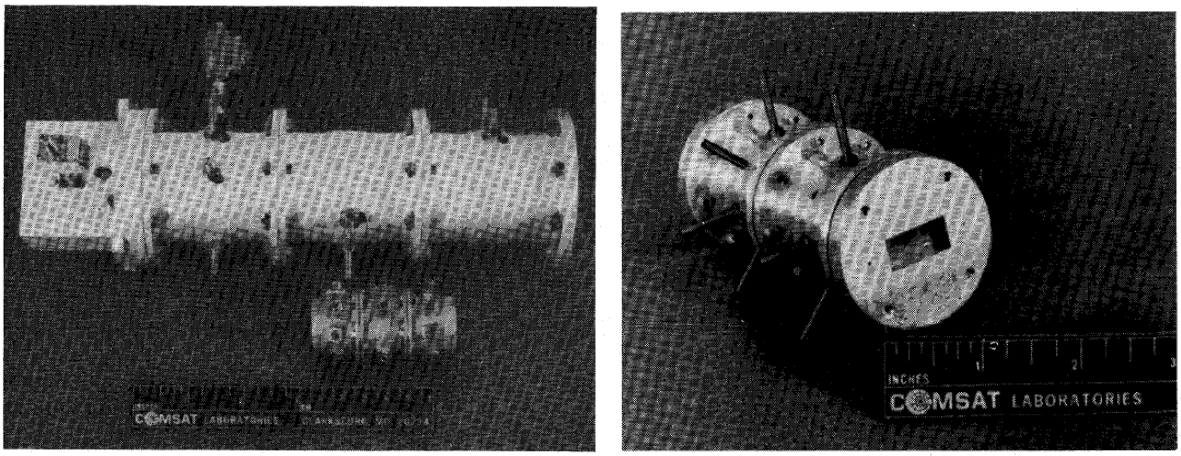

(*a*) (*b*)

Figure 2.3. ***a***) 3.986 GHz 6-pole C-band dual-mode dielectric-function filter and 3.986 GHz 6pole C-band air-filled dual-mode filter. ***b***) 12-GHz 4-pole predistorted elliptic-function filter [5].

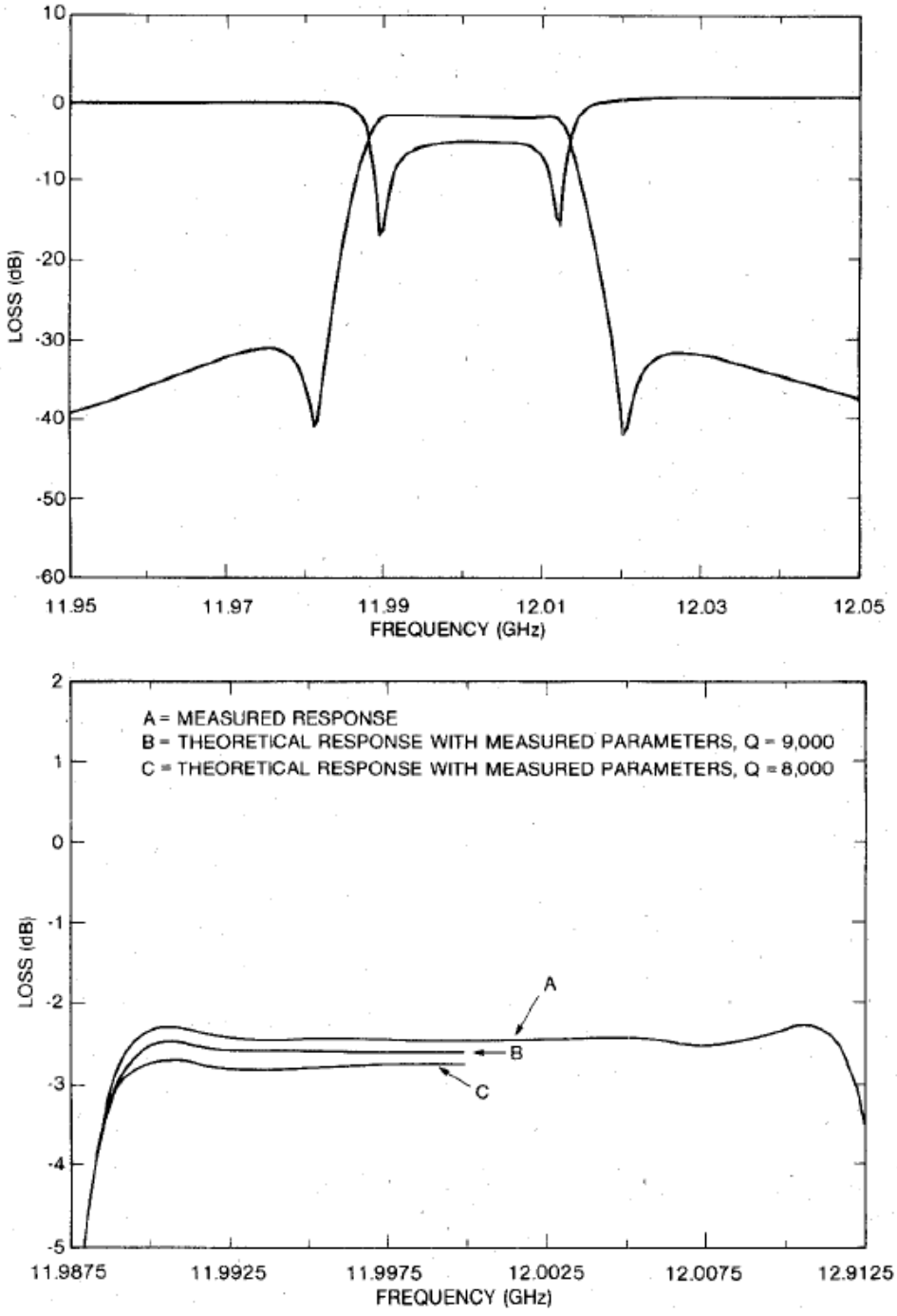

Figure 2.4. Transmission and return loss response of a predistorted, 12-GHz 20-MHz bandwidth 4-pole elliptic-function filter [5].

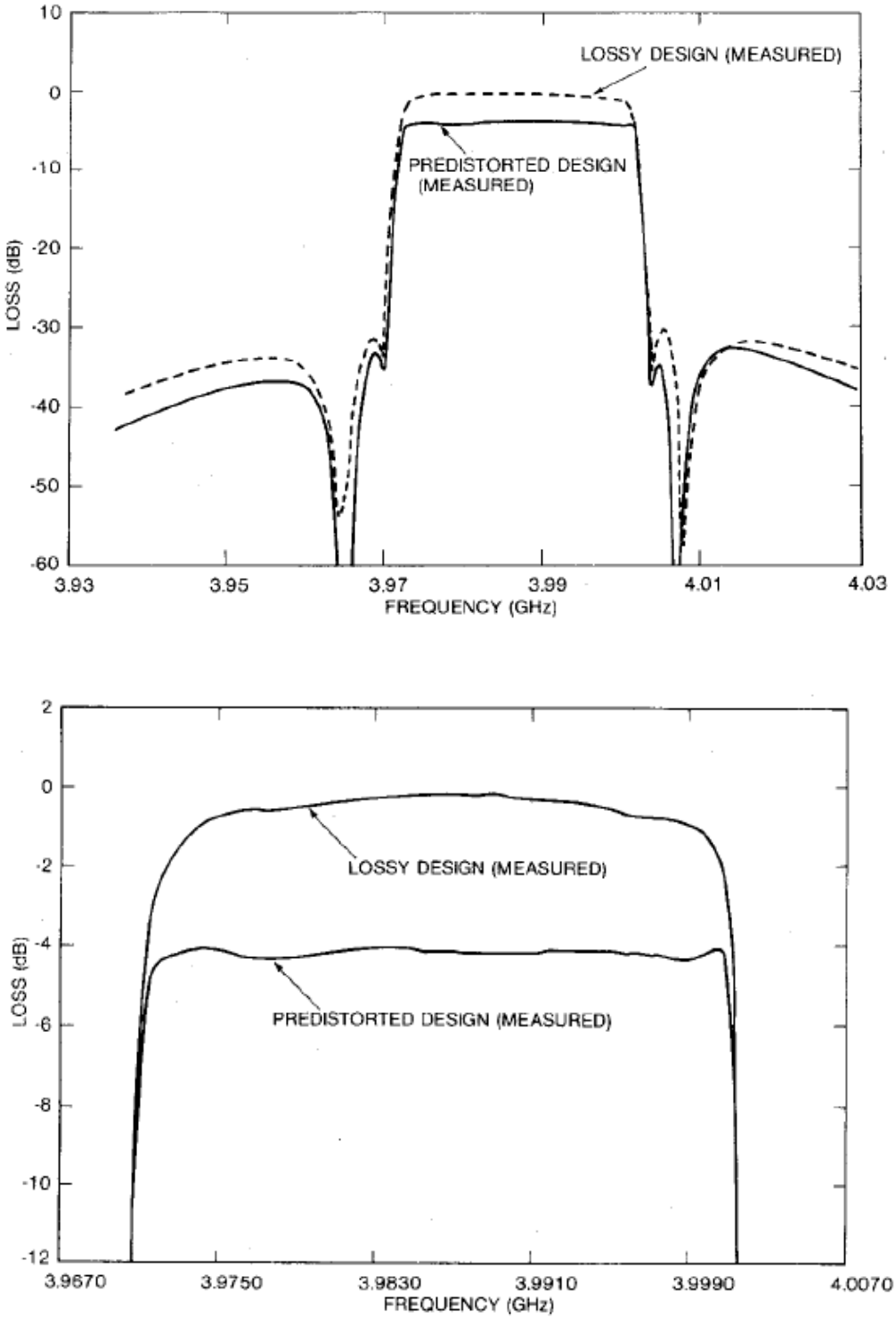

Figure 2.5. Transmission response of low Q and predistorted 6-pole C-band elliptic function filters [5].

In the conventional predistortion technique, the poles of the transfer function are shifted towards the imaginary axis in the S-plane by a fixed amount, which corresponds to the unloaded Q factor of the resonator. In [5], we see that "the pole closest to the imaginary axis dominates the band-edge response" and that it is primarily "the movement of this pole in the lossy, non-predistorted design that leads to rounding of the band-edge". Thus, unlike the conventional predistortion technique, the shifting value may not be fixed for all poles of the transfer function. This idea was studied in [7], where the effects of adaptive predistortion techniques were compared with conventional ones. This adaptive predistortion technique results in much less insertion loss, despite using low-Q resonators. A tenth-order typical filter used in satellite communication was analyzed with an actual Q of 3000 and a target Q of 8000. Using the adaptive technique, an improvement of 1.9 dB in insertion loss and 1.6 dB in return loss was reported in comparison with the results in [5] (Figure 2.7). A 10-4-4 coaxial resonator filter at C-band using resonators with an actual Q of 3000 and a 10-4-4 dielectric resonator filter at Ku-band using resonators with an actual Q of 8000 were designed and tested based on the proposed method, to an equivalent Q of 20000. Using adaptive predistortion reduced the volume and mass of the filter by 75% and 65%, respectively, compared to existing dielectric resonator technology in the cost of in-band insertion loss.

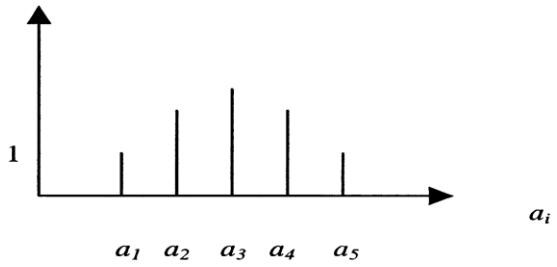

Figure 2.6. Adaptive values used to shift the transfer function poles [7].

Parameters (dB)	Adaptive predistortion	Predistortion
Insertion loss	-5 dB	-6.9 dB
Return loss	-3.6 dB	-2 dB

Figure 2.7. Comparison between adaptive and conventional predistortion [7].

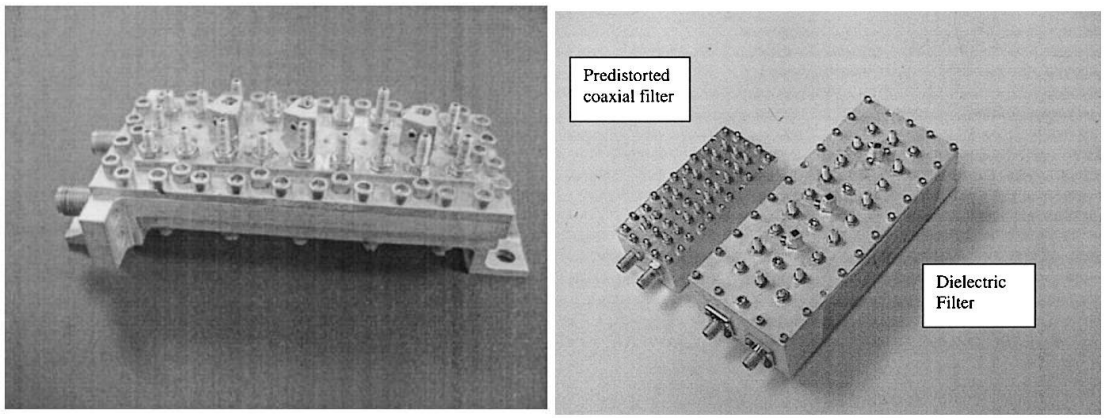

(*a*) (*b*)

Figure 2.8. ***a***) Predistorted dielectric-resonator filter at Ku-band; ***b***) size comparison between coaxial resonator predistorted and conventional dielectric resonator filter [7].

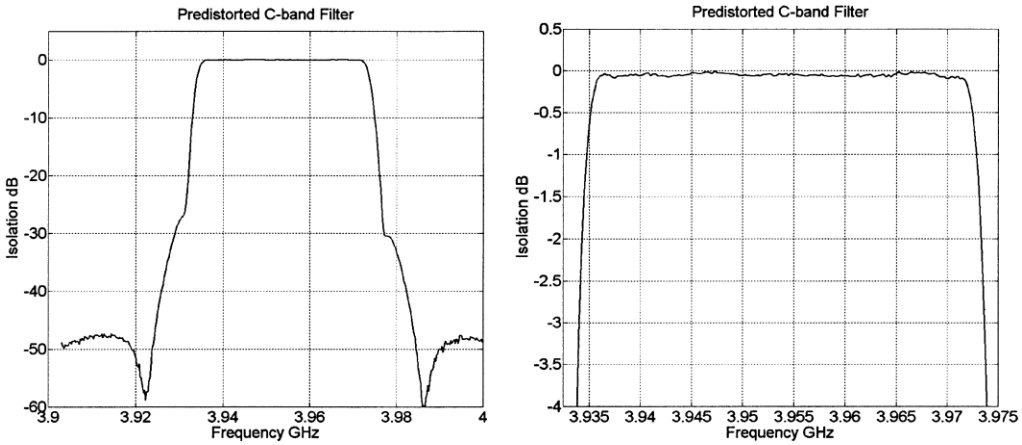

Figure 2.9. Measured insertion loss performance of 10-4-4 C-band filter (normalized to 5.9 dB) [7].

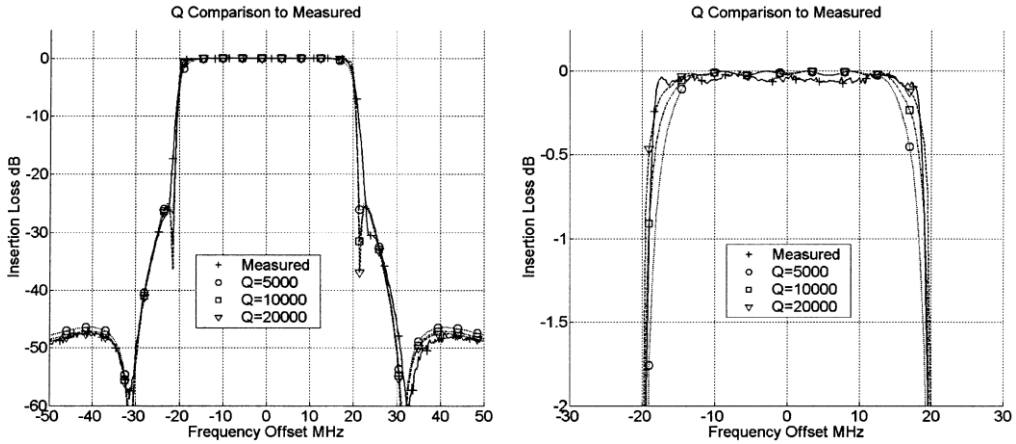

Figure 2.10. Measured loss versus simulated with ideal Q of 10-4-4 C-band filter [7].

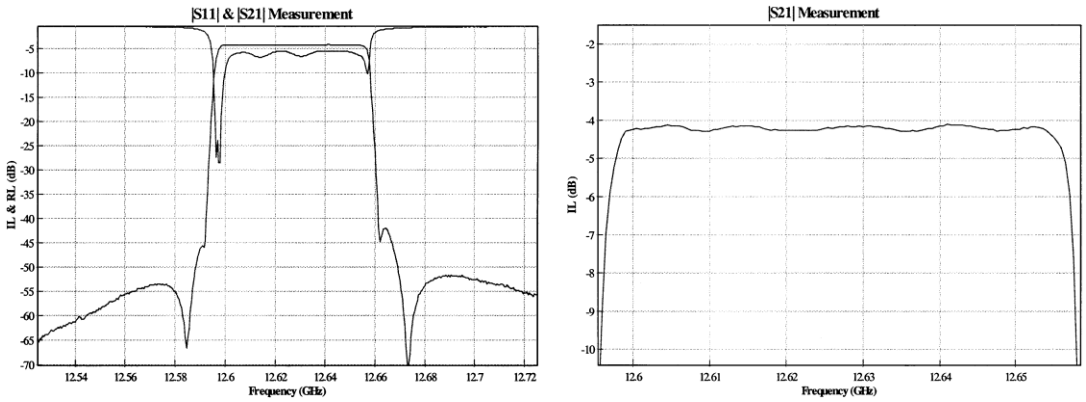

Figure 2.11. Measured insertion loss performance of 10-4-4 Ku-band filter [7].

As mentioned previously, the predistorted transfer function can be calculated from the lossless transfer function by shifting the poles towards the imaginary axis of the s-plane. Thus, regardless of transmission zeros, the zeros of reflection function would no longer be located on the imaginary axis, as with the lossless case. For a realizable network, the reflection zeros, however, must be located in the form of a mirror-image about the imaginary axis. Depending on how the reflection zeros are selected, there would be three different syntheses for the filter elements values (Figure 2.12), as studied in [5] and [8]. Briefly, different choices of reflection zeros would result in a symmetry about the physical center of the network (symmetric coupling matrix about the cross-diagonal) and with a shift in center frequency (asynchronous tuned) or an asymmetry about the physical center of the network (asymmetric coupling matrix about the cross-diagonal) without any shift in the center frequency (synchronously tuned) filter.

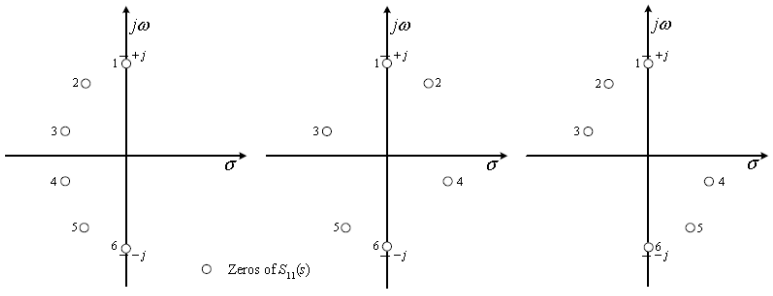

Figure 2.12. Possible arrangements for the reflection zeros for the symmetric 6-2 quasi-elliptic characteristic. Left is asymmetrical synchronous design; middle and right are symmetrical asynchronous designs [8].

Another structure to which the predistortion technique has been applied is a planar SIW (Substrate Integrated Waveguide) [9]. A 4-pole symmetric K-band SIW filter with an actual unloaded resonator

Q of 500, a target Q of 2500 and a FBW (Fractional Bandwidth) of 1% was designed, simulated, and tested. Based on the results reported in [9], unlike the dielectric cavity resonator filter, predistortion does not have a substantial effect on size reduction in SIW (Figure 2.13). Nonetheless, it did improve the effective bandwidth by flattening the in-band insertion loss.

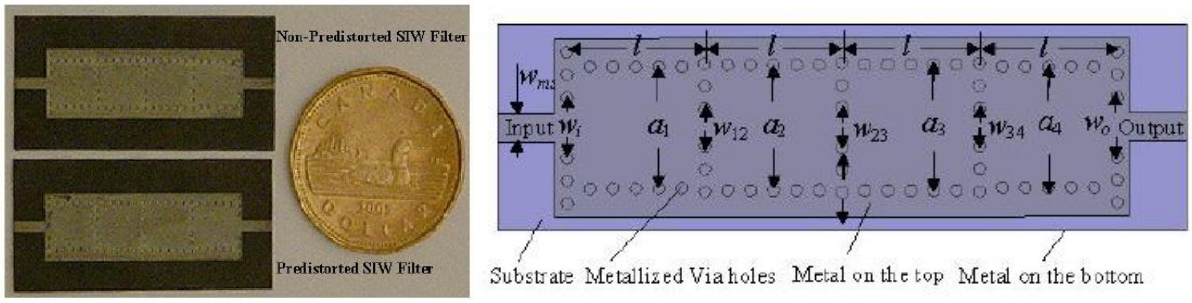

Figure 2.13. SIW K-band filter: up, non-predistorted; down, predistorted [9].

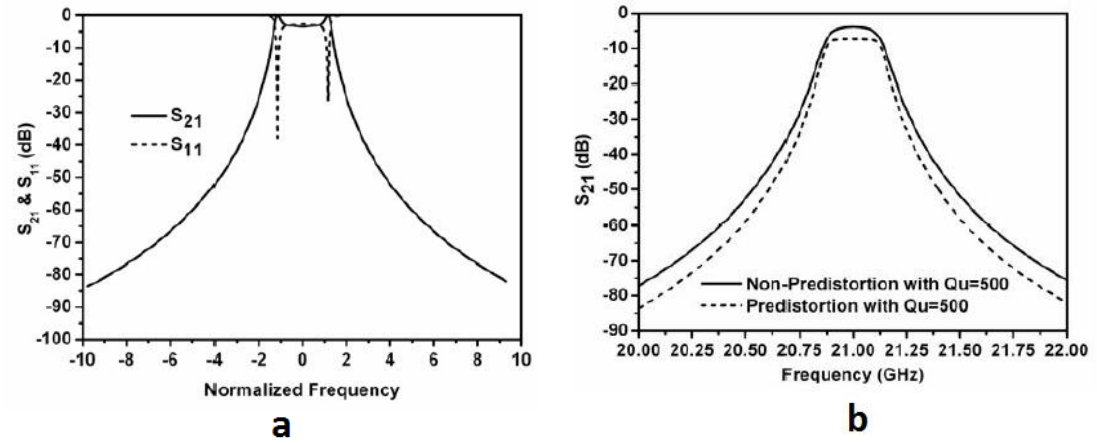

Figure 2.14. ***a***) Synthesized predistorted prototype. ***b***) Ideal circuit responses of non-predistorted and predistorted filters [9].

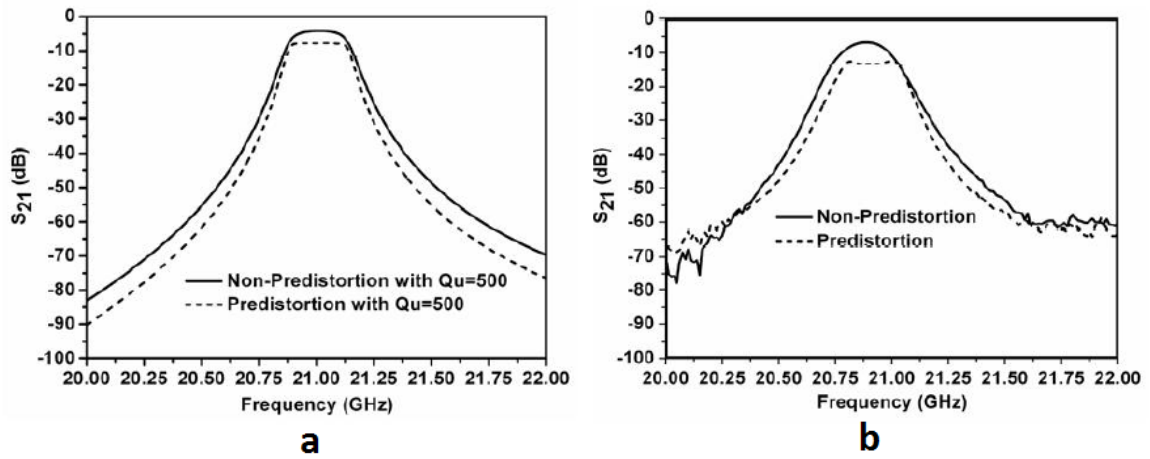

Figure 2.15. ***a***) Simulated results of non-predistorted and predistorted filters. ***b***) Measured results of non-predistorted and predistorted filters [9].

In the same vein, another application of the predistortion technique in optical frequency bands was reported in [10], where a 6-pole, multi-coupled, micro-ring resonator elliptic filter with a 30 GHz bandwidth, 0.1 dB in band ripple and 40 dB out-of-band rejection was designed and tested. One application of the predistorted filter in optical communication was reported on, as follows [10]: "*It may be desirable to optimize the through-port response (insertion loss response) of a micro-ring add/drop filter to achieve a maximum extinction and hence minimum channel crosstalk at the through-port in the presence of loss*". As suggested in [10], group delay can be restored exactly as a lossless case, in which circumstance insertion loss response would have exactly the same shape (selectivity and flatness) as the lossless case, other than for the 3.25 dB loss.

Furthermore, in optical communication circuits, the amount of loss of each resonator consists of coupling and bending losses, surface roughness scattering and material absorption. These can be directly calculated using the formulation equivalent to the definition of the Q factor [10].

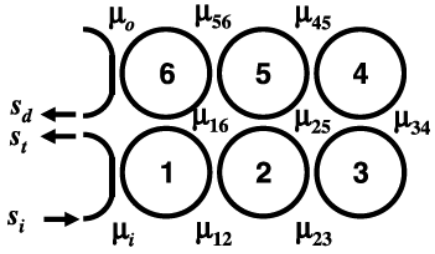

Figure 2.16. Schematic of a six-pole elliptic micro-ring filter with four transmission zeros (μs are coupling values) [10].

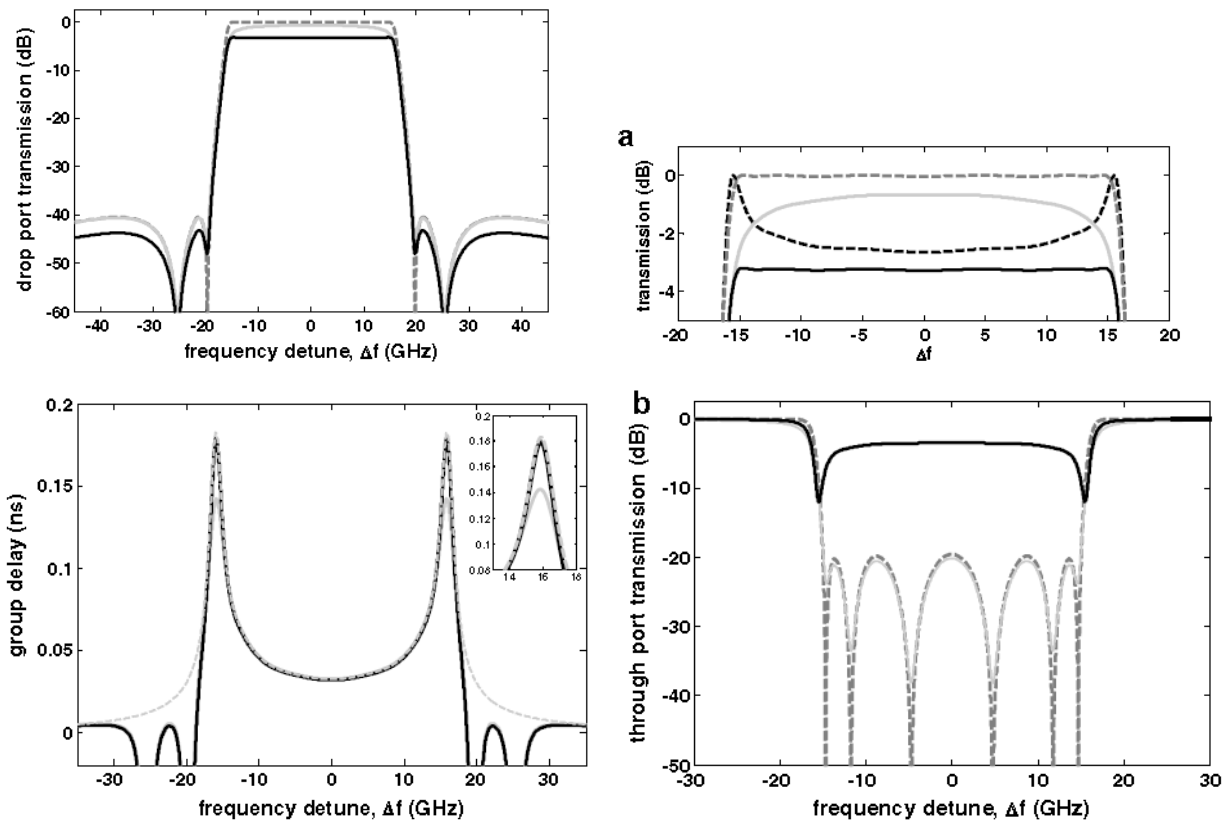

Figure 2.17. Dashed and solid gray lines are the responses of the lossless non-predistorted filter design and when the Q factor is degraded, respectively. Dashed and solid black lines are the responses of the predistorted filter with no loss and when the Q factor is degraded, respectively[10].

2.3 Lossy Filters: Concept and history

As mentioned in section 2.1, the predistortion technique flattens the insertion loss response but deteriorates the return loss, which is why it is not reasonable to design ultra-low Q resonator filters. The lossy filter concept seems to be derived from Hunter's [11] investigations into predistortion in the late 1990s. The terminology (lossy filter) developed from the introduction of extra losses as resistances in the network in addition to intrinsic loss contained in circuit reactive elements, i.e., inductors and capacitors. These extra resistances impose prescribed insertion and return losses to the frequency response. Hunter continued his initial work on lossy filters in [12] by introducing a reflection mode narrow band (0.12%) lossy filter synthesis with prescribed reflection coefficients based on low resonators. In this method, the effect of losses in the resonators is taken into account by multiplying the reflection function S_{11} by a constant value of K and then shifting the poles of the transfer function by a certain amount (the same as predistortion design). Here, the method and filter topology being used is effective only for all-pole Chebyshev low pass filters. The authors extended

their design to the asymmetrical transfer function realizable based on a ladder network in [13]. The reflection mode filter networks mentioned above are synthesized based on the topology of the network, which are different from well-known multi-coupled filter networks.

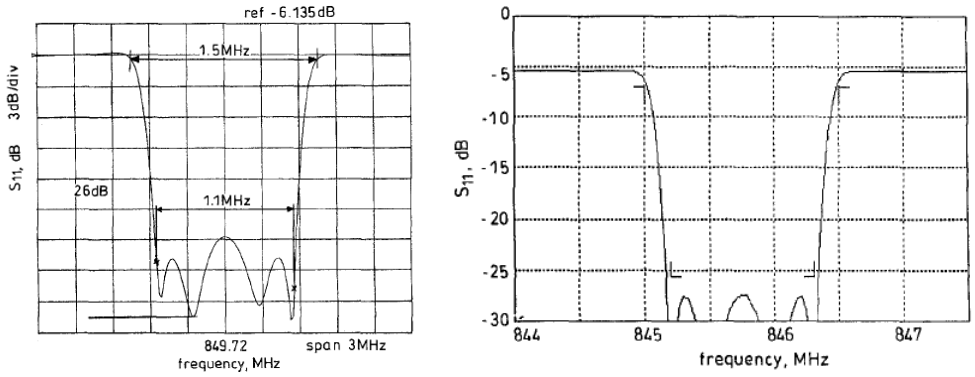

Figure 2.18. Measured performance [12].

The first direct lossy filter synthesis method was proposed in [14]. As we are dealing with lossy networks, the unitary condition does not apply, meaning that it is not possible to use the unitary condition to calculate the reflection function from the transfer function. In this method, assuming the reflection function coefficients are unknown, the authors used the concept of even and odd decomposition in order to calculate the unknown coefficients. Although no circuit topology is proposed in the reference, several examples of maximally flat filter function synthesis are presented in the paper.

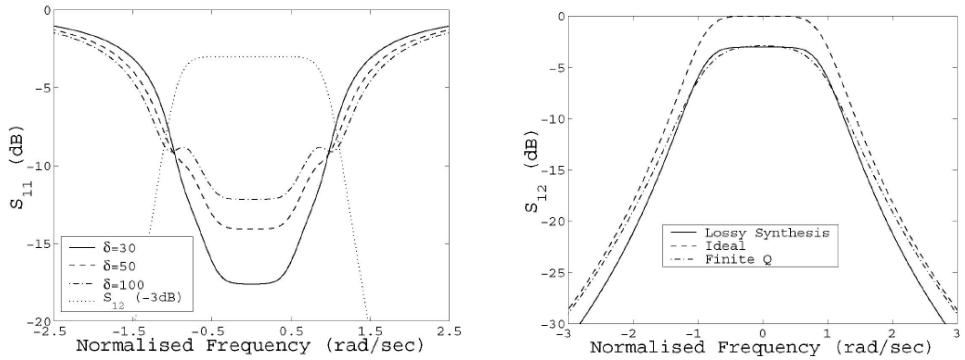

(*a*) (*b*)

Figure 2.19. ***a***) Effect of loss factor on S11 for lossy 5th degree Butterworth. ***b***) 3rd Degree Butterworth networks [14].

The research work on lossy filter realization and circuit topology encountered a breakthrough by introducing a new topology in [15]. The first lossy bandpass filter synthesis with non-uniform Q was introduced using resistive cross coupling, whereas all previous circuit topologies were synthesized

using ladder networks with no cross coupling. The method of finding the reflection function is the same as that in [14], which introduced losses only in the first and last resonators. Employing resistive cross coupling (which comes from additional transmission zeros and/or poles) flattens the insertion loss response, multiplies the transfer function by a constant amount of attenuation, and lowers the reflection function.

In dealing with loss, it is important to distribute it in between the resonators. After synthesizing the multi-coupled network and calculating the coupling matrix, hyperbolic and trigonometric matrix rotation is applied to distribute the loss to the lossless resonator. The effect of proper loss distribution is verified and based on what is reported in[15] when loss is distributed appropriately; the dependence of insertion loss increment on group delay is effectively reduced. This allows for an increase in selectivity". The authors extended the same design procedure of lossy filter synthesis to the multi-path resonator filters in [16]. The proposed example circuit designs along with microstrip prototypes serve as a validation of the concept.

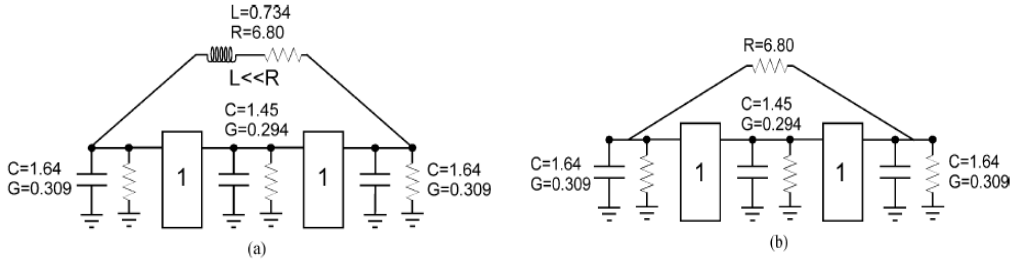

Figure 2.20. ***a***) Lossy third-order Butterworth with resonant resistive cross coupling. ***b***) Non-resonant approximation of the resistive cross coupling [15].

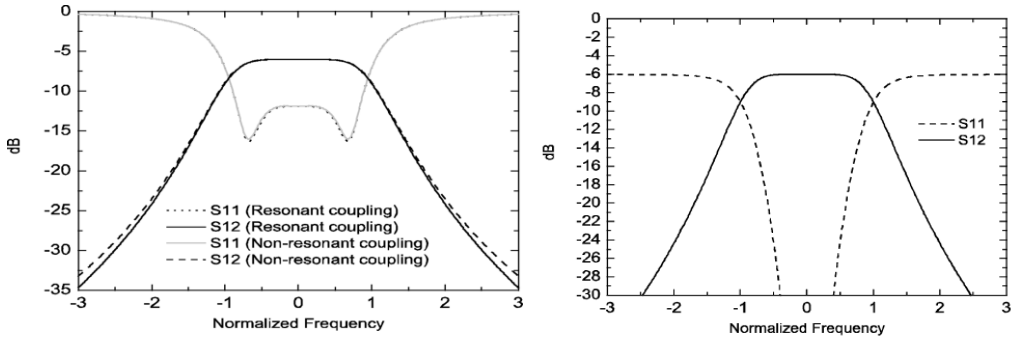

Figure 2.21. Responses of lossy third-order Butterworth filters with resonant and non-resonant resistive cross couplings: ***a***) before multiplying the reflection function by attenuation factor of K; ***b***) after attenuation K multiplication [15].

The lossy technique is suitable for filter structures which have low Q intrinsically, such as coaxial filters, to get more selective response. The application of the lossy synthesis technique which is proposed in previous references, was verified on a coaxial resonator filter with non-uniform Q for the first time in [16][17]. The filter response is chosen to be 3rd order Chebyshev, and the filter topology is designed based on the even and mode technique, explained in [16]. Q_1 and Q_2 have an equal value of 5.319 in the prototype network, and Q_3 has a value of 2.558, after frequency transformation. The unloaded Q factors of each resonator are 1063 and 511 for $Q_{1,2}$ and Q_3, respectively. Also, there are two additional resistances with the value of G=0.333 mho at input and output to preserve the flat insertion loss and return loss response while shifting them with a certain amount, i.e. 6 dB corresponding to G=0.333 mho.

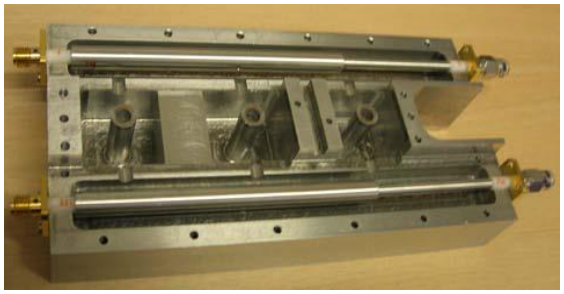

(*a*)

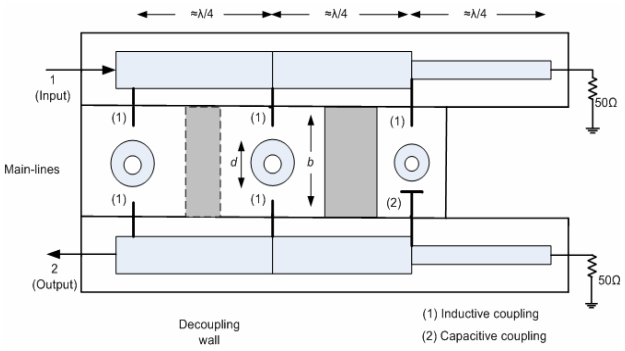

(*b*)

Figure 2.22. ***a***) fabricated filter. ***b***) The proposed physical layout [17].

A more straight-forward and systematic lossy filter synthesis technique is introduced in [18], based on a conventional multi-coupled cavity model coupling matrix synthesis technique [6]. The design procedure of the proposed method starts with the synthesis of a lossless network, where the scattering parameters are multiplied by a prescribed loss factor. Afterwards, the lossy filter coupling matrix can be obtained from the scattering parameters using an iterative technique regarding the algebraic properties of the coupling matrix, including matrix decomposition technique and orthogonalization process. Unlike the previous synthesis techniques, the presented method is applicable for both reciprocal and non-reciprocal microwave filters and has no limitation on higher order filters. The multi-coupled model contains complex cross-coupling values. Also, due to the higher number of resonators in the main line from input to the output, this model improves the out-of-band performance. For the experimental verification, a 4th order Chebyshev filter is designed at 12 GHz, with an additional loss value of 2.9 dB.

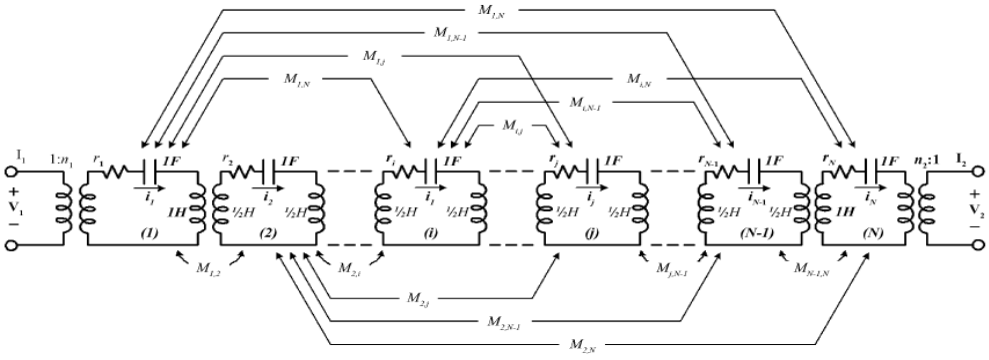

Figure 2.23. Generalized coupled cavity model [18].

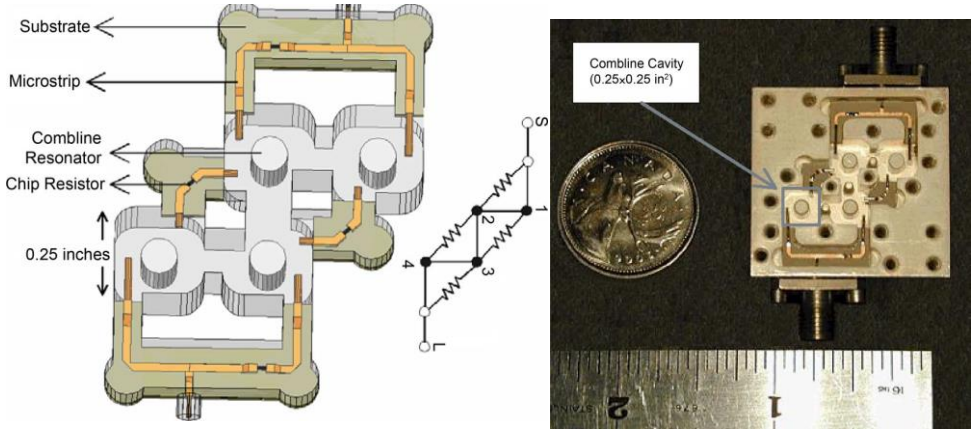

(*a*) (*b*)

Figure 2.24. ***a***) HFSS model of lossy filter and its node diagram. ***b***) Fabricated filter [18].

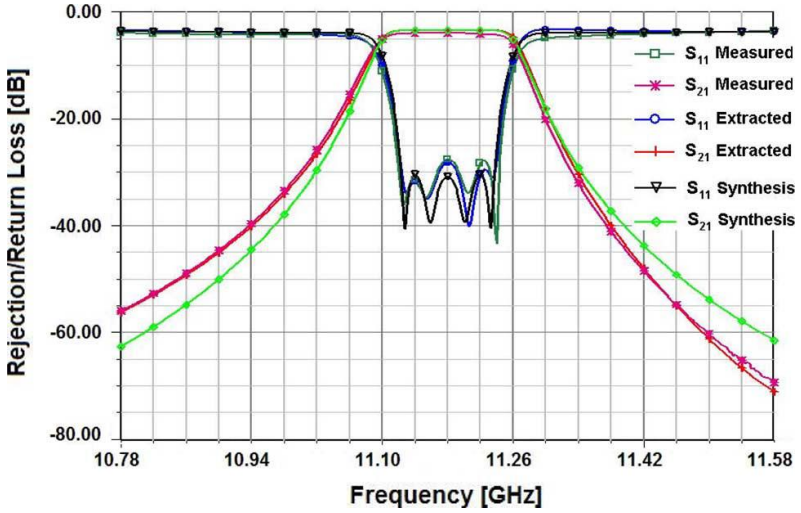

Figure 2.25. Measurement versus synthesis results at 11.18 GHz (tuned due to the fabrication tolerance) [18].

The iteration process explained in detail in [18] is a time-consuming routine. This issue has been addressed and the method modified in a recent publication [19]. A more direct method to obtain the proper complex coupling matrix for lossy synthesis is proposed to avoid the long-winded iteration process. The rest of the procedure is the same as previous work, i.e., the coupling matrix decomposition process and orthogonalization.

In 2003, Richard Cameron proposed an advanced analytical coupling matrix synthesis for microwave lossless filters, based on a network topology called a "transversal model". In this technique, a lossless coupling matrix for a canonical filter response is synthesizable, a feat which was not possible in multi-coupled mode, as it requires a direct coupling between source and load. This systematic technique was sufficiently interesting to be considered in lossy filter synthesis, as discussed in detail in [21]. Unlike the lossless case in the transversal model, there are two additional resistances at the source and the load. It also includes complex inverter values, since the network is lossy. The method proposed in [21] is more general than previous techniques and almost any filter configuration is synthesizable using this method, e.g., filter responses with different combinations of transmission zeros, non-reciprocal and reciprocal networks (different loss levels for S_{11} and S_{22}), and asymmetrical and symmetrical frequency responses. However, the initial coupling matrix obtained using this transversal is now realizable and must be reduced to a feasible coupling matrix. This is possible by applying the similarity rotation method or matrix reduction, which has been extensively used in the literature. The matrix can be reduced to any feasible form, depending on the physical design of the filter, e.g., reduced to the folded form [22], right-hand justified [23], etc. The reduction is followed by a hyperbolic rotation in order to appropriately (i.e., equally or unequally) distribute the loss among the resonators.

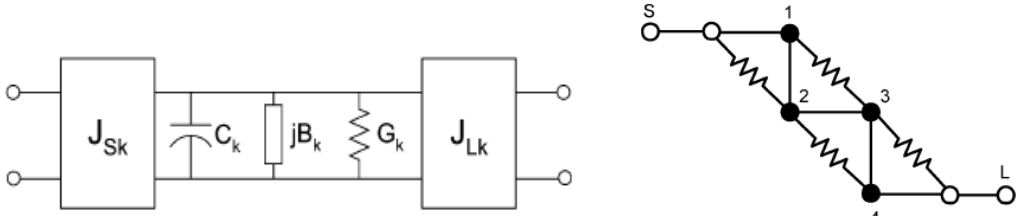

(*a*) (*a*)

Figure 2.26. ***a***) Equivalent lossy circuit for the K^{th} resonator in the array. ***b***) Equally distributed Q configuration after hyperbolic rotation [21].

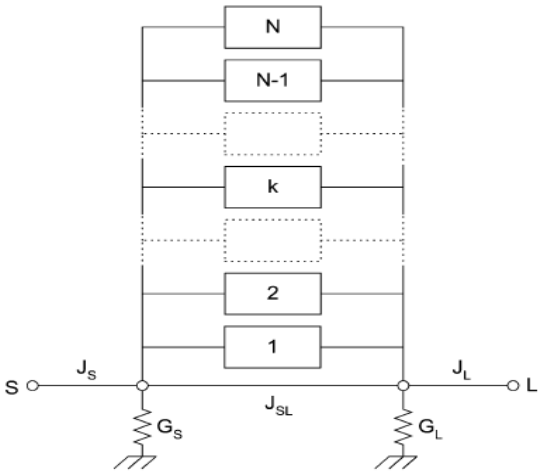

Figure 2.27. *N* resonator transversal array including direct source-to-load complex coupling J_{SL} [21].

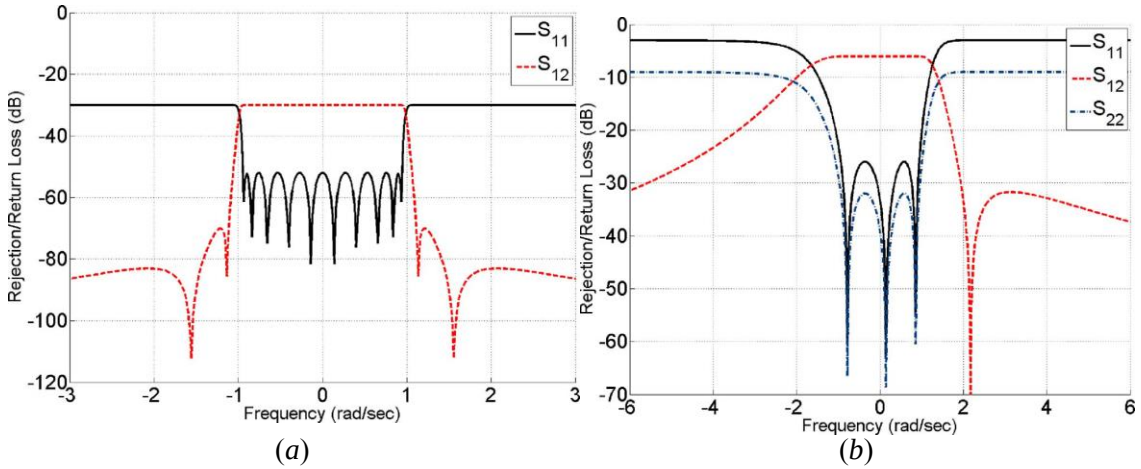

Figure 2.28. ***a***) Lossy 10–4–4 pseudoelliptic bandpass filter function with equal return loss levels of -30 dB. ***b***) Lossy asymmetrical three-pole pseudoelliptic filter response with different return loss levels of -3dB and -9 dB, respectively [21].

Chapter 3

3.1 Introduction

In the theory of microwave resonator-based filters, high quality factor (Q) resonators play an important role in creating a high-performance and sharp frequency response. However, in practice, designers are constrained with Q limitations. In order to maintain good filter response performance, the size of the filter must be increased in some cases, while in other cases (e.g., planar filters), using low-loss materials would increase the cost. Nevertheless, using low Q resonators results in insertion loss in the passband, less selective filter response, and band-edge rounding of the response.

In order to address Q limitation issues, the concept of lossy filters synthesis has been developed, as mentioned in Chapter 2. By using the concept of lossy filters, one can design a very sharp response filter with high equivalent Q (even a Q equal to infinity) with low Q resonators which consequently, miniaturized the filter dimensions in the cost of having degraded insertion loss. By improving the selectivity and flatness of the passband, lossy filters impose a significant degraded insertion loss, and this extra loss imposed by the filter in the communication system will increase the noise figure (NF) of the whole system, e.g., a radio frequency receiver. It is thus of utmost importance for the lossy filter to be preceded by a further low noise amplifier which would have just enough gain to minimize the effect of the passband loss on the NF.

3.2 Coupling matrix synthesis methods

In the literature, there are three main techniques for synthesizing a filter coupling matrix based on the filter specifications. These are the direct method, the transversal network model, and the element extraction method. In the following section, the first two of these techniques are explained in detail. The third technique is not explained in detail because it has some limitations in terms of the type of filter configurations, such as:

- it only applies for lossless network, and
- it is not a general method for all filters network topologies, i.e., it applies only to a folded filter configuration.

It should be pointed out that, for all methods mentioned above, a recursive procedure is used to obtain the filter polynomial, i.e., F(s), E(s) and P(s) (eq. (3.5)) of all types of Chebyshev filters.

3.2.1 Direct Method: Multi-coupled sequential network

For a multi-coupled sequential resonator lossless filter (Figure 3.1), meaning that there is no cross coupling between resonators, the synthesis of the coupling matrix is as easy as calculating filter elements (the g-values) of the desired filter function, e.g., Chebyshev or maximally flat (Butterworth), etc., and then finding the elements of the coupling matrix, as follows:

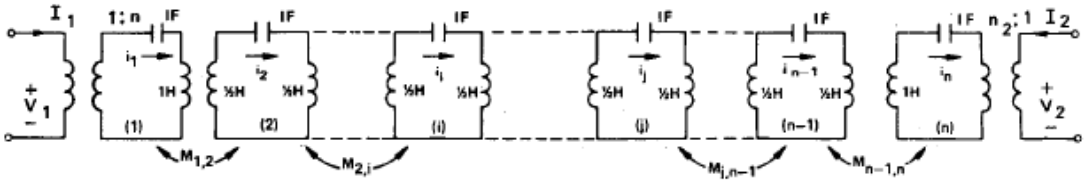

Figure 3.1. Sequential low-pass prototype multi-coupled filter.

For maximally flat filter function, g-values can be derived from the following formulas:

$$g_k = 2\sin[\frac{(2k-1)\pi}{2n}], k = 1, 2, 3, \ldots, n$$
$$g_0 = 1, \quad g_{n+1} = 1 \tag{3.1}$$

For the Chebyshev filter function, g-values can be derived from the following formulas:

$$g_0 = 1$$
$$g_1 = \frac{2a_1}{\gamma}$$
$$g_k = \frac{4a_{k-1}\,a_k}{b_{k-1}g_{k-1}}, k = 2, 3, \ldots, n$$
$$g_{n+1} = \begin{cases} 1 & n\ odd \\ \coth^2\frac{\beta}{4} & n\ even \end{cases}$$
$$a_k = \sin[\frac{(2k-1)\pi}{2n}], \qquad k = 1, 2, 3, \ldots, n$$
$$b_k = \gamma^2 + \sin^2\frac{k\pi}{n}, \qquad k = 1, 2, 3, \ldots, n$$
$$\gamma = \sinh\frac{\beta}{2n}$$
$$\beta = \ln[\coth(\frac{L_{ar}}{17.37})] \tag{3.2}$$

L_{ar} is ripple level in the passband in dB (Insertion loss ripple), which can be calculated from the desired filter return loss, RL in dB. In the next step, coupling matrix elements can be calculated as follows:

$$L_{ar} = 10\log\frac{1}{(1-10^{-\frac{RL}{10}}))} \tag{3.3}$$

$$M_{j,j+1} = \frac{1}{\sqrt{g_j}g_{j+1}}\ ,j = 1\ ,2\ ,3\ ,\ldots,N-1$$

$$R_1 = \frac{1}{g_1 g_0}\ , \qquad R_N = \frac{1}{g_N g_{N+1}} \tag{3.4}$$

In dealing with multi-coupled resonator filters with cross-couplings, the first step is to filter polynomials F(s), E(s) and P(s) for the general class of Chebyshev filters (which may have some or all transmission zeros in the finite position). These can be calculated using a recursive technique [24] and [25], after which the scattering parameter functions can be calculated as follows:

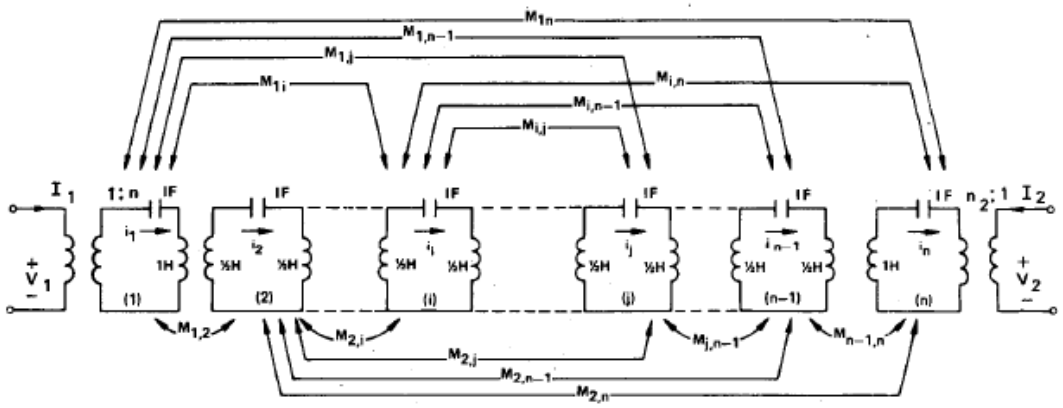

Figure 3.2. A general 2-port composed of synchronously tuned coupled cavities [26].

$$S_{11} = \frac{F(\omega)/\epsilon_R}{E(\omega)},\quad S_{22} = \frac{F_{22}(\omega)/\epsilon_R}{E(\omega)},\quad S_{21} = S_{12} = \frac{P(\omega)/\epsilon}{E(\omega)} \tag{3.5}$$

in which ε and ε_R are normalization factors to set $|S_{11}(s)|$ and $|S_{21}(s)| \leq 1$ at any value of frequency variable *s*.

Unknown coupling matrix elements can be obtained by first converting the scattering parameters to admittance parameters and then calculating the admittance parameters from the unknown coupling matrix itself, using Eigendecomposition and orthonormalization [26].

Regarding the eigenvector matrix T in Eigendecomposition theory, the orthogonality property is used to construct the entire matrix T from its first two rows. It exists only when the coupling matrix is symmetric with the complex conjugate elements over and below its diagonal. In lossy cases, the coupling matrix has complex entries and is symmetric, but not with complex conjugate entries

(Hermitian matrix), and therefore a modified orthogonalization process is used, as in [18] and [28]. It is also important to point out that, with this method, the maximum number of TZs (transmission zeros) of the filter is N-2, based on the Nfz rule of thumb (N_{fzmax}=N-N_{min} , where N is filter degree, N_{min} is the number of resonators in the shortest path through the network between the source and the load).

The main points to be considered in the direct method can be summarized as follows:

- This technique is based on a multi-coupled array network model.
- The eigendecomposition theory is applied to obtain coupling matrix.
- It needs an orthonormalization process to obtain the initial coupling matrix.
- For lossless cases, the Gram Schmitt orthonormalization process is usually used.
- For lossy cases, because of the complex entries of the coupling matrix, a modified orthonormalization process is required.

3.2.2 Transversal network model

According to the N_{fz} rule, the maximum number of finite transmission zeros equals the total number of resonators minus the number of resonator nodes in the shortest signal path between source and load ($N_{fzmax} = N - N_{min}$). In this method [29], since there is a direct coupling between sources, then N_{min}=0, and the fully canonical filter response is realizable. The polynomial calculation process and *Y*-parameter calculation are the same as in the previous section. The only facilitating difference in this transversal model compared with the previous one is that because there is no direct coupling between resonators, formulating the Y-parameter to the two-port, short-circuit admittance parameter will result directly in coupling *N*+2 matrix, with no need for any matrix algebra.

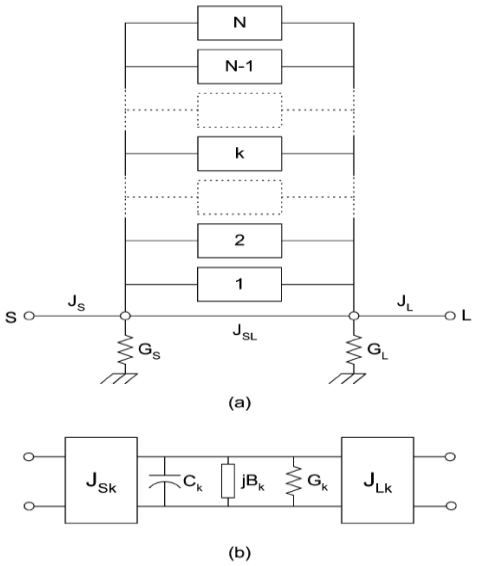

Figure 3.3. ***a***) N-resonator transversal model, ***b***) equivalent lossy circuit for the Nth resonator [30].

	S	1	…	k	…	N	L
S	$-jG_S$	J_{S1}	…	J_{Sk}	…	J_{SN}	J_{SL}
1	J_{S1}	$B_1 - jG_1$					J_{1L}
⋮	⋮		⋱				⋮
k	J_{Sk}			$B_k - jG_k$			J_{kL}
⋮	⋮				⋱		⋮
N	J_{SN}					$B_N - jG_N$	J_{NL}
L	J_{SL}	J_{1L}	…	J_{kL}	…	J_{NL}	$-jG_L$

Figure 3.4. N+2 fully canonical complex coupling matrix for the lossy transversal array [30].

The calculation of the elements of a coupling matrix is formulated as follows. Using nodal analysis (Figure 3.5), the N+2 matrix of the Y-parameter of a multi-coupled resonator filter can be written as

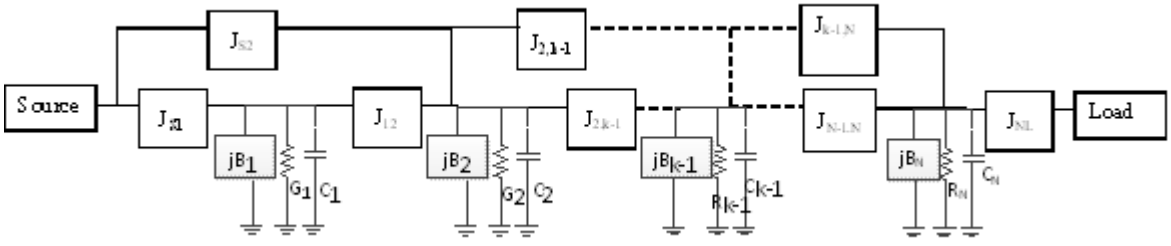

Figure 3.5. Admittance inverter model of low-pass prototype filter.

$$\begin{bmatrix} I_S \\ 0 \\ \vdots \\ \vdots \\ I_L \end{bmatrix} = \begin{bmatrix} 1/R_s & -jJ_{S1} & \cdots & \cdots & -jJ_{SN} & -jJ_{SL} \\ -jJ_{S1} & G_1 + jB_1 + s & -jJ_{12} & \cdots & -jJ_{1N} & -jJ_{1L} \\ \vdots & \ddots & & \ddots & \vdots & \vdots \\ \vdots & & \ddots & & & \vdots \\ -jJ_{SN} & \cdots & \cdots & G_N + jB_N + s & & -jJ_{NL} \\ -jJ_{SL} & -jJ_{1L} & \cdots & \cdots & -jJ_{NL} & 1/R_L \end{bmatrix}_{N+2\ by\ N+2} = \begin{bmatrix} V_S \\ V_1 \\ \vdots \\ \vdots \\ V_L \end{bmatrix} \tag{3.6}$$

where Is is current source, R_S and R_L are source and load impedances which are normalized to $R_S=R_L=1$, J_k are values of admittance invertors between resonator (couplings), B_k are frequency invariant elements (FIR) which are necessary for non-symmetrical frequency response, G_k are resonators' loss values, and $S=j\omega$ is the frequency variable.

This can be written as

$$[Y_N] = j[M] + [R] + [s] \tag{3.7}$$

where M is the coupling matrix, S is the frequency variable matrix and R is normalized source and load resistance matrix.

In order to reduce the N+2 by N+2 matrix to 2-by-2 resultant Y-matrix (short-circuit admittance matrix), multi-port network analysis is applied. Here, we define I_p, I_c, V_p, and V_c vectors and the matrix-relation between these valuables, as follows:

$$\begin{bmatrix} I_p \\ I_c \end{bmatrix} = \begin{bmatrix} Y_{pp} & Y_{pc} \\ Y_{cp} & Y_{cc} \end{bmatrix} \begin{bmatrix} V_p \\ V_c \end{bmatrix} \tag{3.8}$$

where

$$[I_p] = \begin{bmatrix} I_s \\ I_L \end{bmatrix}, [I_c] = \begin{bmatrix} 0 \\ \vdots \\ 0 \end{bmatrix}, [V_p] = \begin{bmatrix} V_s \\ V_L \end{bmatrix} \text{ and } [V_c] = \begin{bmatrix} V_1 \\ \vdots \\ V_N \end{bmatrix}$$

$$[Y_{pp}] = \begin{bmatrix} 1 & -jJ_{sL} \\ -jJ_{sL} & 1 \end{bmatrix}, [Y_{pc}] = \begin{bmatrix} -jJ_{s1} & \cdots & -jJ_{sN} \\ -jJ_{1L} & \cdots & -jJ_{NL} \end{bmatrix}, [Y_{cp}] = [Y_{pc}]^T$$

$$[Y_{cc}] = \begin{bmatrix} G_1 + jB_1 + s & -jJ_{12} & \cdots & -jJ_{1N} \\ -jJ_{12} & & \ddots & \vdots \\ \vdots & & & -jJ_{N-1,N} \\ -jJ_{1N} & & -jJ_{N-1,N} & G_N + jB_N + s \end{bmatrix}_{\text{NxN}} \tag{3.9}$$

According to these definitions, since $I_c=0$, I_p is calculated as below:

$$\begin{bmatrix} I_S \\ I_L \end{bmatrix} = [I_p] = [Y_{pp} - Y_{pc}[Y_{cc}]^{-1}Y_{cp}][V_p]$$
$$= \begin{bmatrix} Y_{11_t} & Y_{12_t} \\ Y_{21_t} & Y_{22_t} \end{bmatrix}_{2x2} \begin{bmatrix} V_S \\ V_L \end{bmatrix} = [Y_N]_{2x2} \begin{bmatrix} V_S \\ V_L \end{bmatrix}$$
$$\Rightarrow [Y_N] = \begin{bmatrix} Y_{11_t} & Y_{12_t} \\ Y_{21_t} & Y_{22_t} \end{bmatrix}_{2x2} = [Y_{pp} - Y_{pc}[Y_{cc}]^{-1}Y_{cp}] \quad (3.10)$$

As we know that, in a transversal model, there is no direct coupling between resonators (meaning, $J_{nm}=0$, $n \neq m$ and therefore Y_{cc} is a diagonal matrix and its inverse is equal to Y_{cc} with inverse elements), by simplifying the above matrix equations, one can rewrite the Y parameter of a 2-by-2 overall network as follows:

$$[Y_N] = j\begin{bmatrix} 0 & J_{SL} \\ J_{SL} & 10 \end{bmatrix} + \begin{bmatrix} G_S & 0 \\ 0 & G_L \end{bmatrix} + \sum_{k=1}^{N} \frac{1}{s + jB_k + G_k} \begin{bmatrix} J_{Sk}^2 & J_{Sk}J_{Lk} \\ J_{Sk}J_{Lk} & J_{Lk}^2 \end{bmatrix} \quad (3.11)$$

Two important points about the transversal technique is that it results in the N+2 coupling matrix directly with no need for the orthonormalization process. Furthermore, a fully canonical filter is realizable using this method.

3.3 Lossy Filter

3.3.1 Lossy Coupling Matrix Synthesis

The synthesis procedure of an N^{th} order lossy filter with different loss levels of S_{11} and S_{22} starts from a rational representation of the lossless scattering parameters of a low-pass prototype, simply by multiplying Eq. (3.5) with attenuation factor *K*,

$$S_{11} = K_1 \frac{F(\omega)/\epsilon_R}{E(\omega)} = K_1 \frac{\bar{F}(\omega)}{E(\omega)}, \quad S_{22} = K_2 \frac{F_{22}(\omega)/\epsilon_R}{E(\omega)} = K_2 \frac{\bar{F}_{22}(\omega)}{E(\omega)}, \quad S_{21} = S_{12} = K \frac{P(\omega)/\epsilon}{E(\omega)} = K \frac{\bar{P}(\omega)}{E(\omega)}$$
$$K_1 = \sqrt{10^{-\frac{L_1}{10}}}, \; K_2 = \sqrt{10^{-\frac{L_2}{10}}}, \; K = \sqrt{K_1 K_2} = \sqrt{10^{-(L_1+L_2)/20}}, \; \alpha \triangleq \sqrt{\frac{K_1}{K_2}} \quad (3.12)$$

in which L_1 and L_2 are loss values of S_{11} and S_{22} in dB, respectively. Based the procedure presented in [30], and using classic two-port S matrix to Y matrix transformation formulas, with normalized characteristic impedances, the -parameter functions can be derived as:

$$Y_{11} = \frac{E - (K\alpha)\bar{F} + \left(\frac{K}{\alpha}\right)\bar{F}_{22} + V}{E + (K\alpha)\bar{F} + \left(\frac{K}{\alpha}\right)\bar{F}_{22} - V}$$

$$Y_{22} = \frac{E + (K\alpha)\bar{F} - \left(\frac{K}{\alpha}\right)\bar{F}_{22} + V}{E + (K\alpha)\bar{F} + \left(\frac{K}{\alpha}\right)\bar{F}_{22} - V}$$

$$Y_{12} = Y_{21} = \frac{E - (K\alpha)\bar{F} + \left(\frac{K}{\alpha}\right)\bar{F}_{22} + V}{E + (K\alpha)\bar{F} + \left(\frac{K}{\alpha}\right)\bar{F}_{22} - V}$$

$$V = K^2 \frac{\bar{P}^2 - \alpha\bar{F}\left(\frac{\bar{F}_{22}}{\alpha}\right)}{E} \tag{3.13}$$

The rational function V can be simplified by applying reciprocity and matching properties of the two-port network on phase conditions, after which V can be calculated as

$$V = K^2 \frac{\bar{P}^2 - \alpha\bar{F}\left(\frac{\bar{F}_{22}}{\alpha}\right)}{E} = K^2\,(-1)^{N+1}\,E^* \tag{3.14}$$

in which E^* is the complex conjugate of the denominator polynomial E and its poles are located at the mirror image of poles of polynomial E with respect to the imaginary axis, i.e., $s_{i\,conj} = -s_i^*$.

Imposing loss into the network would make the coupling matrix have complex entries both in the resonators and in the coupling in addition to the reactive path. Complex values can be modeled as admittance or impedance inverters with complex values. One approach to finding a lossy coupling matrix is using the transversal array model [29][30]. Although the *N+2* lossy coupling matrix can be synthesized from the transversal array circuit model in Figure 3.3, the circuit model is different from the lossless model. First of all, there is loss in all resonators representing the finite Q factor; secondly, there is loss in the coupling values; and finally, two additional resistors are present at source and load.

Using nodal analysis in transversal array model, one can calculate the overall admittance matrix $[Y_N]$ as:

$$[Y_N] = \begin{bmatrix} G_s & -jJ_{S1} & \cdots & \cdots & -jJ_{SN} & -jJ_{SL} \\ -jJ_{S1} & G_1 + jB_1 + s & -jJ_{12} & \cdots & -jJ_{1N} & -jJ_{1L} \\ \vdots & \ddots & & \ddots & \vdots & \vdots \\ \vdots & & \ddots & & & \vdots \\ -jJ_{SN} & \cdots & \cdots & G_N + jB_N + s & -jJ_{NL} & \\ -jJ_{SL} & -jJ_{1L} & \cdots & \cdots & -jJ_{NL} & G_L \end{bmatrix}_{N+2\ by\ N+2} \quad (3.15)$$

Furthermore, because$[Y_N] = j[M] + [R] + [s]$, the coupling matrix $[M]$ can be expressed as

$$[M] = \begin{bmatrix} -jG_s & J_{S1} & \cdots & \cdots & J_{SN} & J_{SL} \\ J_{S1} & B_1 - jG_1 & J_{12} & \cdots & J_{1N} & J_{1L} \\ \vdots & \ddots & & \ddots & \vdots & \vdots \\ \vdots & & \ddots & & & \vdots \\ J_{SN} & \cdots & \cdots & B_N - jG_N & J_{NL} & \\ J_{SL} & J_{1L} & \cdots & \cdots & J_{NL} & -jG_L \end{bmatrix}_{N+2\ by\ N+2} \quad (3.16)$$

The admittance matrix of the overall network can be written calculating the residues of the Y-matrix polynomial, as follows:

$$[Y_N] = j\begin{bmatrix} 0 & k_\infty \\ k_\infty & 0 \end{bmatrix} + \begin{bmatrix} g_1 & 0 \\ 0 & g_2 \end{bmatrix} + \sum_{k=1}^{N} \frac{1}{s - j\lambda} \begin{bmatrix} r_{11k} & r_{12k} \\ r_{21k} & r_{22k} \end{bmatrix} \quad (3.17)$$

$k_\infty \neq 0$ only in fully canonical case, which indicates that the number of transmission zeros is the same as the order of the filter (N_{fz}= N), g_1 and g_2 are scalars remaining from partial fraction expansion of Y_{11} and Y_{22}, λ are the Eigen values of Y parameter, and $r_{11}, r_{21}, r_{12}, r_{22}$ are the residues of Y matrix polynomials. On the other hand, by simplifying the transversal array network in Figure 3.3, the overall admittance matrix can be written as:

$$[Y_N] = j\begin{bmatrix} 0 & J_{SL} \\ J_{SL} & 0 \end{bmatrix} + \begin{bmatrix} G_S & 0 \\ 0 & G_L \end{bmatrix} + \sum_{k=1}^{N} \frac{1}{sC_k - jB_k + G_k} \begin{bmatrix} J_{Sk}^2 & J_{Sk}J_{Lk} \\ J_{Sk}J_{Lk} & J_{Lk}^2 \end{bmatrix} \quad (3.18)$$

By equating Eq.(3.18) and Eq.(3.17), elements of the transversal array model coupling matrix can be found, as follows:

$$C_k = 1\ , B_k = -Re\{\lambda_k\}, G_k = Im\{\lambda_k\}\ ,$$
$$J_{Lk} = \pm\sqrt{r_{22k}}\ , J_{Sk} = \pm\ \frac{r_{21k}}{\sqrt{r_{22k}}}$$
k=1, 2 ,3 ,….., N (3.19)

3.3.2 Lossy Filter Synthesis Using an Attenuator

Another approach to finding a lossy coupling matrix has been presented in [31]. In this approach, the lossless filter network is sandwiched between two attenuators, which represent the loss of the overall network. Since the attenuators are matched at both ends, the lossy scattering parameters of the overall network can be written as:

$$\begin{aligned} S_{11}^{lossy} &= K^2 S_{11} \\ S_{21}^{lossy} &= K^2 S_{21} \\ S_{22}^{lossy} &= K^2 S_{22} \end{aligned} \tag{3.20}$$

where K is the loss level. The equivalent network of the attenuators illustrated in Figure 3.7 and its equivalent circuit after moving the resistors to the right-hand side of the admittance inverter and using appropriate scaling, the inverter can be scaled to unity and removed.

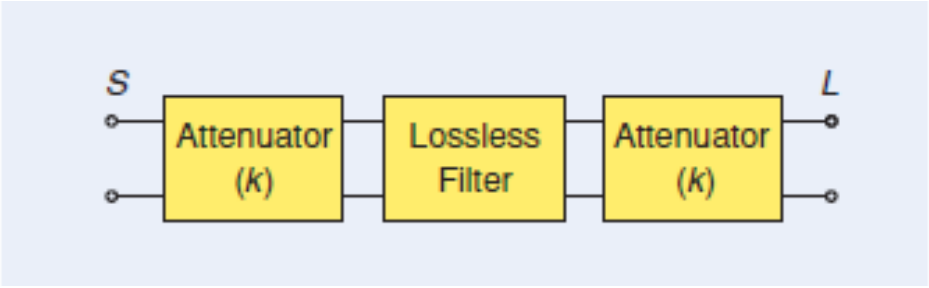

Figure 3.6. Possible representation of a lossy filter [31]

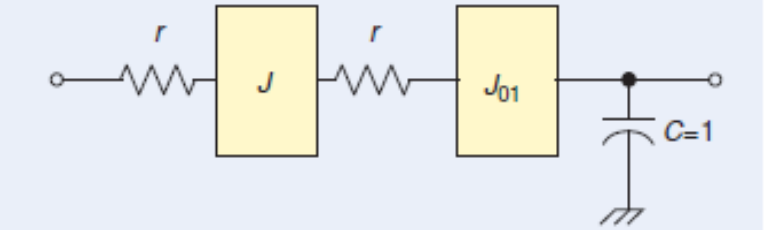

Figure 3.7. Attenuator network attached to the first (last) resonator [31].

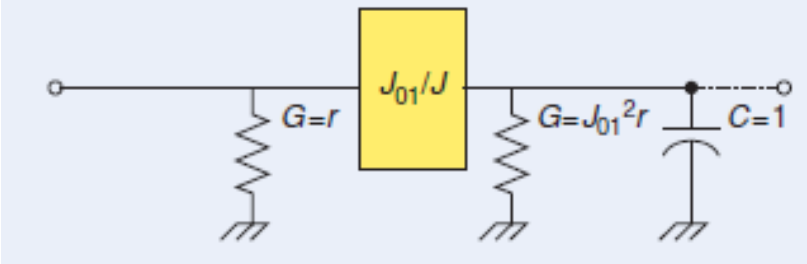

Figure 3.8. Equivalent model for attenuator attached to the first (last) resonator [31].

The relations between resistance, the inverter value and loss level can be defined as follows:

$$J = \pm\frac{1}{\sqrt{1-r^2}} \quad and \; K = \sqrt{\frac{1-r}{1+r}} \tag{3.21}$$

For synthesis, the lossy coupling of this model and the initial lossless coupling matrix of the order *N* (non-transversal) should be synthesized at the first step, as in [31]. Furthermore, as illustrated in the equivalent circuit model Figure 3.8, some elements must be modified to change the lossless coupling matrix to a lossy one. Comparing Figure 3.7 and Figure 3.8 , we can see that a conductance of *G* would be added to the first and last resonators and that there would be a conductance *G* at the non-resonating source and load nodes (and, being divided by the value of *J*, at the first and last admittance inverters as well). The new entries' values and the resultant lossy coupling matrix are shown below.

	S	1	2	...	*N*–1	*N*	*L*
S	0	J_{S1}	0	...	0	0	0
1	J_{S1}	J_{11}	J_{12}	...	$J_{1,N-1}$	J_{1N}	0
2	0	J_{12}	J_{22}	...	$J_{2,N-1}$	J_{2N}	0
⋮	⋮	⋮	⋮	⋱	⋮	⋮	⋮
N–1	0	$J_{1,N-1}$	$J_{2,N-1}$	...	$J_{N-1,N-1}$	$J_{N-1,N}$	0
N	0	J_{1N}	J_{2N}	...	$J_{N-1,N}$	J_{NN}	J_{NL}
L	0	0	0	...	0	J_{NL}	0

Figure 3.9. Lossless N+2 coupling matrix [31].

	S	1	2	...	*N*–1	*N*	*L*
S	$-jG'_S$	J'_{S1}	0	...	0	0	0
1	J'_{S1}	$J_{11}-jG'_1$	J_{12}	...	$J_{1,N-1}$	J_{1N}	0
2	0	J_{12}	J_{22}	...	$J_{2,N-1}$	J_{2N}	0
⋮	⋮	⋮	⋮	⋱	⋮	⋮	⋮
N–1	0	$J_{1,N-1}$	$J_{2,N-1}$	...	$J_{N-1,N-1}$	$J_{N-1,N}$	0
N	0	J_{1N}	J_{2N}	...	$J_{N-1,N}$	$J_{NN}-jG'_N$	J'_{NL}
L	0	0	0	...	0	J'_{NL}	$-jG'_L$

Figure 3.10. Lossy N+2 coupling matrix [31].

$$G_L' = G_S' = r = \frac{1-K^2}{1+K^2}$$
$$J_{S1}' = \pm J_{S1}\sqrt{1-r^2}\,, J_{NL}' = \pm J_{NL}\sqrt{1-r^2}$$
$$G_1' = J_{S1}^2 r\,, G_N' = J_{NL}^2 r \tag{3.22}$$

The above formulation applies for the identical loss level of S_{11} and S_{22}. However, it would be simple to modify the formulation for different loss level cases, as follows:

$$K_1 = \sqrt{\frac{1-r_1}{1+r_1}}\,, K_2 = \sqrt{\frac{1-r_2}{1+r_2}}$$
$$G_L' = r_1 = \frac{1-K_1^2}{1+K_1^2}$$
$$G_S' = r_2 = \frac{1-K_2^2}{1+K_2^2}$$
$$J_{S1}' = \pm J_{S1}\sqrt{1-r_1^2}\,, J_{NL}' = \pm J_{NL}\sqrt{1-r_2^2}$$
$$G_1' = J_{S1}^2 r_1\,, G_N' = J_{NL}^2 r_2 \tag{3.23}$$

3.3.3 Coupling Matrix Rotation (reduction)

Having *N+2* couplings between source and resonators and the same amount between load and resonators, a transversal coupling matrix seems to be infeasible in practice. In order to obtain a practical coupling matrix, some unwanted couplings should be annihilated with a sequence of similarity transforms (rotations) until a more convenient form with a minimal number of couplings is obtained. Of course, using the similarity transforms ensures that the eigenvalues and eigenvectors of the coupling matrix are preserved in such a way that the transformed matrix will retain exactly the same transfer and reflection frequency response as that of the original matrix. In terms of practice, there are two well- known canonical forms of coupling matrix out of several ones. One is the "*right-column justified*" (RCJ) [32] and the more generally useful one is the "*folded*" form [33].

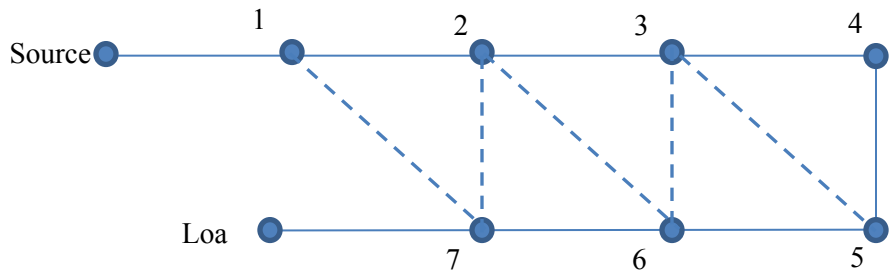

Figure 3.11. N=7 degree folded representation of the coupling matrix.

s	m	0	0	0	0	x
.	s	m	0	0	x	x
.	.	s	m	x	x	0
.	.	.	s	m	0	0
.	.	.	.	s	m	0
.	.	.	.	.	s	m
.	.	.	.	.	.	s

Figure 3.12. Folded coupling matrix representation of N=7: *x*, cross couplings; *m*, main-line couplings; and *s*, self-couplings.

The procedure to reduce the coupling matrix to the folded form is as follows. The initial transversal coupling matrix must be pre- and post-multiplied by a rotation matrix R with the same order of coupling matrix, meaning $M_r = R_r M_{r-1} R_r^t$, in which M_{r-1} is the coupling matrix before rotation, M_r is the coupling matrix after rotation, and R_r is r^{th} rotation matrix. A 6-by-6 rotation matrix with pivot [3, 4] is shown below. Rotation matrix R with pivot $[i,j]$,$i \neq j$ means that $R_{ij} = -R_{ji} = \sin(\theta_r)$ and $R_{ii} = R_{jj} = \cos(\theta_r)$ and $ij \neq 1$ or N, and θ_r is r^{th} the rotation angle. All other elements are equal to zero.

1	0	0	0	0	0
0	1	0	0	0	0
0	0	$\boldsymbol{C_r}$	$\boldsymbol{-s_r}$	0	0
0	0	$\boldsymbol{-s_r}$	$\boldsymbol{C_r}$	0	0
0	0	0	0	1	0
0	0	0	0	0	1

Figure 3.13. A 6-by-6 rotation matrix with pivot =[3, 4].

The sequence of annihilation is as follows. Starting with elements right to left along rows and top to bottom down columns, as shown in Figure 3.14, it starts with the element in the first row and the $(N\text{-}1)^{th}$ column.

s	m	4	3	2	1	x
.	s	m	9	8	x	x
.	.	s	m	x	x	5
.	.	.	s	m	10	6
.	.	.	.	s	m	7
.	.	.	.	.	s	m
.	.	.	.	.	.	s

Figure 3.14. Elements of coupling matrix to be annihilated.

Summary of the formulation used in similarity transforms is listed below, the general formulas of rotated entries with pivot [i,j] and angle θ_r are:

$$M'_{ik} = c_r M_{ik} - s_r M_{jk}\,, \quad fir\ the\ k^{th} element\ of\ row\ i$$
$$M'_{jk} = s_r M_{ik} + c_r M_{jk}\,, \quad fir\ the\ k^{th} element\ of\ row\ j$$
$$M'_{ki} = c_r M_{ki} - s_r M_{kj}\,, \quad fir\ the\ k^{th} element\ of\ column\ i$$
$$M'_{kj} = s_r M_{ki} + c_r M_{kj}\,, \quad fir\ the\ k^{th} element\ of\ column\ i \tag{3.24}$$

The formulas for rotation angles for annihilation of elements with pivot [i,j] are summarized below.

$$\theta_r = \tan^{-1}(M_{ik}/M_{jk}), \quad for\ annihilation\ the\ K^{th}\ element\ of\ row\ i$$
$$\theta_r = -\tan^{-1}(M_{jk}/M_{ik}), \quad for\ annihilation\ the\ K^{th}\ element\ of\ row\ j$$
$$\theta_r = \tan^{-1}(M_{ki}/M_{kj}), \quad for\ annihilation\ the\ K^{th}\ element\ of\ column\ i$$
$$\theta_r = -\tan^{-1}\left(\frac{M_{kj}}{M_{ki}}\right), \quad for\ annihilation\ the\ K^{th}\ element\ of\ column\ j$$

$$\theta_r = -\tan^{-1}\left(\frac{M_{ij} \pm \sqrt{M_{ij}^2 - M_{ii}M_{jj}}}{M_{jj}}\right),$$

$$for\ annihilation\ cross\ pivot\ element\ M_{ii}$$

$$\theta_r = \tag{3.25}$$

$$-\tan^{-1}\left(\frac{-M_{ij}\pm\sqrt{M_{ij}^2-M_{ii}M_{jj}}}{M_{ii}}\right), for\ annihilation\ cross\ pivot\ element\ M_{jj}$$

$$\theta_r = -0.5\tan^{-1}\left(\frac{2M\_ij}{M_{ii}-M_{jj}}\right), \quad for\ annihilation\ cross\ pivot\ element\ M_{ij}$$

There are three important properties of similarity transformation. First, only those elements in the rows and columns of the pivot may be affected by the rotation. Second, a pair of zero elements across the rows and columns of the pivot would remain zero after the transformation. And third, electrical properties (i.e., eigenvalues and eigenvectors) of the new the coupling matrix would remain exactly the same as that of the original coupling matrix.

3.3.4 Loss Distribution Technique

The resultant coupling matrix after rotation would be feasible in terms of practice and implementation. After rotation, the coupling matrix includes the resistive entries in the resonators and resistive/complex entries in the coupling. However, the loss in the resonators is not distributed evenly, indicating that each resonator has a different Q factor from the others. In some cases, it is desirable to have the loss distributed equally between all resonators in order to simplify the fabrication. In other cases, some resonators need to have equal Q values different from other resonators, e.g. a pair of resonators have the same Q value for a specific design. A hyperbolic rotation makes it possible to distribute the loss among the resonators[34].

The concept of hyperbolic rotation is the same as trigonometric rotation, which is used to rotate the matrix to the folded form. The exception here is that the rotation is not sine and cosine anymore, but rather hyperbolic sine and hyperbolic cosine, or a combination of both. Furthermore, there is no formulation to find the proper rotation angle because it depends on the desired Q factor on each resonator; however, it can be done by programing a code with the objective quality factor. The rotation matrix is the same as in the previous section except for c_r and s_r. This means that the elements $R_{ij} = -R_{ji} = \sinh(\theta_r)$ and $R_{ii} = R_{jj} = \cosh(\theta_r)$ and $ij \neq 1$ or N, and θ_r is r^{th} the rotation angle. An example in the results section below will illustrate this concept.

3.3.5 Simulation and Results

To illustrate the procedures explained above, let us consider the following example. A 4-pole fully canonical pseudoelliptic filter with 25 dB return loss in passband and four transmission zeros at +j1.1 -j1.1 +j1.5 -j1.5 with different loss values of 5dB and 10dB for S11 and S22 respectably is presented. For the first step, we need to calculate the filter polynomials coefficients based on the recursive technique.

Table 3.1. Roots of filter polynomials.

roots of E(s)	-1.0149 +*j*0.86476i	-0.22681 -*j*1.2539	0.22681 +*j*1.2539	-1.0149- *j*0.86476i	ε=7.0262
roots of F(s)	*j*0.9405	*j*0.9405	*j*0.42839	*j*0.42839	ε_r=1.0103

Coefficients of the polynomials in descending order are,

Table 3.2. Coefficients of filter polynomials.

n	4	3	2	1	0
E(s) coefficients	1	2.4834	4.3222	4.1021	2.8866
F(s) coefficients	1	0	1.0681	0	0.16233
P(s) coefficients	1	0	9.49	0	20.25

To familiarize ourselves with the transversal array network model, the lossless transversal coupling matrix is synthesized [29], after which the attenuation factor is taken into consideration.

Table 3.3. Coefficients of Y-parameters.

n	4	3	2	1	0
Y(s) denominator	1	0	2.7034	0	1.5314
Y_{11}(s) matrix numerator	0	1.248	0	2.0615	0
Y_{22}(s) matrix numerator	0	1.248	0	2.0615	0
Y_{21}(s)/Y_{12}(s) matrix numerator	*j*0.071527	0	*j*0.67879	0	*j*1.4484

Coupling matrix elements i.e., FIR elements conductance, source to resonators' and load to resonators' coupling values can be calculated as below, based on Eq.(3.19).

Table 3.4. Coupling matrix elements.

B_K	G_K	J_{SK}	J_{LK}	J_{SL}	k
1.3768	0	0.3739	0.3739	0.0715	1
0.8988	0	-0.6958	0.6958	-	2
-0.8988	0	0.6958	0.6958	-	3
-1.3768	0	-0.3739	0.3739	-	4

Table 3.5. Transversal coupling matrix, lossless network.

	S	1	2	3	4	L
S	0	0.3739	-0.695	0.6958	-0.3739	0.0715
1	0.3739	1.3767	0	0	0	0.3739
2	-0.6958	0	0.8988	0	0	0.6958
3	0.6958	0	0	-0.8988	0	0.6958
4	-0.3739	0	0	0	-1.3767	0.3739
L	0.07152	0.3739	0.6958	0.6958	0.3739	0

The feasible folded form of the coupling matrix, after the rotation procedure has been carried out on the transversal matrix, is as follows:

Table 3.6. Feasible folded form of the coupling matrix after the rotation.

	S	1	2	3	4	L
S	0	1.1172	0	0	0	0.0715
1	1.1172	0	0.9489	0	-0.3889	0
2	0	0.9489	0	0.8669	0	0
3	0	0	0.8669	0	0.9489	0
4	0	-0.3889	0	0.9489	0	1.1172
L	0.0715	0	0	0	1.1172	0

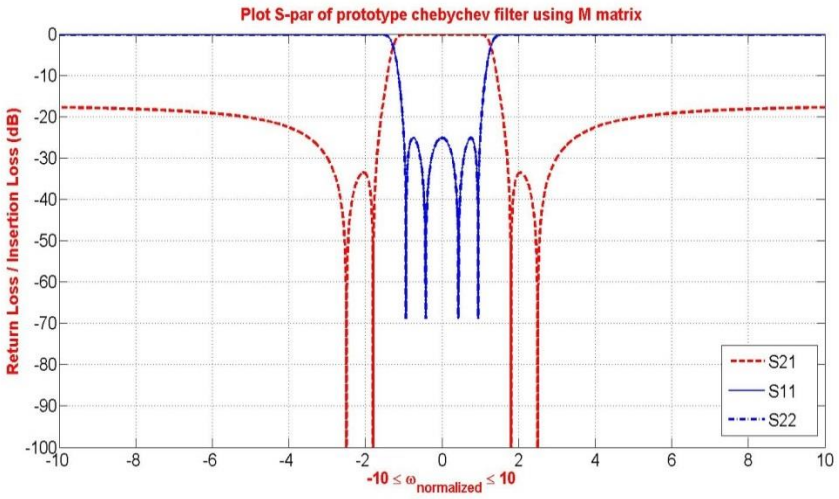

Figure 3.15. Lossless canonical pseudoelliptic filter.

Using the attenuator at the source and load, the lossy coupling matrix can be obtained by applying the method explained in section 3.3.2.

Using the formulas in Eq.(3.23), the lossy elements and modified admittance inverter values can be calculated as:

Table 3.7. Lossy elements and modified admittance inverter values.

G_L'	G_S'	J_{NL}'	J_{S1}'	G_1'	G_N'
0.5195	0.2801	0.9546	1.0724	0.3496	0.6483

Alternatively, using the method described in 3.3.1, the lossy coupling matrix might be constructed by applying attenuation factors calculated as K_1 = 0.5623, K_2 = 0.3162 and α=1.3335, based on Eq.(3.12).

Admittance parameters coefficients are derived as below, using Eq. (3.13).

Table 3.8. Coefficient of Y-parameters.

n	4	3	2	1	0
Y(s) denominator	1	0.99721	2.94	1.6472	1.7295
$Y_{11}(s)$ matrix numerator	0.28258	1.4286	1.6085	2.3598	1.1398
$Y_{22}(s)$ matrix numerator	0.52054	1.4286	1.8627	2.3598	1.1784
$Y_{21}(s)/Y_{12}(s)$ matrix numerator	*j*0.058627	0	*j*0.55637	0	*j*1.1872

Using the transversal array network, the elements of the initial coupling matrix Eq. (3.16) can now be derived based on Eq. (3.19), as follows:

Table 3.9. Elements of the initial coupling matrix

B_K	G_K	J_{SK}	J_{LK}	J_{SL}	k
1.3509	0.1025	0.3993 - *j*0.0143	0.2598 -*j*0.1112	0.0586	1
0.8862	0.3961	-0.6436 - *j*0.0113	0.6334 -*j*0.0404	-	2
-0.8862	0.3961	0.6436 - *j*0.0113	0.6334 +*j*0.0404	-	3
-1.3509	0.1025	-0.3993 - *j*0.0143	0.2598 +*j*0.1112	-	4

The *N*+2 transversal coupling matrix would be:

Table 3.10. N+2 transversal coupling matrix.

	S	1	2	3	4	L
S	-*j*0.2826	0.3993-*j*0.0143	-0.6436-*j*0.0113	0.6436-*j*0.0113	-0.3993-*j*0.0143	0.0586
1	0.3993-*j*0.0143	1.3509-*j*0.1025	0	0	0	0.2568-*j*0.1112
2	-0.6436-*j*0.0113	0	0.8862-*j*0.3961	0	0	0.6334-*j*0.0404
3	0.6436-*j*0.0113	0	0	-0.8862-*j*0.3961	0	0.6334+*j*0.0404
4	-0.3993-*j*0.0143	0	0	0	-1.3509-*j*0.1025	0.2568+*j*0.1112
L	0.0586	0.2568-*j*0.1112	0.6334-*j*0.0404	0.6334+*j*0.0404	0.2568+*j*0.1112	*J*0.5205

After reducing the coupling matrix to the feasible folded form using the rotation technique as described in section 3.3.3, the folded coupling matrix is presented as follows.

Table 3.11. Folded coupling matrix.

	S	1	2	3	4	L
S	-*j*0.2826	1.0709	0	0	0	0.0586
1	1.0709	-*j*0.3119	0.9489	0	-0.4141	-*j*0.0546
2	0	0.9489	-*j*0.0645	0.8693	0	0
3	0	0	0.8693	*j*0.0645	0.9489	0
4	0	-0.4141	0	0.9489	-*j*0.6782	0.9552
L	0.0586	-*j*0.0546	0	0	0.9552	*J*0.5205

The scattering parameter plot of the folded coupling matrix with different loss levels of S_{11} and S_{22} is shown below.

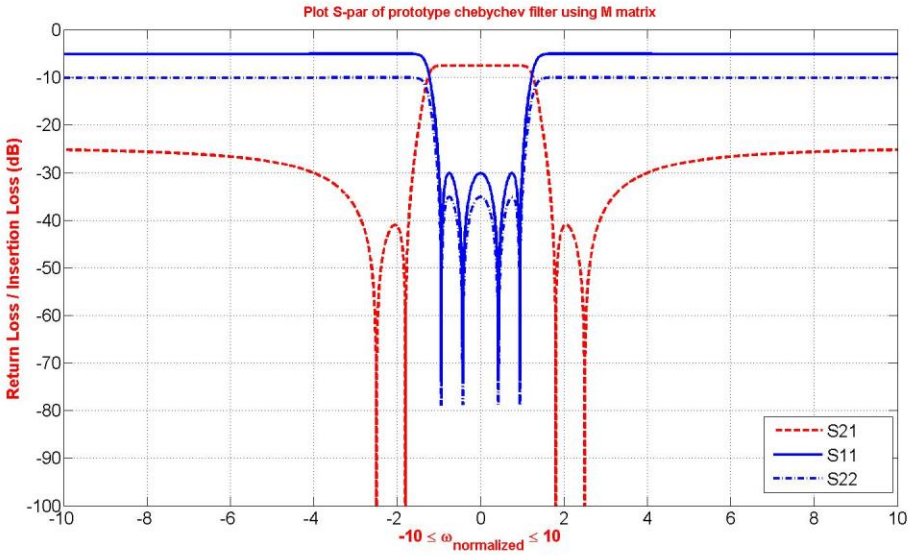

Figure 3.16. S-parameter of folded coupling matrix with different loss level

3.3.6 Actual Physical Q vs. Achievable Equivalent Q

Although the reduced coupling matrix is feasible in terms of practice, as mentioned in the previous section, in some cases it is needed to have the loss distributed among the resonators for ease of fabrication. Depending on the physical structure and the filter type, for example, one might need to distribute the loss equally among the resonator to have an equal actual Q factor of all resonators or each pair of an equal actual Q factor. This would be achieved using the loss distribution technique based on hyperbolic rotation of the coupling matrix.

Consider the 4-pole Chebyshev filter as an example, with a 22 return loss. The lossless coupling matrix can be calculated using the multi-coupled sequential network explained in section 3.2.1 or the transversal array model in section 3.2.2, followed by the similarity transform, as below.

Table 3.12. Lossless coupling matrix of 4-pole Chebyshev filter with RL=22 dB.

	S	1	2	3	4	L
S	0	1.0822	0	0	0	0
1	1.0822	0	0.95999	0	0	0
2	0	0.95999	0	0.72676	0	0
3	0	0	0.72676	0	0.95999	0
4	0	0	0	0.95999	0	1.0822
L	0	0	0	0	1.0822	0

Figure 3.17. Lossless 4-pole Chebyshev filter response.

Simulating the circuit model in ADS software based on the coupling matrix will give the same results as the MATLAB results in Figure 3.17.

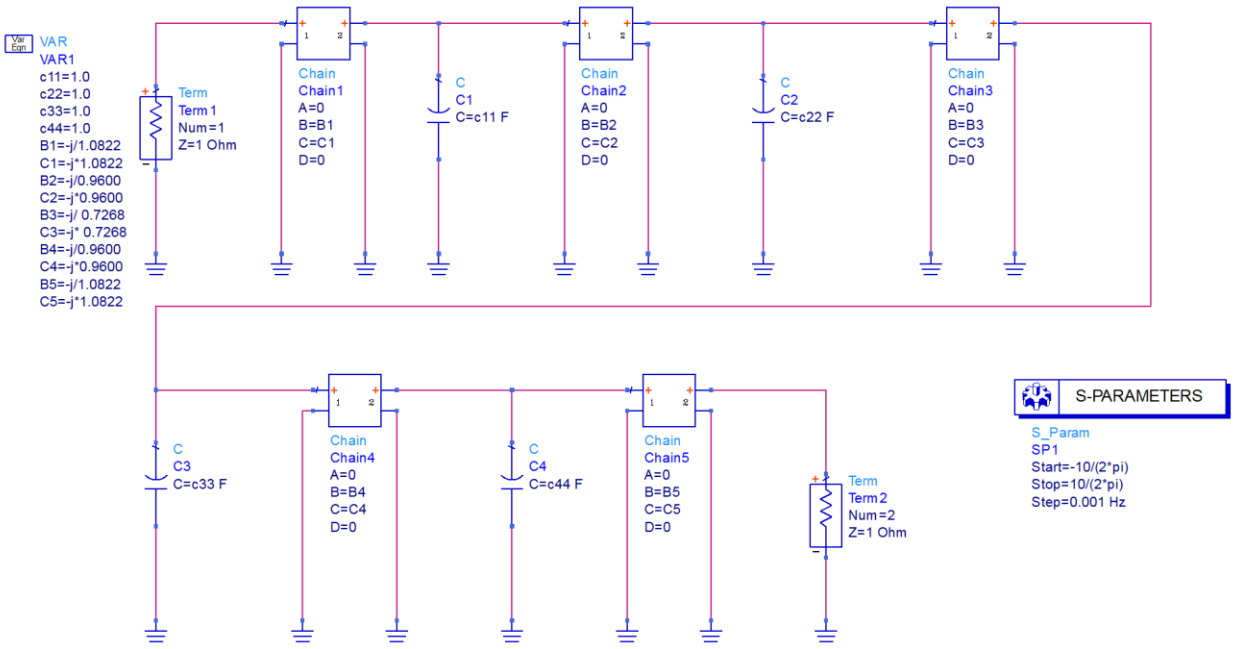

Figure 3.18. Lossless circuit model of a 4-pole Chebyshev filter.

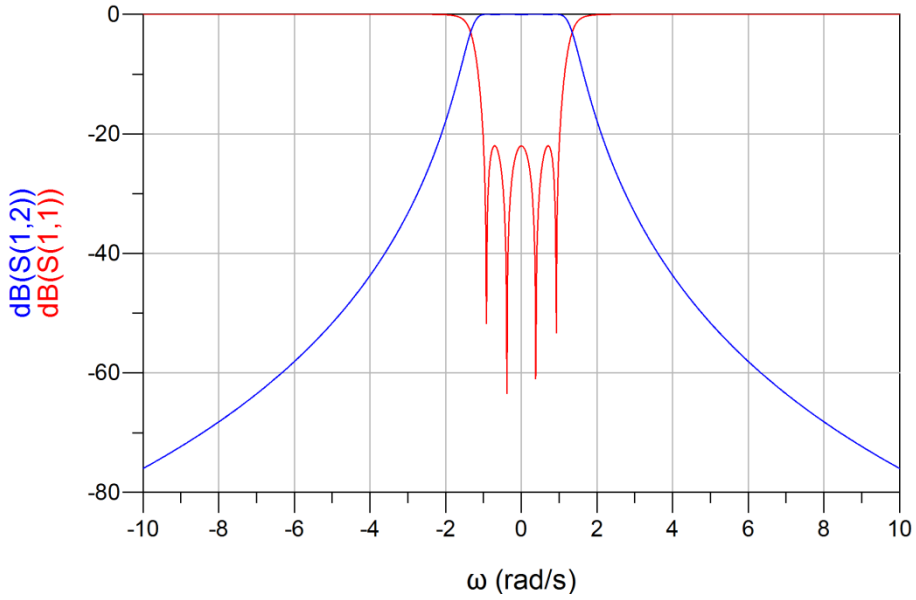

Figure 3.19. ADS simulation result of a lossless 4-pole Chebyshev filter.

Based on the relation between the *dissipation factor* and the Q factor of a filter, which is discussed in detail in [35], one can find the amount of loss to insert in an ideal infinity Q resonator of the lowpass prototype filter.

$$\delta = \frac{f_0}{\Delta f \times Q} = \frac{1}{FBW \times Q}$$

$$\delta = \frac{G}{C_k}, k = 1,2,3,\dots,N \qquad (3.26)$$

where δ is the dissipation factor of a lowpass prototype filter, C_k is the kth capacitive element of the prototype filter, G is the conductance value, and FBW is the fractional bandwidth. Since, in prototype filter, $C_k = 1$, then $\delta = G$.

The value of the loss (G) calculated based on Eq.(3.26), such that all the resonators will all have the same Q factor of 400 and *FBW*=1% as a typical example. Consequently, filter frequency response (i.e., S_{21}) would have band edge roundness and degraded insertion loss, as illustrated in Figure 3.21, and the insertion loss would degrade to -4.7 dB at the center frequency.

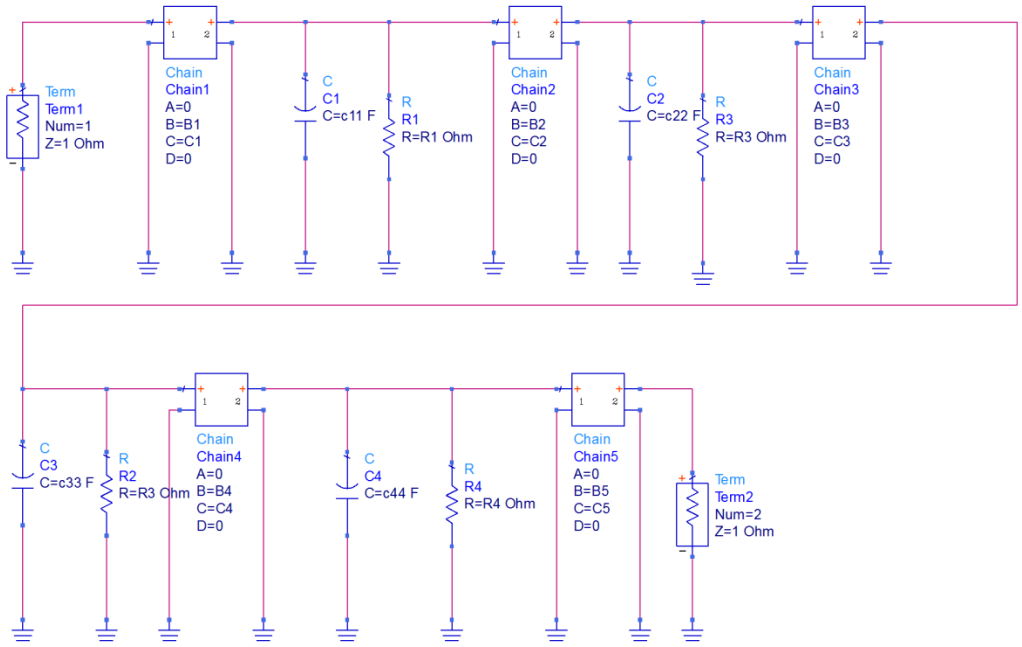

Figure 3.20. Q=400 Chebyshev prototype circuit model.

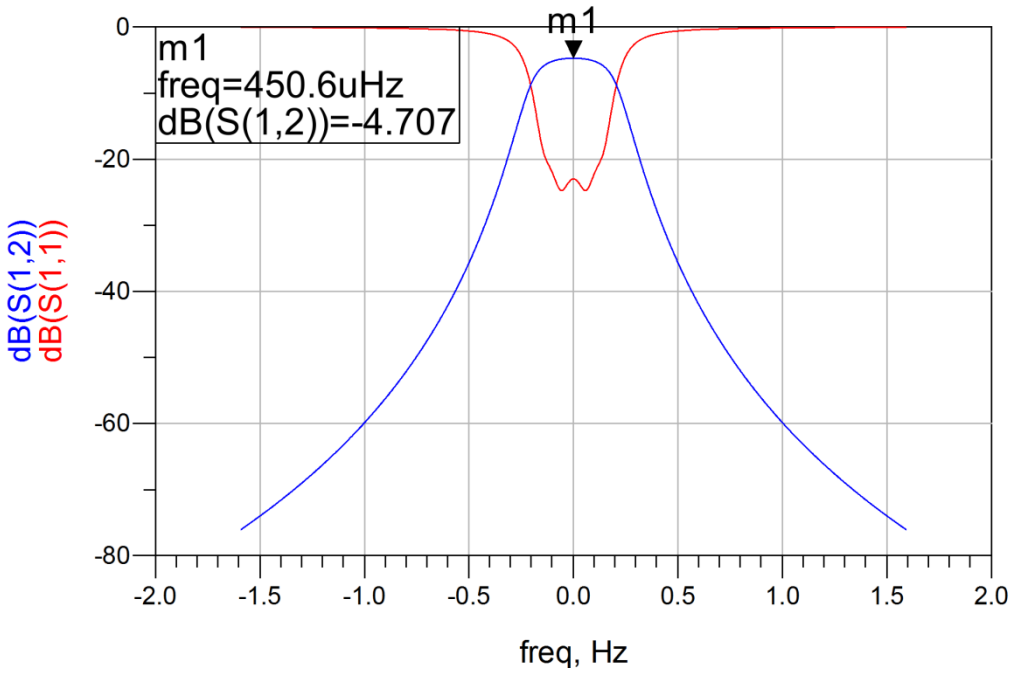

Figure 3.21. S-par simulation results of 4-pole Chebyshev filter with Q=400

We will now investigate the effect of lossy design with the same actual Q factor of 400 on improving the frequency response (S_{21}) shape of the filter. This improvement results in an increment in loss and shifting the S_{21} and $S_{11}$with a certain amount of loss, a typical value of 10 dB as designed. The *N*+2 lossy coupling matrix above, after rotation, is as follows:

Table 3.13. The *N*+2 lossy coupling matrix.

	S	1	2	3	4	L
S	- *j*0.5195	0.9247	0	0	0	0
1	0.9247	- *j*0.6084	0.95999	0	0	0
2	0	0.95999	0	0.72676	0	0
3	0	0	0.72676	0	0.95999	0
4	0	0	0	0.95999	- *j*0.6084	0.9247
L	0	0	0	0	0.9247	- *j*0.5195

Table 3.14 *N*+4 coupling matrix

	S	1	2	3	4	5	6	L
S	0	0.31987	0	0	0	0	0	0
1	0.31987	- *j*0.05315	-0.30052	*j*0.053154	0	0	0	0
2	0	-0.30052	-*j*0.37743	0.91092	*j*0.1327	-0.02347	0	0
3	0	*j*0.05315	0.91092	- *j*0.43092	0.75023	*j*0.1327	0	0
4	0	0	*j*0.1327	0.75023	- *j*0.4309	0.91092	*j*0.05315	0
5	0	0	-0.02347	*j*0.1327	0.91092	- *j*0.37743	-0.30052	0
6	0	0	0	0	*j*0.05315	-0.30052	- *j*0.05315	0.31987
L	0	0	0	0	0	0	0.31987	0

The Q factor of the resonators after rotation would be $Q_1 = Q_4 = 164.3779$ and $Q_2 = Q_3 = \text{Inf}$. The equivalent Q factor (or in other words, the target Q factor in this example) is chosen to be 1000. This means that the lossy filter response would be shifted by 10 dB, but the shape of the response (i.e., the selectivity and flatness in the passband) would be the same as a lossless filter with Q factor of 1000. After applying the loss distribution procedure on pivot [1, 2] with the rotation angle of -0.17876 rad and on pivot [3, 4] with rotation angle of 0.17876 rad and finally scaling the source and load node by the factor of 0.31987, the new N+4 coupling matrix with the equivalent Q of 1000 is shown in Table 3.14.

The scaling force is used to add two extra nodes to the coupling matrix and therefore would become $N+4$ coupling matrix. However, by using this technique, two shunt resistors are eliminated in the two non-resonating nodes.

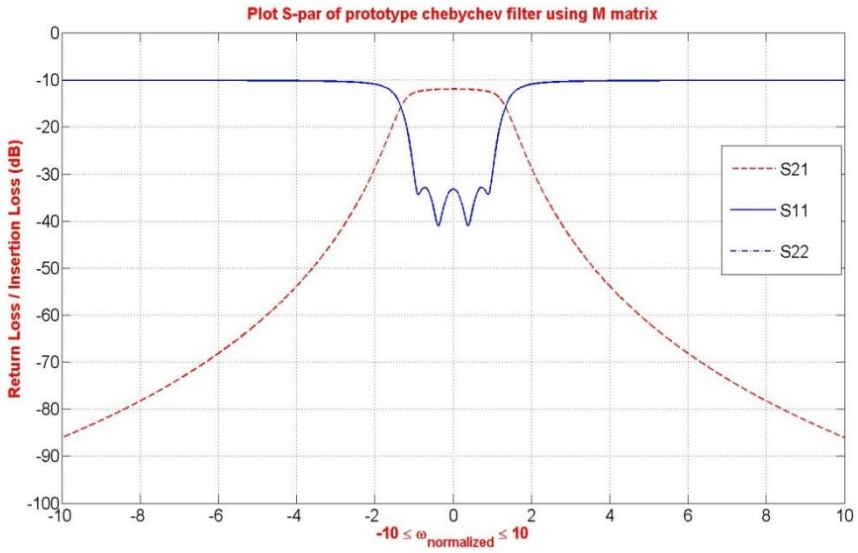

Figure 3.22. MATLAB plot of a 4-pole lossy Chebyshev filter.

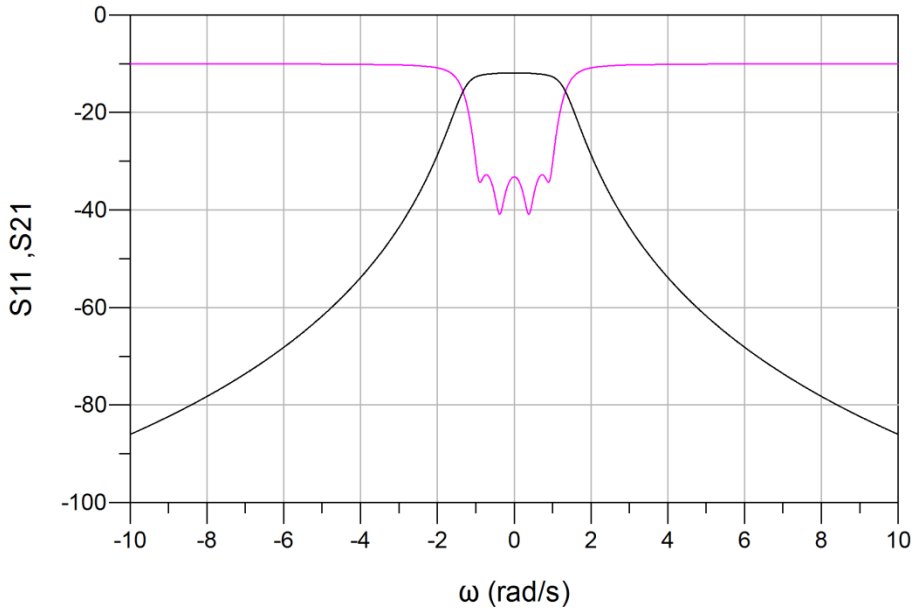

Figure 3.23 ADS plot of a 4-pole lossy Chebyshev filter.

To get a better sense of the relation between the actual (physical) Q factor and the equivalent Q factor, a study was carried out for the above example with the target Q of 1000 and different FBW values with respect to different values of loss level. The results are shown below.

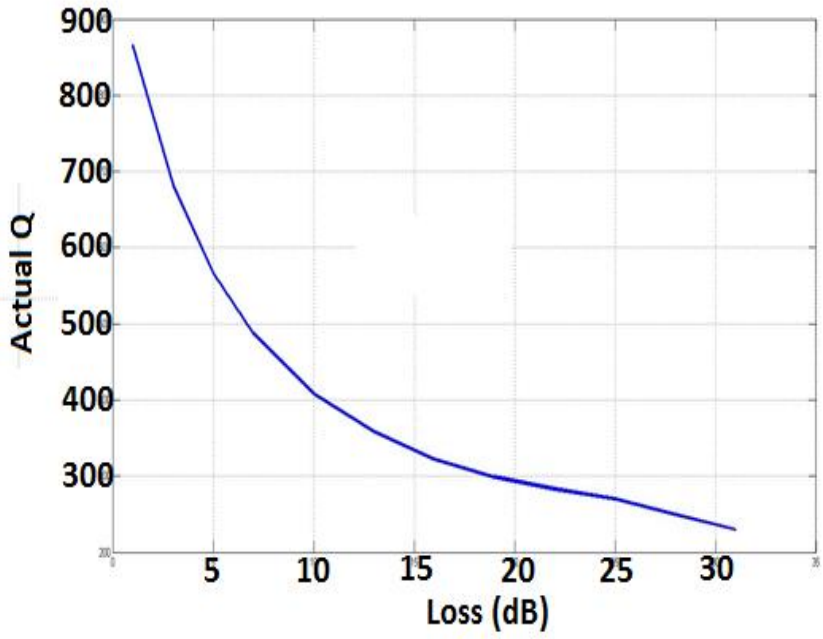

Figure 3.24. Actual Q vs. loss level, equivalent Q=1000, FBW =1%.

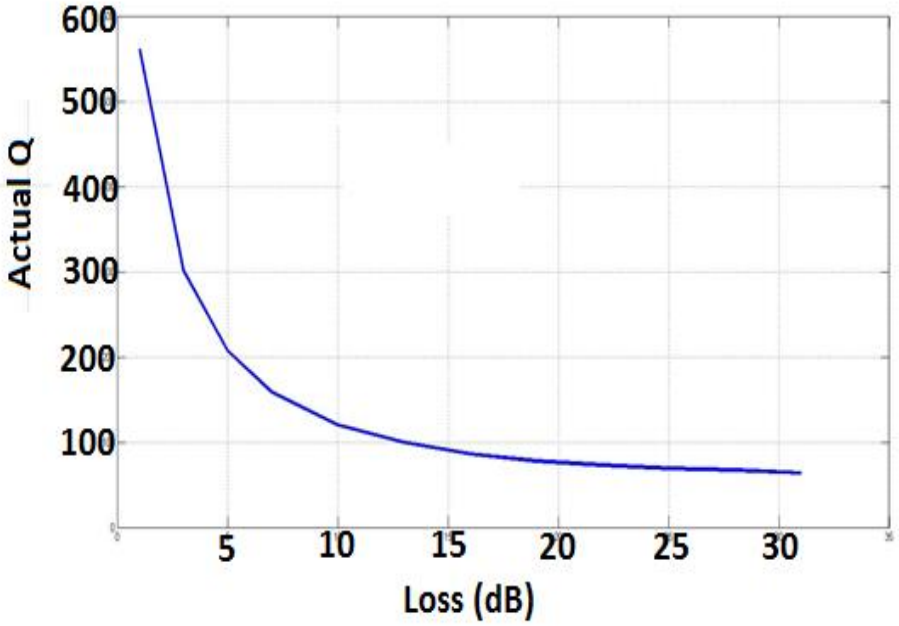

Figure 3.25. Actual Q vs. loss level, equivalent Q=1000, FBW =5%.

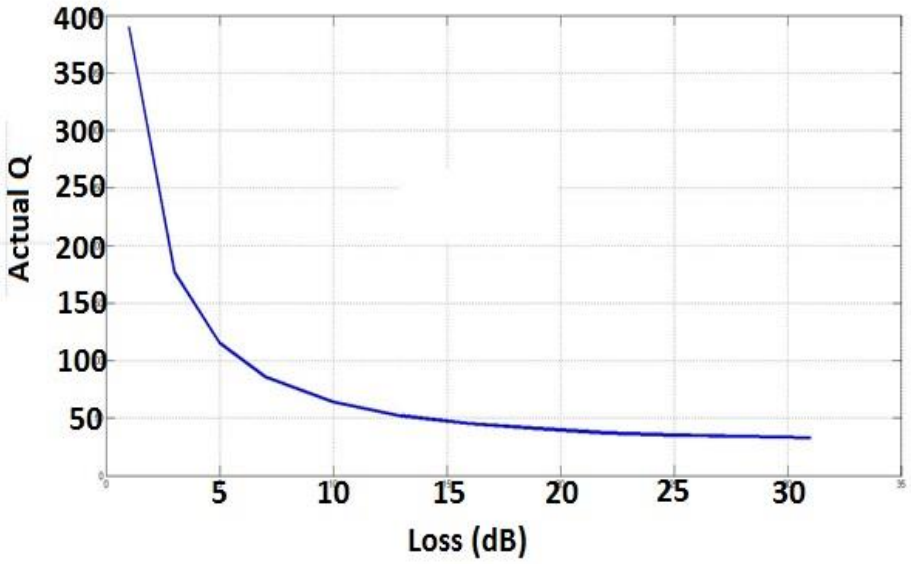

Figure 3.26. Actual Q vs. loss level, equivalent Q=1000, FBW =10%.

3.4 Predistorted Filter

3.4.1 Concept and Formulation

As discussed previously, a low Q factor would affect the band-edge's sharpness and degrade insertion loss. One method to compensate for band-edge roundness is to use a predistortion technique, which was first developed in 1939 [1] by Darlington and then further developed by others on all pole filters [3] [4] and multi-coupled cavity filters [5]. The principle of operation is to design a low-pass prototype filter that has a peaky response near the passband edges. Since loss attenuates the passband edges more than the center of the passband, by adding the sufficient loss (low Q effect), a flattened bandpass response would be recovered. The design of a peaky edge response is obtained by shifting the poles of the transfer function polynomial E(s) of the low-pass prototype filter towards the right-half plane of a complex *s*-plane.

The technique is based on shifting the poles of the polynomial *E*(s) by r, $s ==> s - r$. It should be noted that the poles cannot be shifted out of the left-half of the *s*-plane in order to preserve the Hurwitz condition, because

$$S_{11} = \frac{F'(s)/_{\epsilon'_R}}{E(s-r)}, \quad S_{22} = \frac{F'_{22}(s)/_{\epsilon'_R}}{E(s-r)}, \quad S_{21} = S_{12} = \frac{P(s)/_{\epsilon'}}{E(s-r)}$$

$$r = \frac{f_0}{\Delta f}\left(\frac{1}{Q_u} - \frac{1}{Q_{eq}}\right) \tag{3.27}$$

The procedure of predistortion design can be summarized as follows [35]:

- Deriving the lossless prototype filter polynomials F(s), P(s), and F(s).
- Obtaining the amount of loss factor r (shifting value) from Eq. (3.27).
- Shifting the position of the poles (roots of E(s)) by the amount of r, noting that the Hurwitz condition is not violated.
- Calculating the new values for ε and ϵ_r using the original $P(s)$ polynomial such that $|S_{11}(s)|$ and $|S_{21}(s)| \leq 1$ at any value of frequency variable *s*, thereby ensuring a feasible passive network.
- Recalculating the $F_{22}(s)$ and $F(s)$ polynomials using the conservation of energy equation; $S_{11}S_{11}^* + S_{21}S_{21}^* = 1$

In step 5, a choice can be made in selecting the reflection zeros. If total left- or right-half plane zeros are chosen, an asymmetric, synchronously tuned (meaning there would be no non-zero imaginary parts in the admittances [no FIR elements]) coupling matrix will be realized. If a combination of left- and light-half plane zeros is chosen, the couplings and resistances will be symmetrical. However, in this latter instance, the FIR elements would make the filter asynchronous tuned. Hence, the resonators would have to be re-tuned to compensate for the frequency shift.

Although the predistortion method improves the insertion loss response and recovers passband flatness, changes in reflection zero positions would drastically degrade the return loss. Therefore, pole predistortion is limited to those applications where minimum insertion and maximum return loss are not required and flatness of insertion loss is of the utmost importance.

3.4.2 Illustrative Example

Consider a 4-pole elliptic filter with return loss of 22dB and transmission zeros on -*j*2 and +*j*2. The lossless polynomials of the filter function would be as calculated below, based on a recursive technique, as follows:

Table 3.15. Lossless polynomials coefficients and roots.

roots of E(s)	-0.87929 -*j*0.61997	-0.26177 +*j*1.222	-0.26177 -*j*1.222	-0.87929 +*j*0.6199	ε= 2.2197
roots of F(s)	-*j*0.9333	*j*0.9333	-*j*0.40602	*j*0.40602	ε_r=1
Roots of P(s)	*j*2	-j2	-	-	
n=	4	3	2	1	0
Coefficients of F(s)	1	0	1.0359	0	0.14359
Coefficients of E(s)	1	2.2821	3.64	3.3525	1.8077
Coefficients of P(s)	-	-	1	0	4

The unloaded Q and its equivalent are chosen to be 1000 Q and 5000, respectively. Based on an FBW equal to 1%, the shifting value r can be calculated using Eq. (3.27) as $r = \frac{f_0}{\Delta f}\left(\frac{1}{Q_u} - \frac{1}{Q_{eq}}\right) =$

0.1000. Moreover, a new value of ε = 3.4899. Shifted roots of E(s) along with the original roots of E(s) are shown in Figure 3.27.

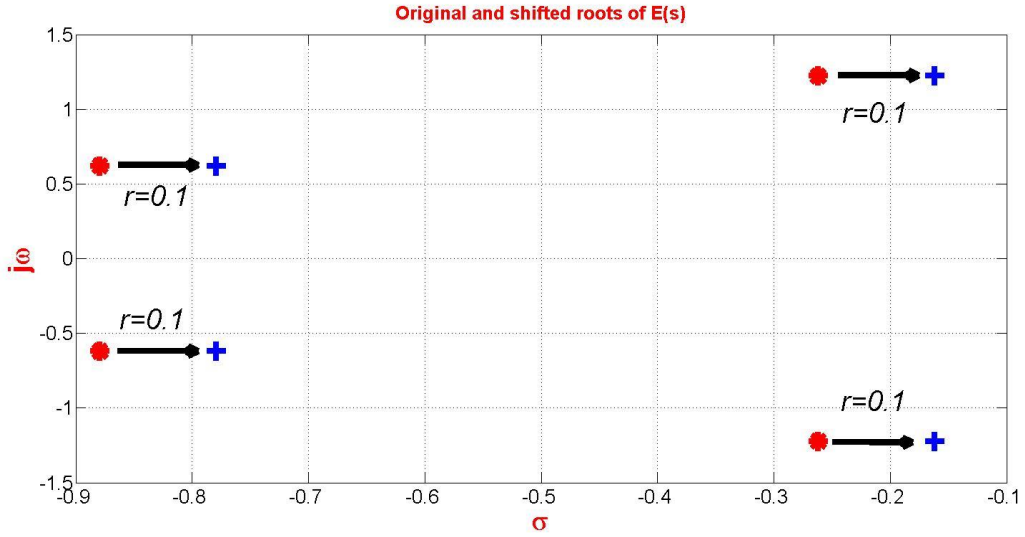

roots of E(s)	-0.77929-j0.61997	-0.16177+j1.222	-0.16177-j1.222	-0.77929+j0.6199	ε= 3.4899

Figure 3.27. Original and shifted roots of polynomial E(s) towards the right-half *s*-plane.

The new roots of $F(s)$ are calculated and illustrated in Figure 3.28,

New roots of F(s)	- j1.1477
	- j1.1476
	0.6386 - j0.5786
	-0.6386 - j0.5786
	-0.6386 + j0.5786
	0.6386 + j0.5786
	+ j1.1477
	+ j1.1476

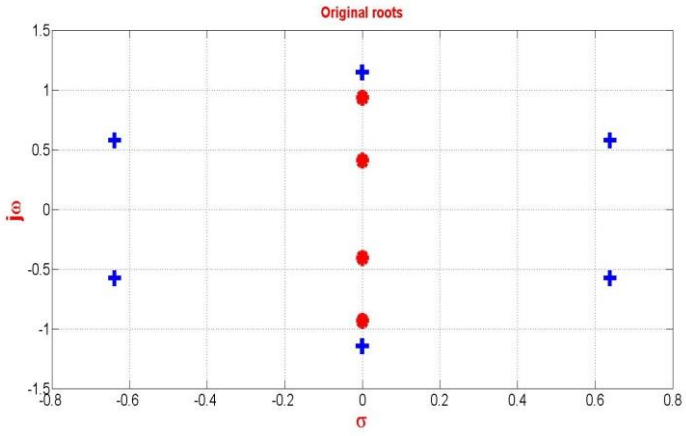

Figure 3.28. New roots of F(s) polynomial.

The predistorted s-parameter plot is below.

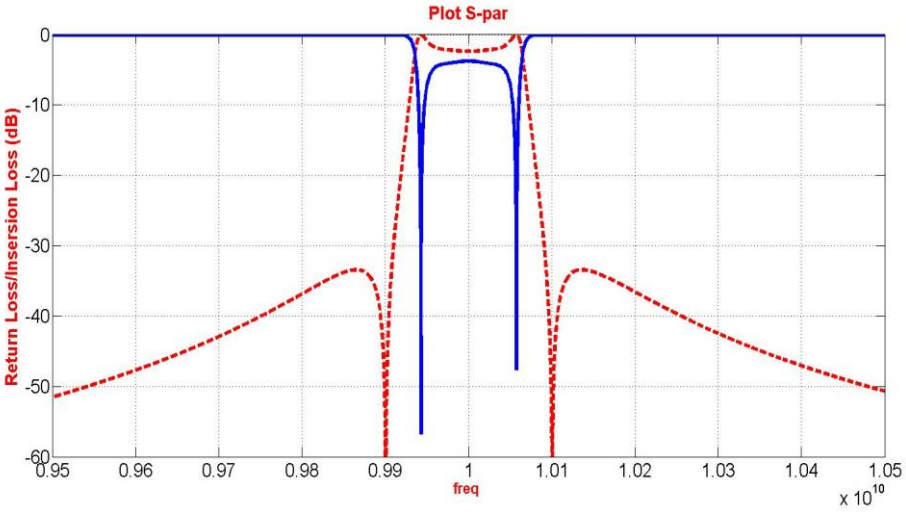

Figure 3.29. Predistorted filter frequency response (MATLAB simulation).

After adding the loss in the resonators with an equivalent Q of 1000, S_{21} would be flattend in the passband, as follows:

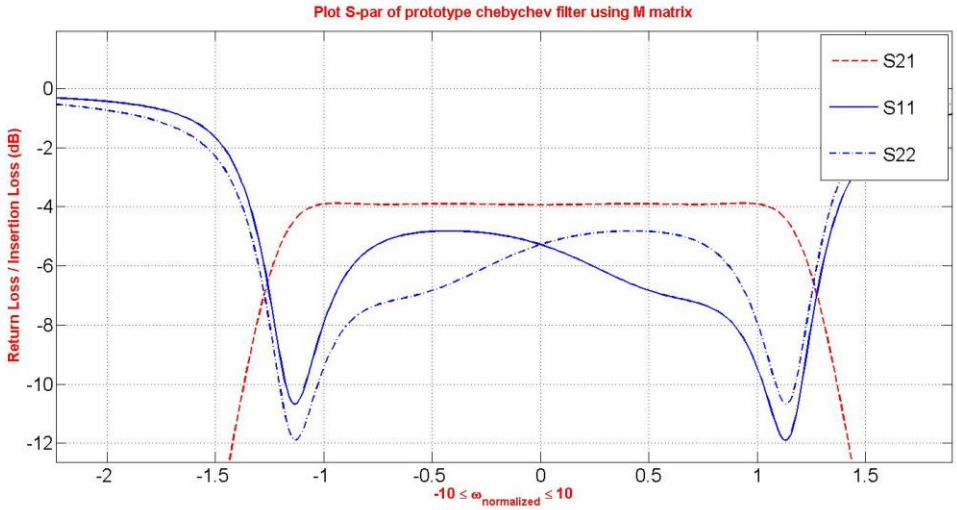

Figure 3.30. Predistorted filter frequency response after adding Q=1000 (MATLAB simulation).

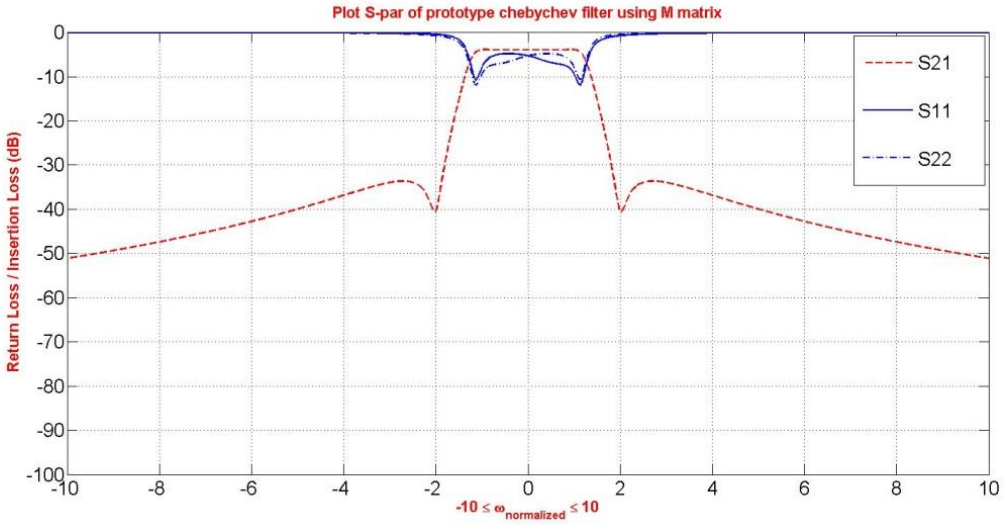

Figure 3.31. Predistorted filter frequency response after adding Q=1000 (MATLAB simulation).

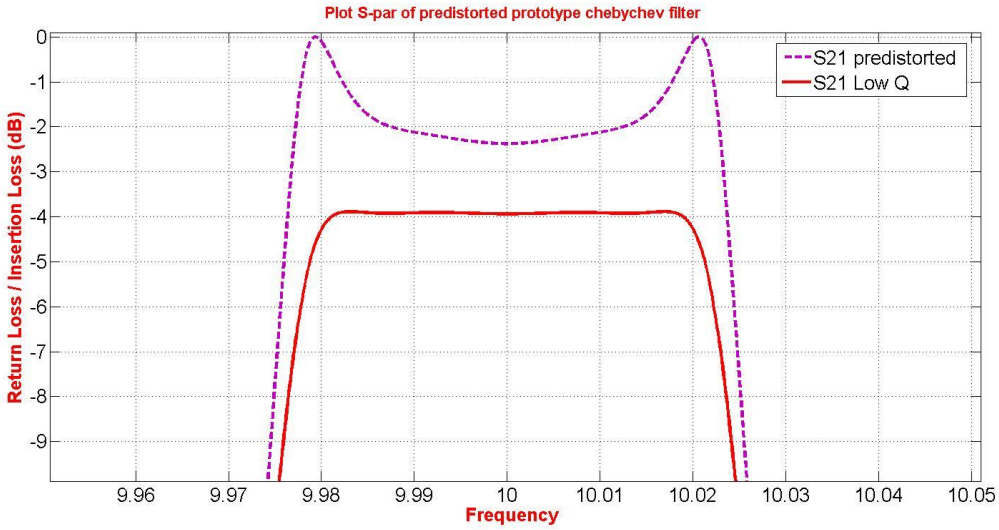

Figure 3.32 Predistorted filter frequency response after adding Q=1000 vs. before adding Q=1000 (MATLAB simulation).

Chapter 4

4.1 Introduction

In this chapter, lossy filter design methods are applied to the design of different lumped element lossy filters. The goal is to obtain improved frequency response with respect to conventional lumped element filters in terms of selectivity and insertion loss.

In the lossy lumped element filter design, Loss distribution among the resonators and circuit realization are two main challenging steps. In other words, the design of higher filter order filters, the more complicated in terms of loss distribution and circuit realization. In the first section of the chapter, 4-pole lossy lumped element lossy filter is simulated to verify the circuit simulation results.

In previous chapters it has been shown that the use of lossy methods improves the filter frequency response in terms of insertion loss selectivity and passband flatness however it introduces certain amount of loss (based on the design) to the whole frequency response (passband and stopband). To address this issue, in the second section of this chapter, a six-pole lumped element filter is designed and compared with an alternative design which is cascading the lower order lossy filters. This is supposed to improve the imposed loss in frequency response while retaining the selectivity compared to the conventional lumped element filters which have low quality factor.

4.2 Four-pole lossy filter

A four-pole lumped element lossy filter with an equivalent Q of 1000 and an actual Q of 100 with 4% bandwidth is targeted for design. The operating frequency is 2 GHz. These values are chosen based on Figure 27 in chapter 3. The design characteristics introduce 18dB insertion loss in addition the 0.5dB loss associated with equivalent Q of 1000 based on $\alpha \approx 20/(Q*FBW)$. The N+2 coupling matrix of the filter is calculated using the developed MATLAB code in Table 4.1.

This indicates that there are capacitive couplings of 0.23997 at the input and output, resistances in each resonator as well as resistive couplings between non-resonating node and second resonator, first and third resonator and between second and fourth resonator.

Table 4.1. Coupling matrix of the 4-pole lossy filter with 18 dB insertion loss

0	0.23997	0	0	0	0	0	0
0.2399	-0.044707i	-0.16967	+0.04470i	0	0	0	0
0	-0.16967	-0.45834i	0.84581	+0.20579i	-0.054224	0	0
0	+0.04470i	0.84581	-0.50082i	0.78099	+0.20579i	0	0
0	0	+0.20579i	0.78099	-0.50082i	0.84581	+0.04470i	0
0	0	-0.054224	+0.20579i	0.84581	-0.45834i	-0.16967	0
0	0	0	0	+0.04470i	-0.16967	-0.04470i	0.2399
0	0	0	0	0	0	0.23997	0

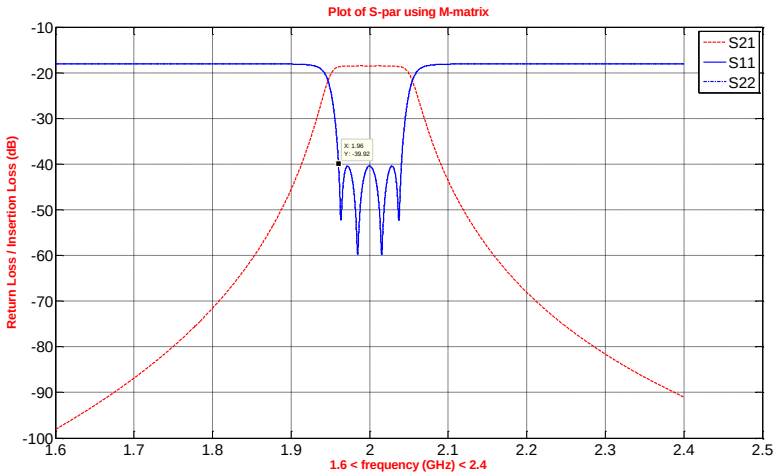

Figure 4.1. Frequency response (S-par) of lossy filter based on the coupling matrix

The initial circuit is not feasible in practice for several reasons, First of all, the input and output couplings are capacitive couplings and they introduce negative capacitors which are not feasible in lumped element model. Second of all microwave resistors come with a phase shift, which would cause the response to deviate from the designed one. Finally, it is also usually preferred to have 50 ohm transmission line at the input and output. Because of mentioned reasons, the initial circuit model based on coupling matrix must be manipulated.

This manipulation introduces two transmission lines of 180 degree and 270 degree at the input and output to the circuit model which can be reduced to one 90 degree transmission line with some circuit simplification. The circuit is simulated on Advanced Design System (ADS) using ideal coupling elements (no frequency dependence) and the scattering parameters are shown in

Figure 4.2 and Figure 4.3 respectively. Some more steps carried out towards further simplification and feasibility using lumped element capacitive coupling instead of ideal coupling. These steps and scattering parameters are indicated in following figures respectively.

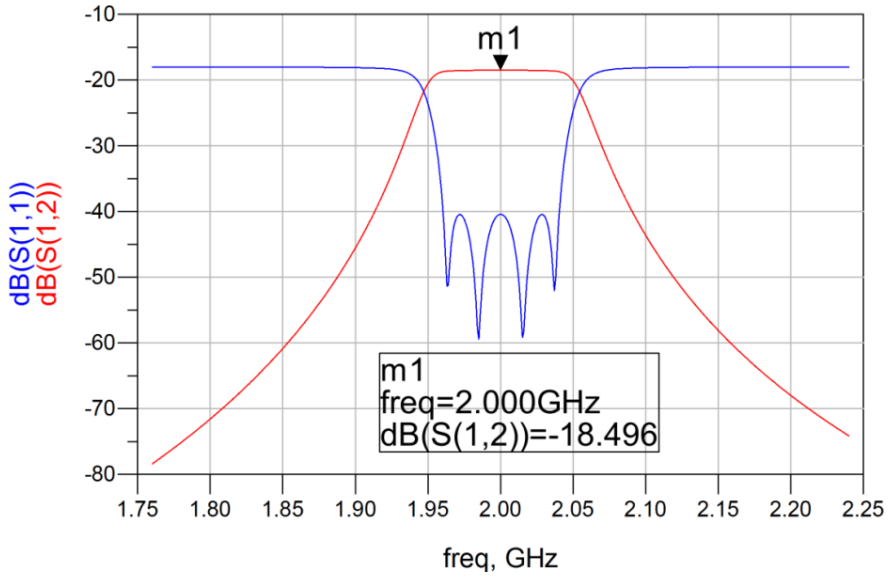

Figure 4.2. ADS simulation of S-parameters using ideal coupling elements

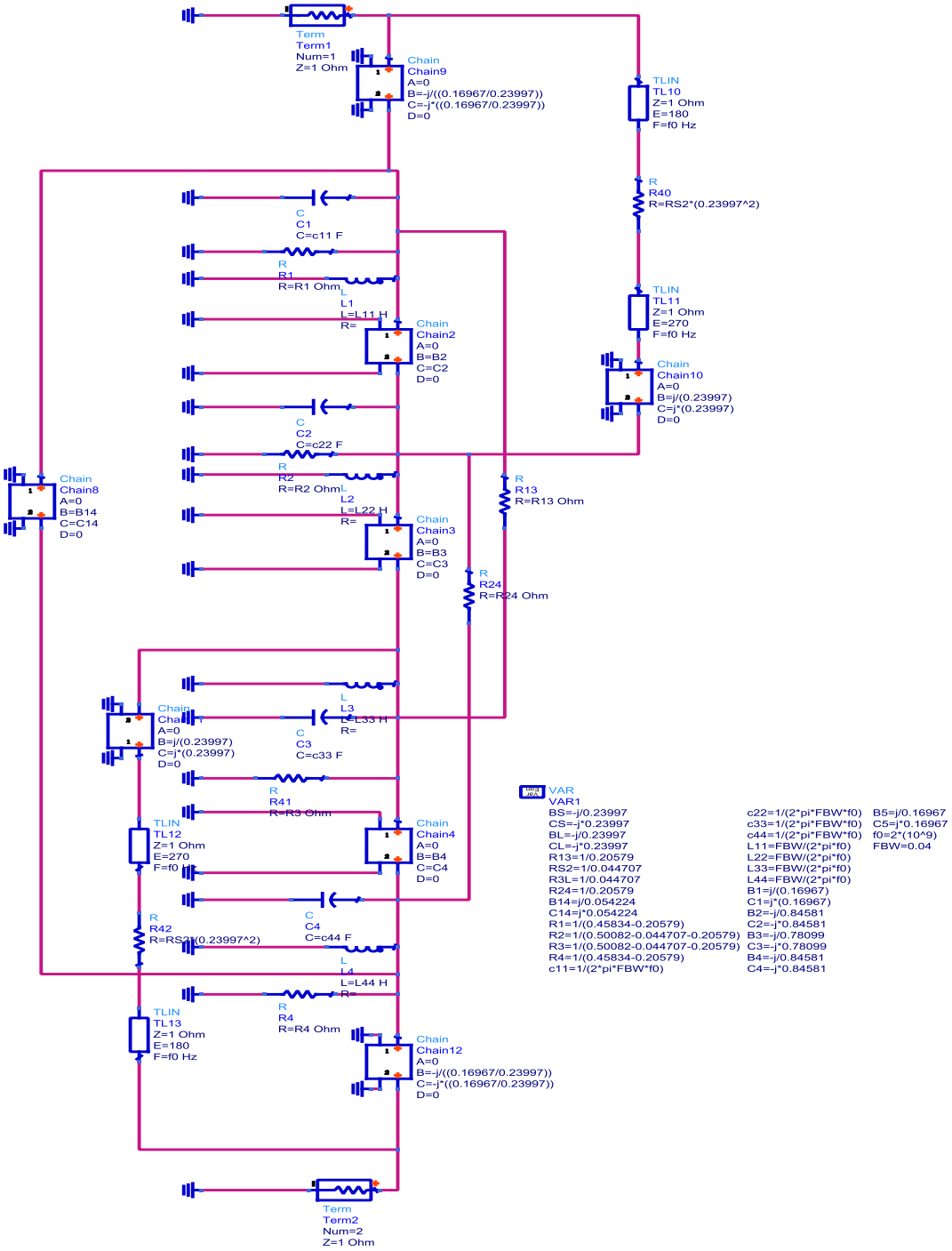

Figure 4.3 Manipulated circuit model in ADS

The frequency dependence of filter response to the circuit elements is investigated in Figure 4.4 and Figure 4.5. Figure 4.4.a shows the circuit model with actual lumped element couplings and ABCD model of transmission line, meaning there is no frequency dependence whereas Figure 4.5 shows the filter response using ABCD model coupling and actual transmission line model. Figure 4.4.b shows the feasible lumped element filter response. As it is shown, the filter response is highly affected by transmission lines rather than the frequency dependence of coupling elements. Further simulation shows that the effect of lumped element coupling is minimum compared to the transmission lines.

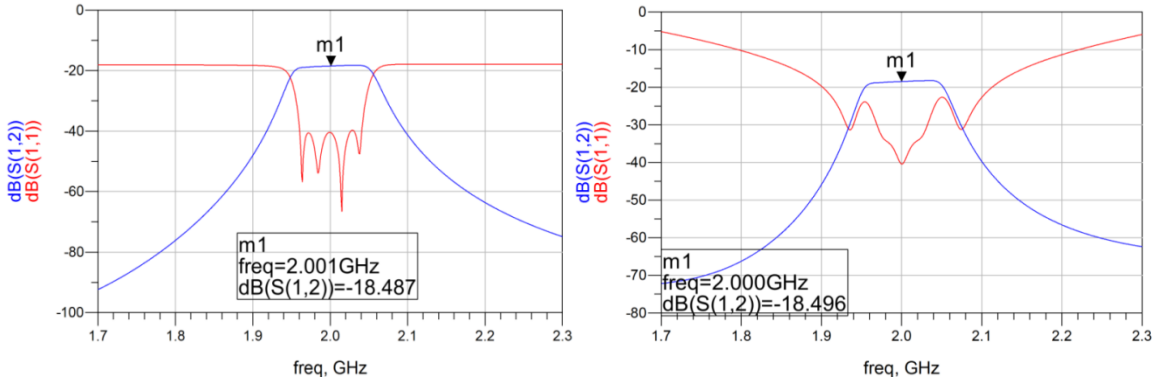

(*a*) (*b*

Figure 4.4. ***a***: Lumped element coupling and ABCD model of TL, ***b***: lumped element coupling and TL

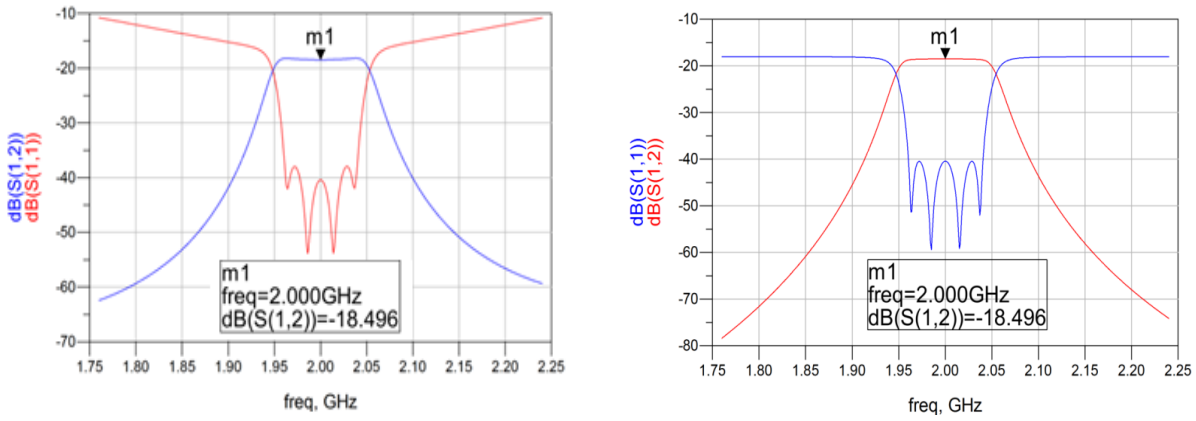

(*a*) (*b*

Figure 4.5. *a*: ABCD model coupling and TL, ***b***: ideal circuit based on ABCD model

The effect of bandwidth is also investigated on the circuit in terms of fractional bandwidth (FBW) and it is shown in Figure 4.6. The greater the bandwidth, the higher effect on the frequency response.

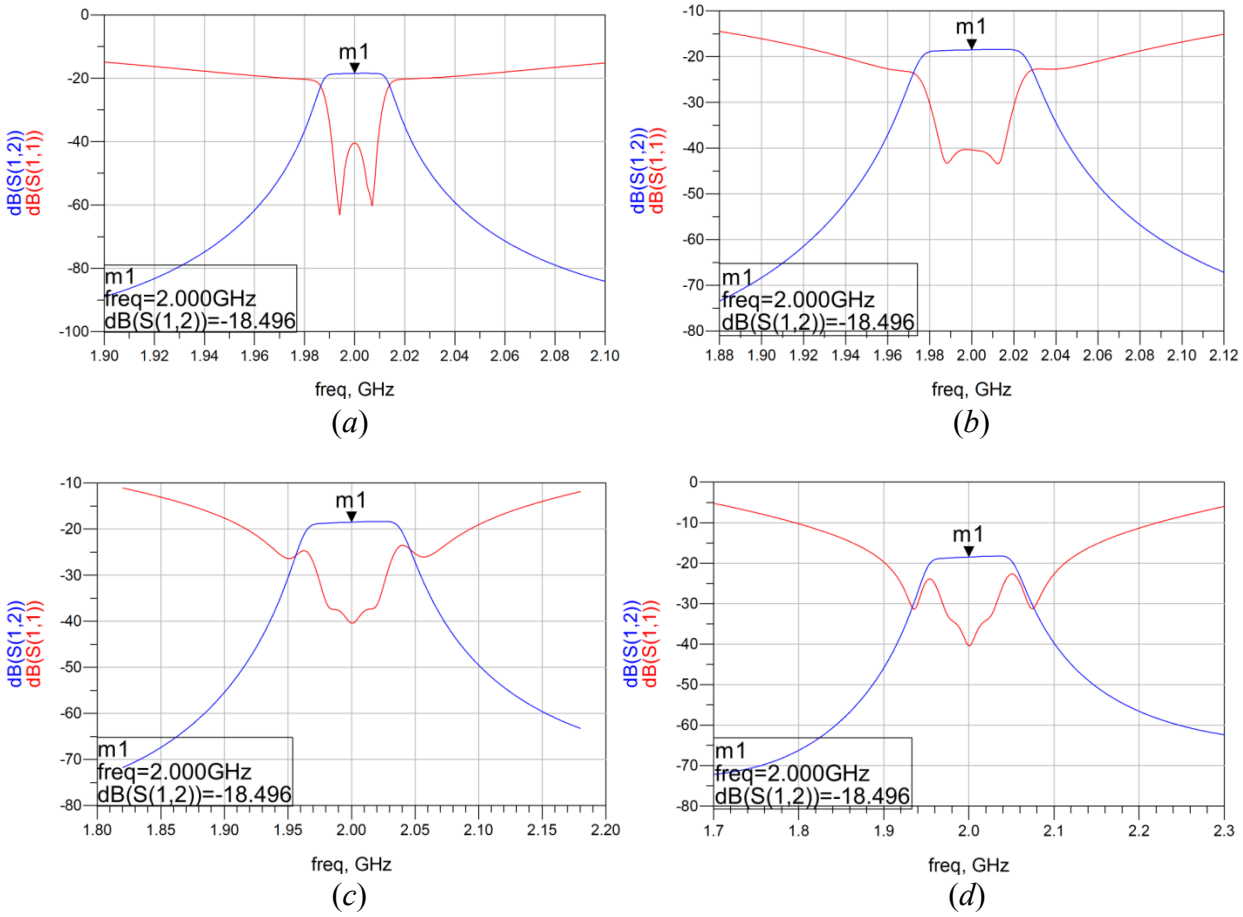

Figure 4.6. ***a***: FBW=1%, ***b***: FBW=2%, ***c***: FBW=3%, ***d***: FBW=4%

In order to address the effect of transmission line on the frequency response of the filter, a lumped lowpass filter replaced the transmission line to achieve two goals as well as retaining the transmission line characteristics which is 90 degree phase shift: one is to eliminate frequency dependence of transmission lines and the second is to reduce the filter size which is the main goal in lumped element filter design approach.

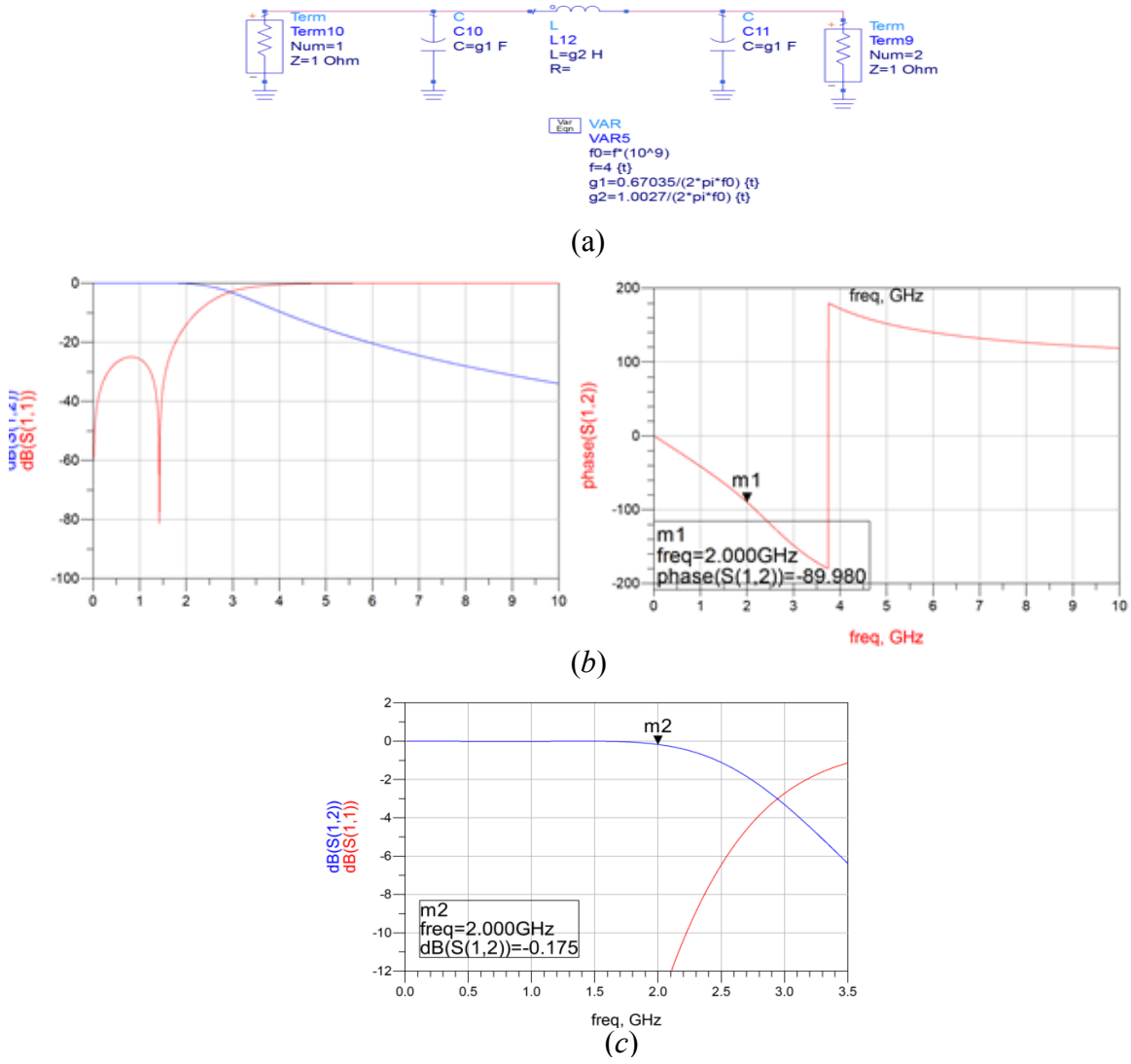

Figure 4.7. ADS simulated S-par results for low pass filter, ***a***: Circuit model, ***b***: Amplitude and phase frequency response, ***c***: zoomed-in Amplitude frequency response

Two lumped element Chebyshev lowpass filters with cut off frequency of 3GHz designed and replaced the transmission line: a five-pole and three-pole lowpass filters. In order to minimize the number of elements the three-pole filter is chosen to replace the input and output transmission lines. The g-values of lowpass prototype Chebyshev filter is g_1=6.506 and g_2= 9.7326. Figure 4.7 shows the simulated results of the lowpass filters.

Also to eliminates the negative capacitors at the input and output coupling, an alternative coupling circuit (impedance inverter) with shunt inductors is used instead of conventional three-capacitor pi network pi network. Since the filter is lumped element, it is feasible to implement shunt inductors.

The scattering parameter simulation (Figure 4.9) shows that for 4% bandwidth the phase response of the impedance inverter has about 2% deviation form ideal 90 degree phase.

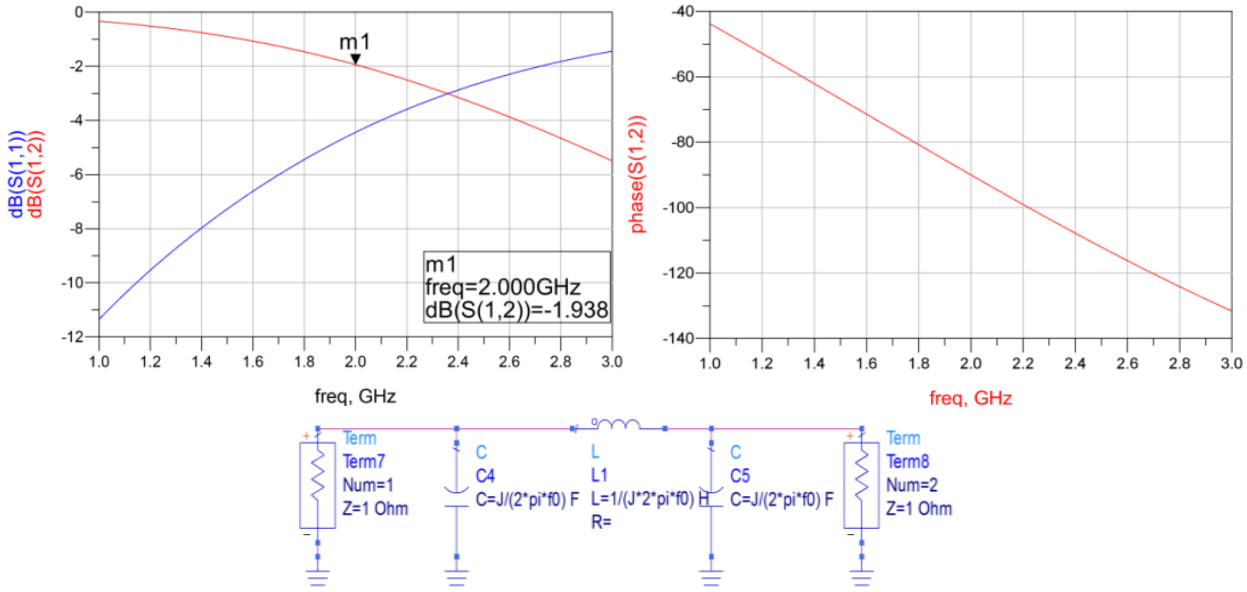

(*a*)

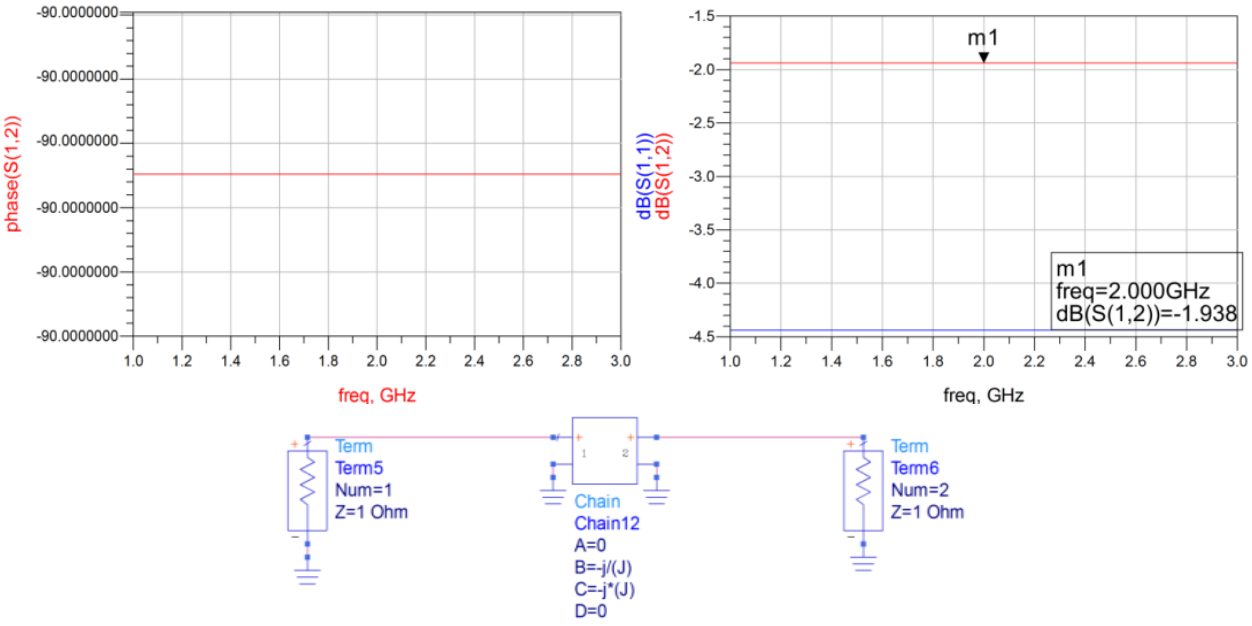

(*b*)

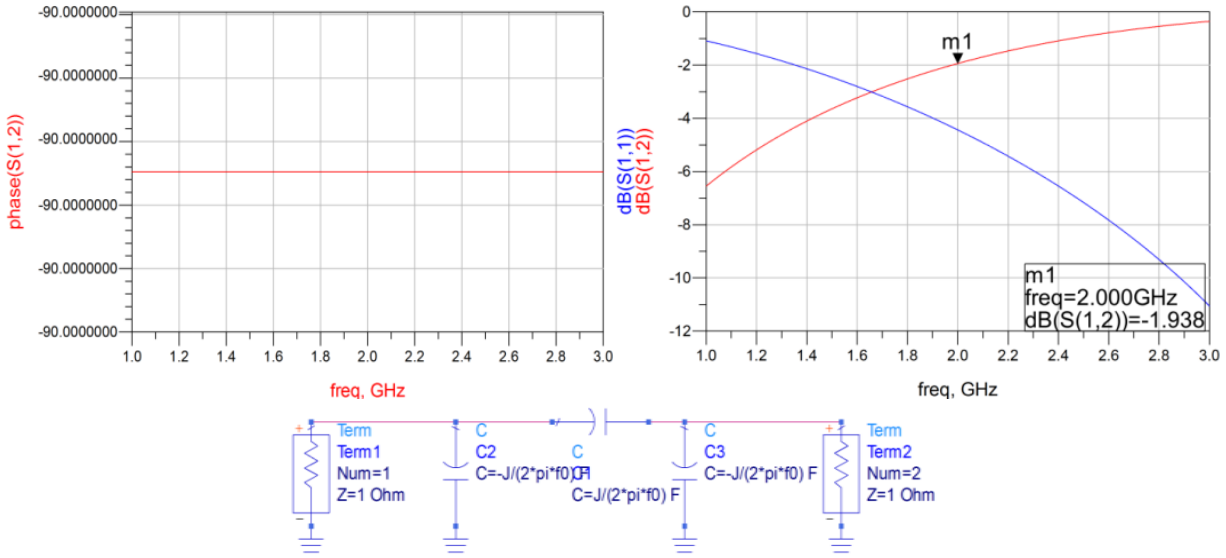

(*c*)

Figure 4.8. Circuit model and simulated S-par of *a*: Proposed inductive-capacitive impedance inverter, ***b***: ideal ABCD impedance inverter model, ***c***: Conventional capacitive impedance inverter with negative capacitor

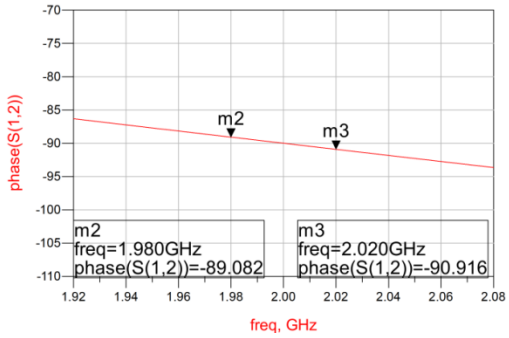

Figure 4.9. The phase characteristic of proposed pi impedance inverter circuit at 2GHz.

Using the proposed impedance inverter, the distortion for FBW of 4% is highly suppressed. Lumped element circuit model turns to be feasible with no negative element and the simulation results are as follow,

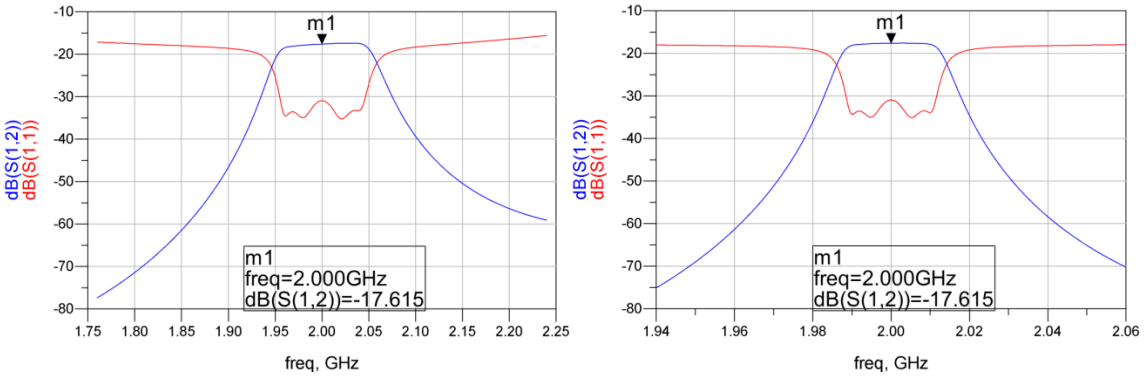

(*a*) (*b*)

Figure 4.10. Circuit model simulation of ***a***: s-parameter of 4-pole lossy filter with FBW=4%, ***b***: s-parameter of 4-pole lossy filter with FBW=1%

After tuning the inverter values, the optimized and scaled (respect to Z=50 ohm) values for circuit elements and the s-parameter of the filter are shown in Figure 4.11 respectively,

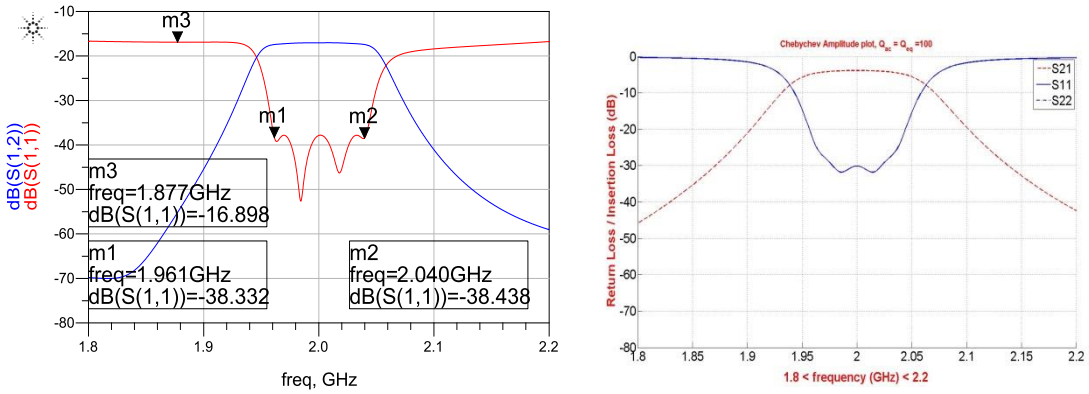

(*a*) (*a*)

Figure 4.11. ***a***) Frequency response of 4-pole lossy filter, ***b***) MATLAB simulation of 4-pole Chebyshev filter with Q=100

Table 4.2. Element values after impedance scaling to Z0=50 ohm

J_{5L}=	0.24	L_{14}=	73.378 nH	C_{R4}=	39.7 pF
J_{45}=	-0.1796	C_{S1}=	1.1912 pF	L_{R4}=	0.16 nH
J_{S0}=	0.24	L_{S1}=	5.3163 nH	R_{S2}=	64.4033 Ω
J_{01}=	-0.1796	C_{12}=	1.3382 pF	R_{24}=	242.9661 Ω
J_{12}=	0.8408	C_{23}=	1.2430 pF	R_{13}=	242.9661 Ω
J_{23}=	0.7810	C_{34}=	1.3382 pF	R_{3L}=	64.4033 Ω
J_{34}=	0.8408	C_{4L}=	1.1912 pF	R_1=	197.9806 Ω
J_{14}=	0.0542	L_{4L}=	5.3163 nH	R_2=	199.7419 Ω
C_{3L}=	0.38192 pF	C_{R1}=	39.7 pF	R_3=	199.7419 Ω
C_{S2}=	0.38192 pF	L_{R1}=	0.16 nH	R_4=	197.9806 Ω
C_{LP}(LP filter Cap)	1.3012 pF	C_{R2}=	39.7 pF		
C_{LP} - C_{S2}	0.91928 pF	L_{R2}=	0.16 nH		
L_{LP}(LP filter Ind)	4.866 nH	C_{R3}=	39.7 pF		
C_{14}=	0.0863 pF	L_{R3}=	0.16 nH		

Values of the inductors and capacitors of each resonator are out of the range to be realizable in lumped element design. To address this issue, scaling technique used to reduce the element values of resonators while retaining the frequency response in an acceptable manner. This can be realized by adding an inductor (capacitor) in series with capacitor (inductor) of a LC resonator which is illustrated in Figure 4.12.

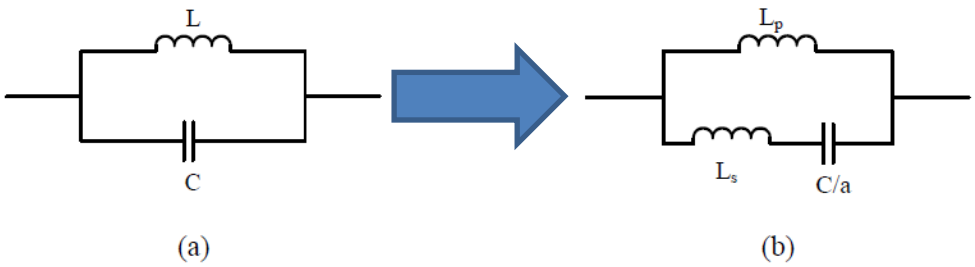

Figure 4.12. ***a***: initial resonator, ***b***: modified Resonator using scaling factor *a*

In order to have the same resonant frequency for both circuits in Figure 4.12, the following equations can be derived consequently,

$$LC = (L_s + L_p) \times \frac{C}{a}$$
$$L_p = aL - L_s \tag{4.1}$$

Assuming that $LC\omega^2 \approx 1$ at center frequency, following formulation can be derived,

$$L_s = aL\left(1 - \frac{1}{\sqrt{a}}\right)$$
$$L_p = \sqrt{a}\,L \tag{4.2}$$

Using this technique with scaling factor a=10 and after some fine tuning, the modified values of the filter would be in a realizable range which is shown in Table 4.3

Table 4.3. Modified values of the 4-pole lossy filter

J_{5L}=	0.2399	L_{14}=	38.6 nH	C_{R3}=	4 pF
J_{45}=	-0.1786	C_{S1}=	1.1845 pF	L_{SR3}=	1 nH
J_{S0}=	0.2399	L_{S1}=	5.346 nH	L_{R3}=	0.5 nH
J_{01}=	-0.1786	C_{12}=	1.3334 pF	C_{R4}=	4 pF
J_{12}=	0.8378	C_{23}=	1.2430 pF	L_{SR4}=	1 nH
J_{23}=	0.7859	C_{34}=	1.3382 pF	L_{R4}=	0.15915 nH
J_{34}=	0.8378	C_{4L}=	1.1845 pF	R_{S2}=	64.4033 Ω
J_{14}=	0.103	L_{4L}=	5.346 nH	R_{24}=	242.9661 Ω
C_{3L}=	0.38192 pF	C_{R1}=	4 pF	R_{13}=	242.9661 Ω
C_{S2}=	0.38192 pF	L_{SR1}=	1 nH	R_{3L}=	64.4033 Ω
C_{LP}(LP filter Cap)	1.3012 pF	L_{R1}=	0.5 nH	R_1=	197.9806 Ω
C_{LP} - C_{S2}	0.91928 pF	C_{R2}=	4 pF	R_2=	199.7419 Ω
L_{LP}(LP filter Ind)	4.866 nH	L_{SR21}=	1 nH	R_3=	199.7419 Ω
C_{14}=	0.164 pF	L_{R2}=	0.5 nH	R_4=	197.9806 Ω

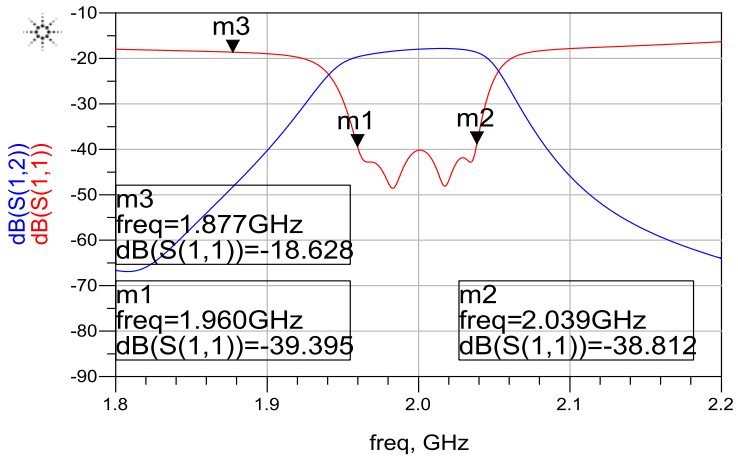

Figure 4.13. Frequency response of the tuned and reduced element circuit

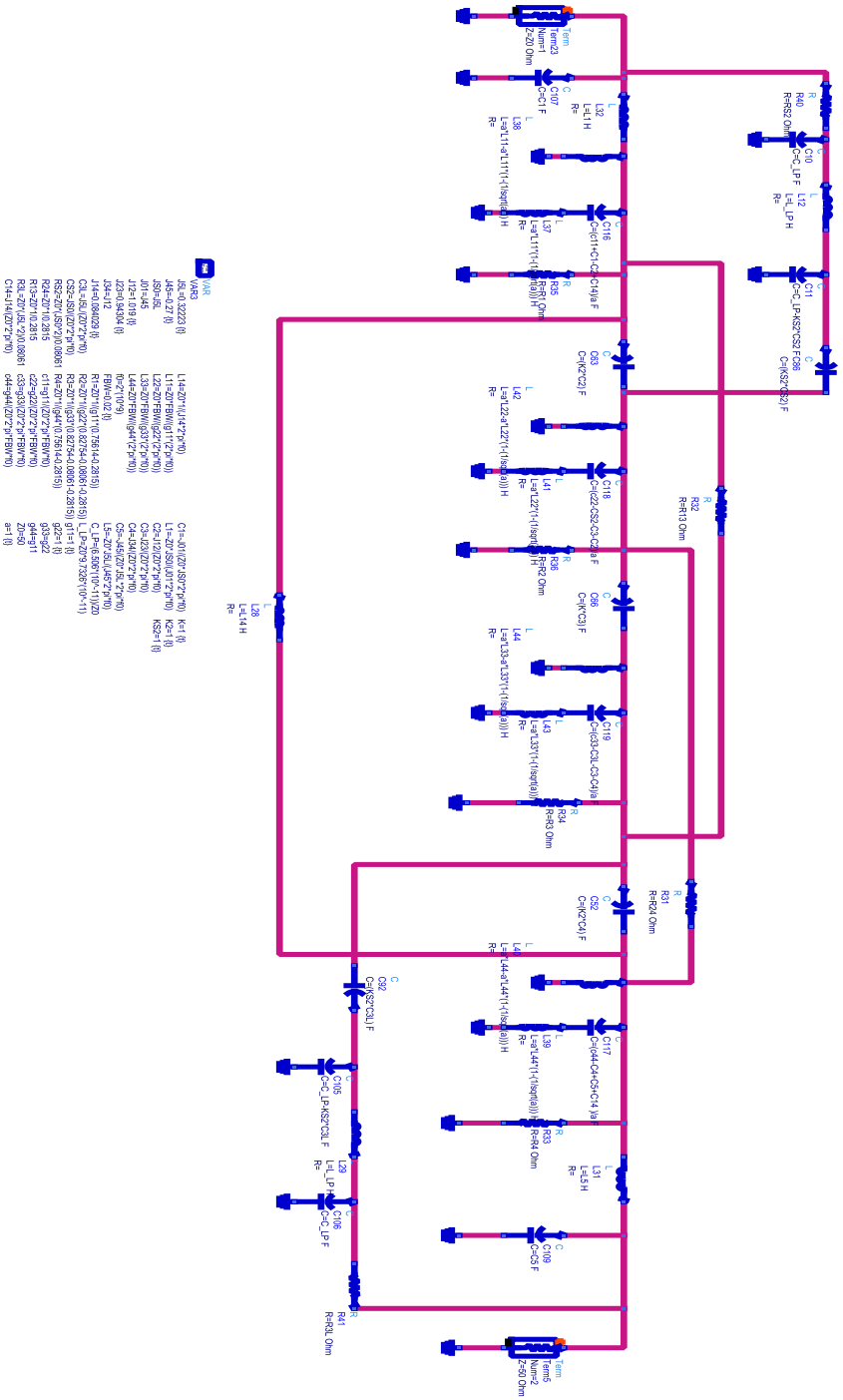

Figure 4.14. Lumped element circuit schematic of 4-pole lossy filter

4.3 Two-pole cascade lossy filters vs. six-pole ideal filter

As discussed in chapter 3, lossy filters have some advantages and disadvantages in comparison with conventional filters. In some applications that the flatness and selectivity is at the utmost importance, it is preferred to use lossy technique, however in the application that inversion loss in the stopband is important it is not reasonable to apply lossy method because it would introduce a significant amount of loss to the reflected signal.

On the other hand, designing a higher order lossy filter has a main difficulty which is equal loss distribution among the resonators. Applying hyperbolic transformation does not necessarily result in a feasible circuit because of the negative resistive coupling elements. To address this issue, we proposed a cascade configuration of three 2-pole filters consisting of two ordinary filters at the input and output and a 2-pole lossy filter in the middle. This configuration is easy to design, feasible and supposed to have better performance in terms of selectivity and flatness.

Table 4.4. Impedance Scaled values

Element	value	Element	Value
Rs=	155.279 Ohm	C12=	4.00892 pF
C11t=	32.99 pF	C23=	5.13464 pF
L11=	0.97025 nH	C34=	8.211636 pF
C22t=	27.8562 pF	C45=	5.13464 pF
L22=	0.97025 nH	C56=	4.00892 pF
C33t=	62.4417 pF	R(Q)	71.4250 Ohm
L33=	0.473675 nH	L66=	0.97025 nH
C44t=	62.4417 pF	C66t=	32.99 pF
L44=	0.473675 nH	L55=	0.97025 nH
C55t=	27.8562 pF		

3x2-pole Chebyshev filter is designed based on recursive method and the coupling matrix is extracted using transversal method. The filter is designed for center frequency of 840 MHz, FBW of 40 MHZ bandwidth (FBW=4.7%) and Q-factor of 30. The impedance scaled values of elements and circuit layout are shown in Table 4.4 and Figure 4.16 respectively.

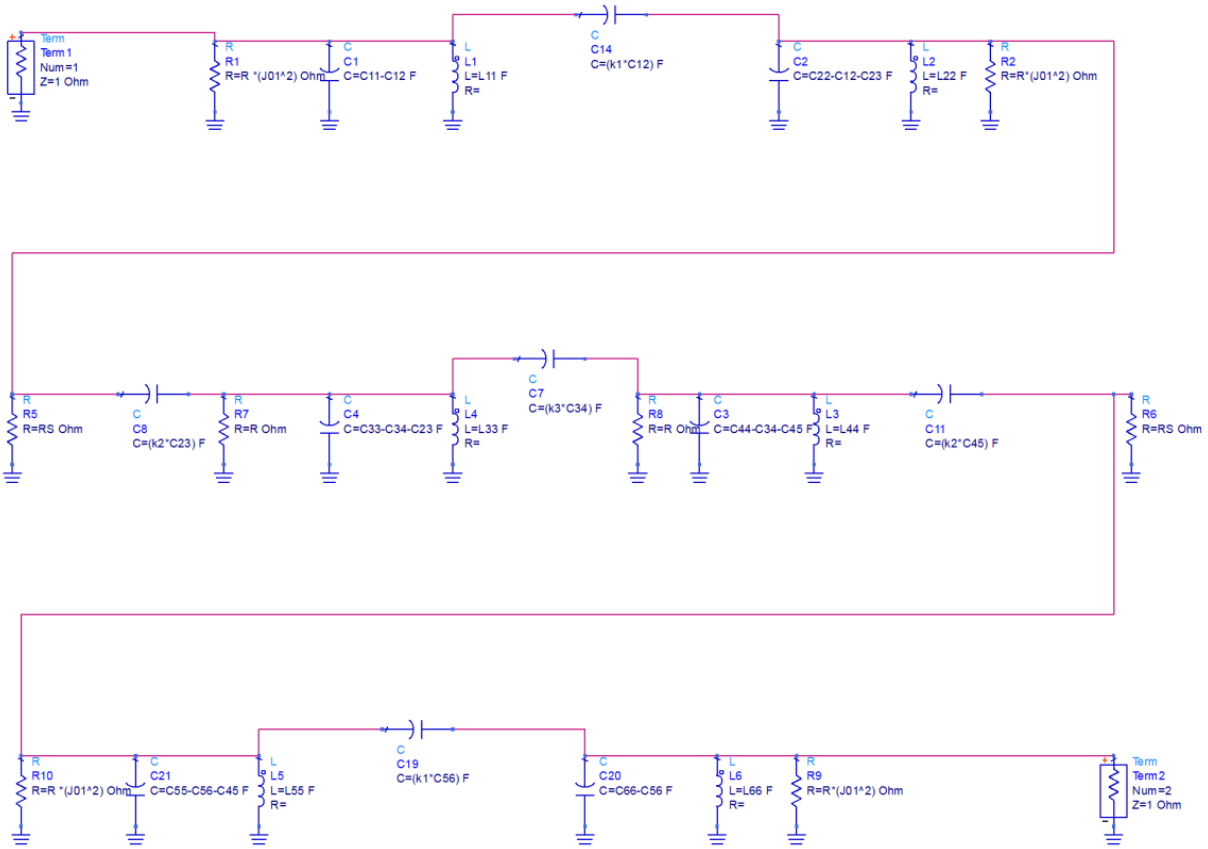

Figure 4.15. Cascaded circuit model

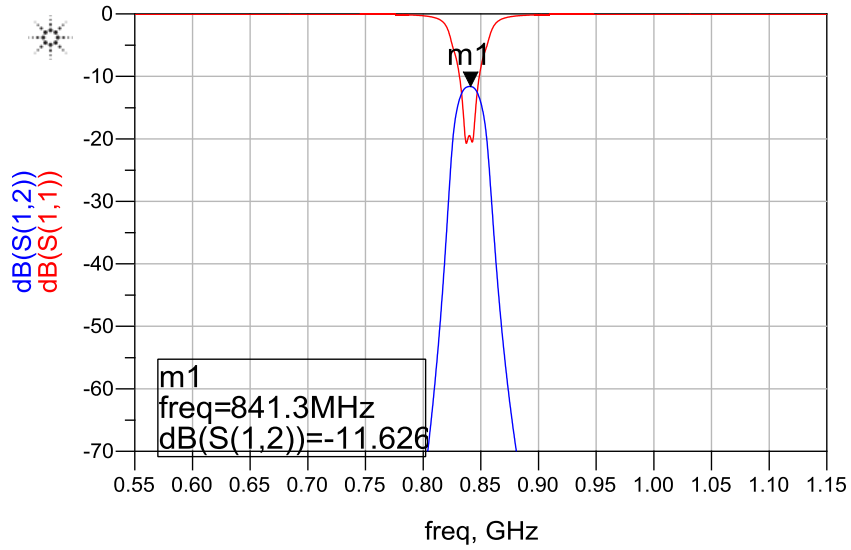

Figure 4.16. Frequency response of three 2-pole filters (ADS simulation)

The inductor and capacitor values which are shown in Table 4.4 are not in an appropriate range to implement on pcb. Meaning that capacitor values are too high and make the circuit big in size and inductor values are not high enough to be realizable by spiral model. This has been investigated by SONET EM simulation software. As an example, Figure 4.17 shows minimal achievable the spiral inductor design of Q =30 using high permittivity material which is about 1.2 nH with one round. As a matter of fact, one round spiral inductor is highly susceptible to the length of connections and loadings in the actual pcb circuit.

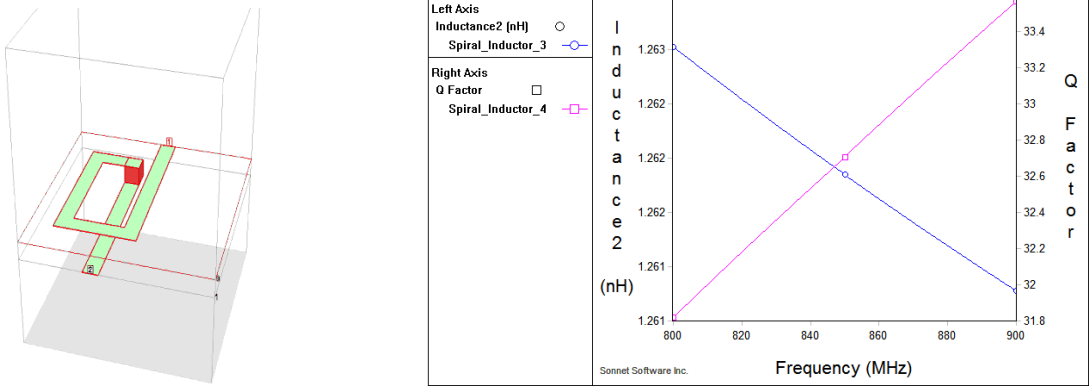

Figure 4.17. Inductance EM simulation in SONNET

Using the same technique mentioned in previous section, the L_s and L_p are multiplied by a scaling factor *a* and value of C is divided by the scaling factor of *a.* After applying the technique to the 2-pole filter, a transmission zero is introduced to the s-parameter. Figure 4.18 shows the modified circuit using scaling value of a=10.

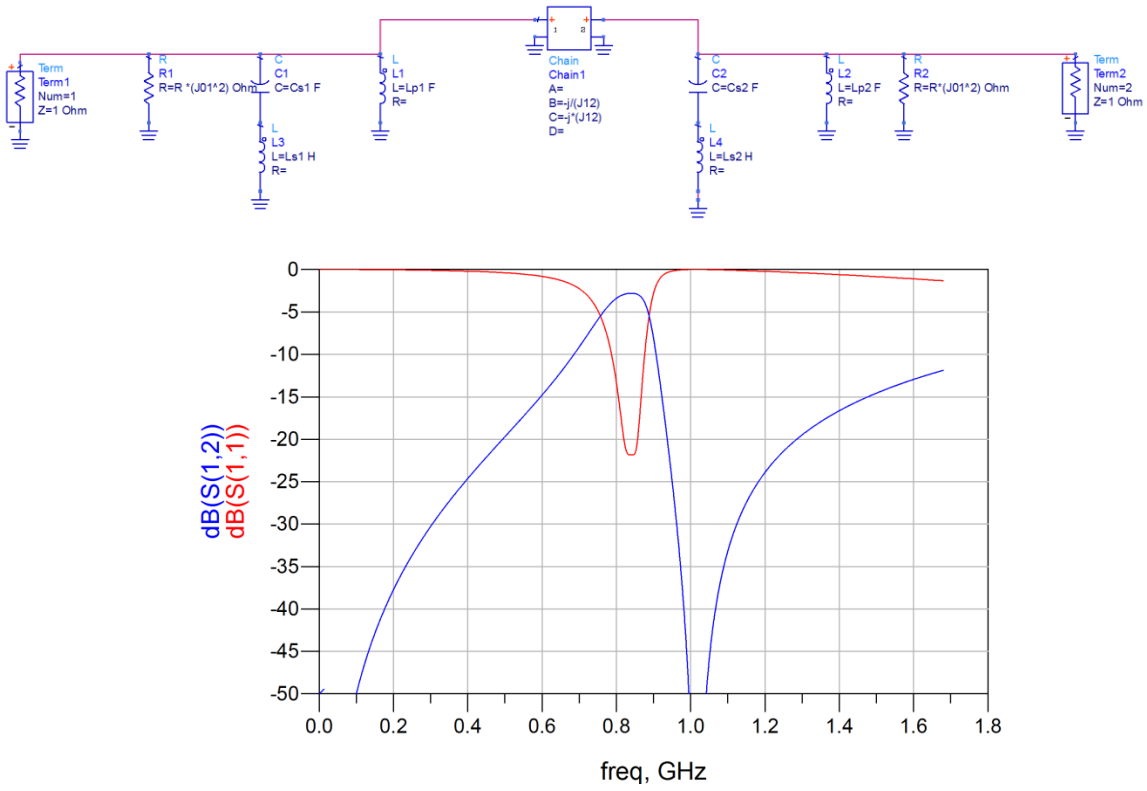

Figure 4.18. Circuit model and frequency response of the modified filter

Using actual capacitive lumped element impedance inverter instead of ideal ABCD model, a unwanted resonance around 1.5 GHz which can be eliminated using inductive impedance inverter.

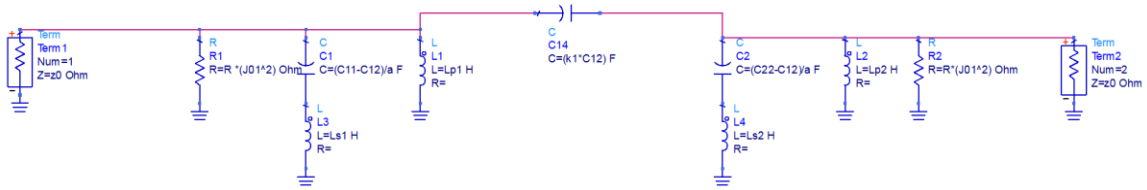

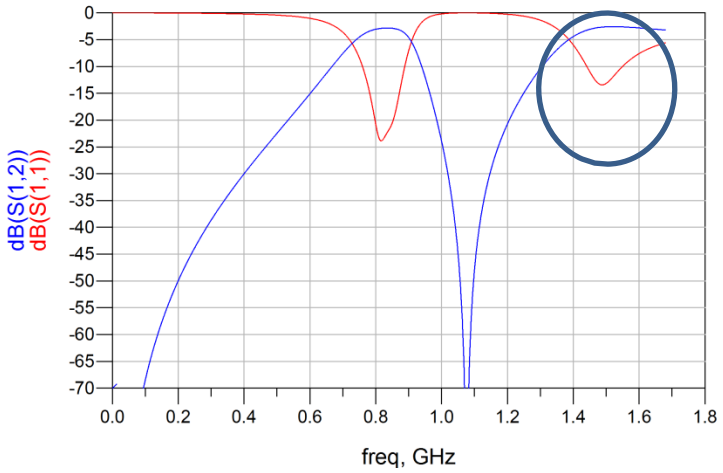

Figure 4.19. Lumped element ccircuit model (capacitive coupling) and frequency response of the modified filter

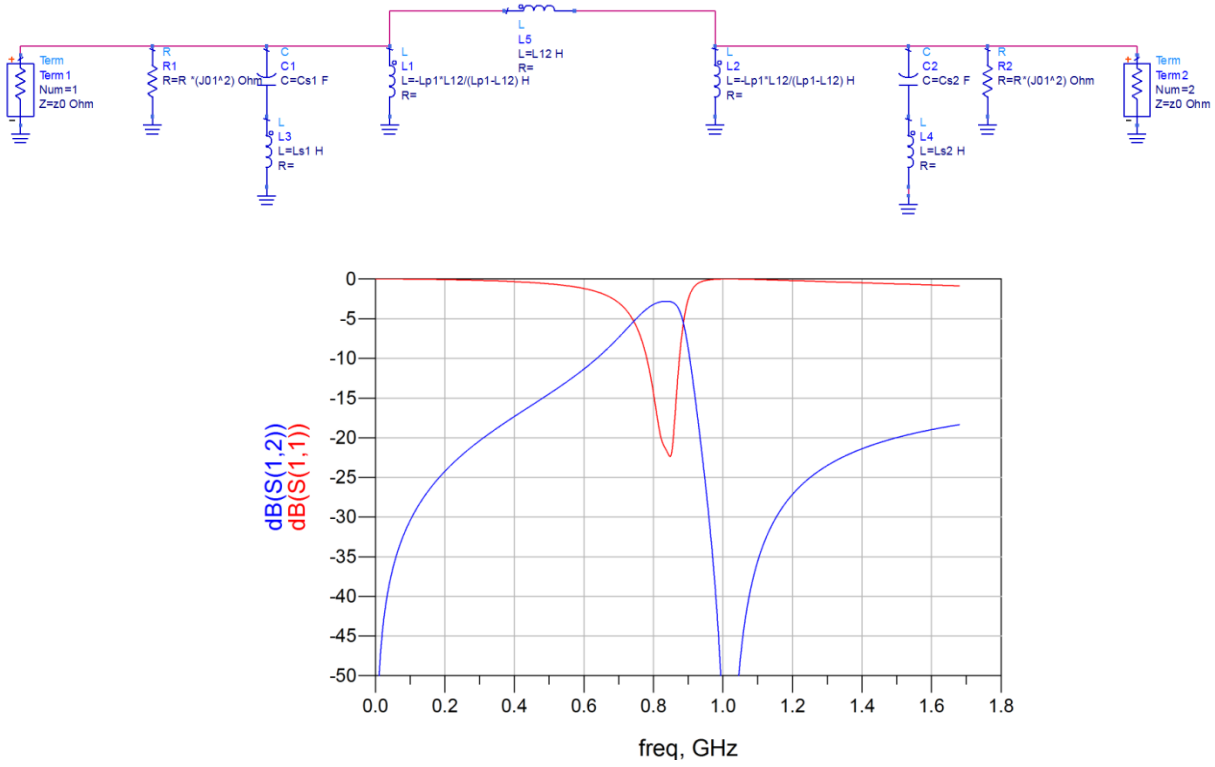

Figure 4.20. Lumped element ccircuit model (inductive coupling) and frequency response of the modified filter

Table 4.5. Modified values of elements of 2-pole filter

Element	*a*	R	Cs1	Cs2	(√a*Lp1 || L12)	(√a*Lp2 || L12)	Ls1	Ls2	L12
value	10	146.30 Ω	3.7 pF	3.7 pF	4.7 nH	4.7 nH	6.6 nH	6.6 nH	8.95 nH

Shows the comparison between the scattering parameter of 2-pole filter with Q=30 before manipulation and after manipulation with different factors of *a*.

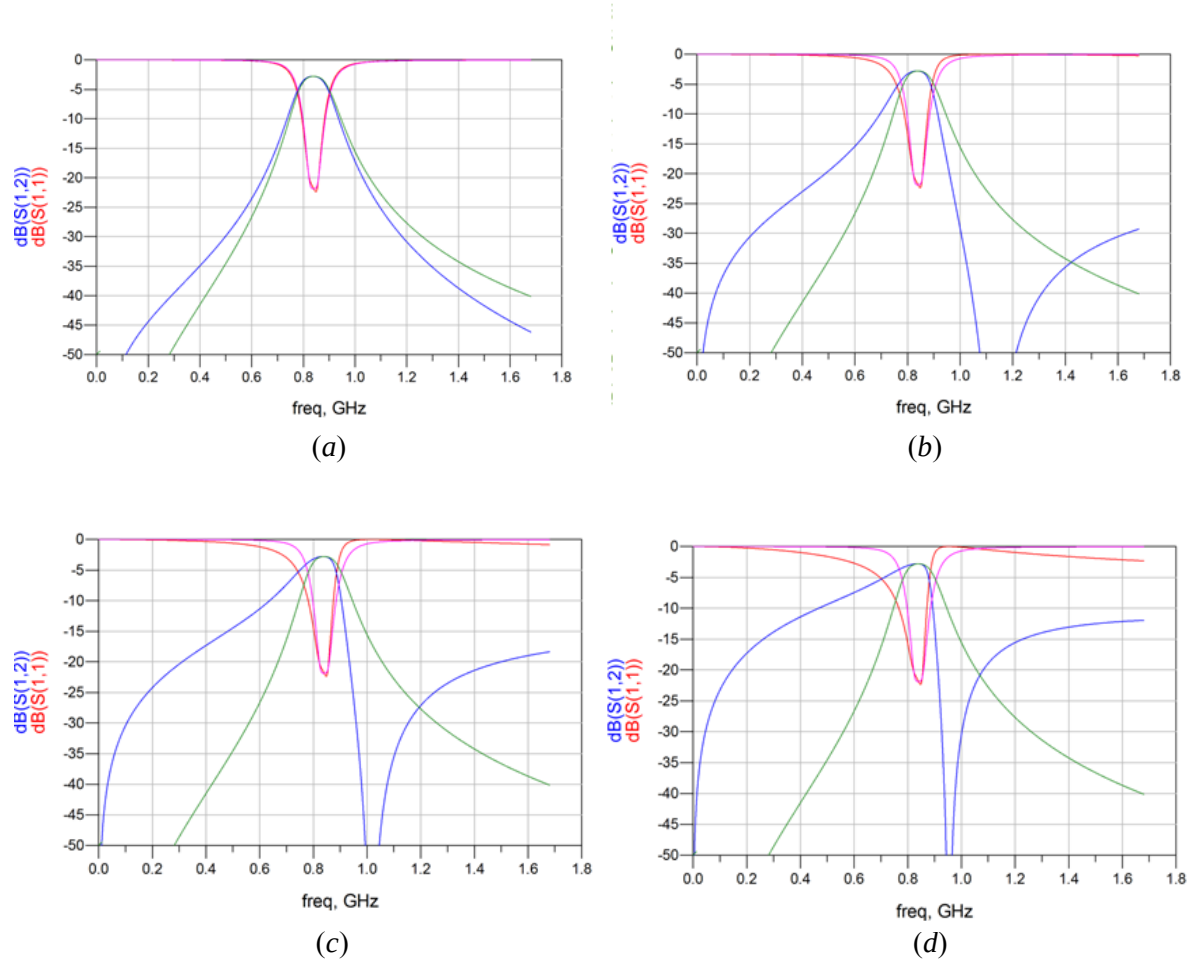

Figure 4.21. ***a***) *a*=1, ***b***) *a*=5, ***c***) *a*=10, ***d***) *a*=20

The middle stage if this cascade design is a 2-pole lumped element lossy filter with Q=30 and consequently passband insertion loss of 6 dB. The same as previous designs, the recursive technique is used to synthesize the filter and two resistors account for the lossy part at the input and output of the 2-pole filter. Figure 4.22 Shows the ideal circuit and scattering parameter using ADS.

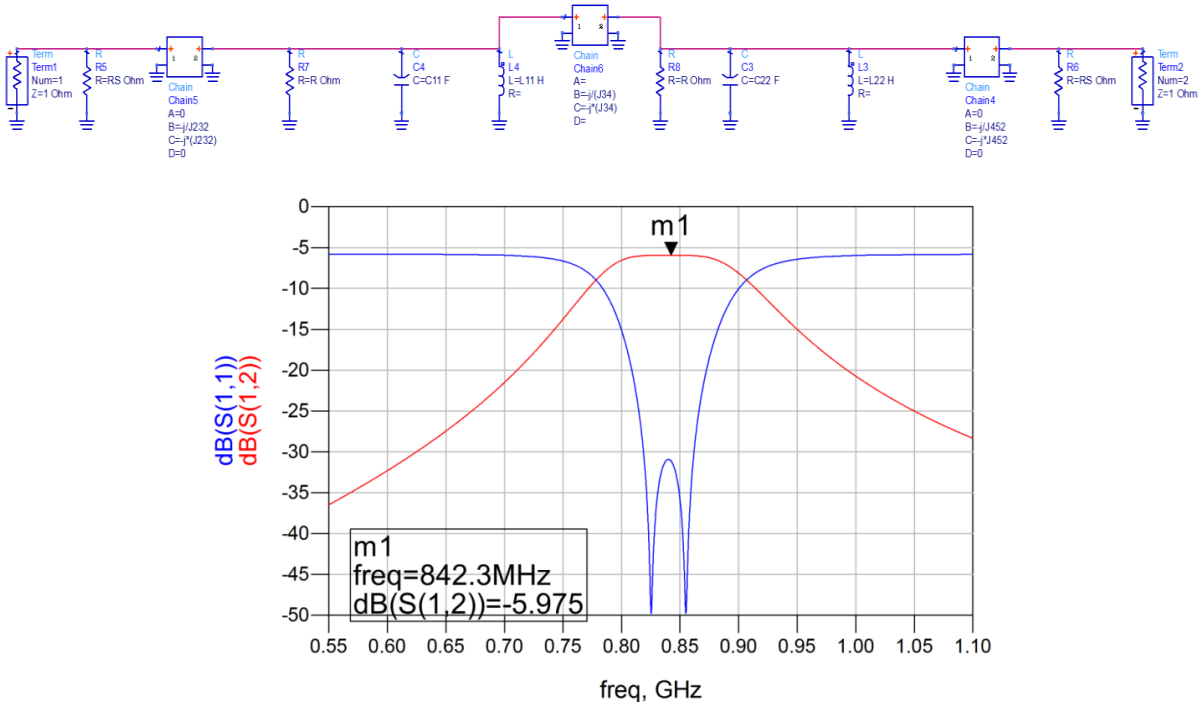

Figure 4.22. Frequency response of 2-pole lossy filter (ADS simulation)

Exact same procedure mentioned in pervious section is carried out with scaling factor a=10 to reduce the elements value to be realizable on PCB board. The circuit with ideal impedance inverters (ABCD model) and modified resonators is shown below along with the scattering parameters.

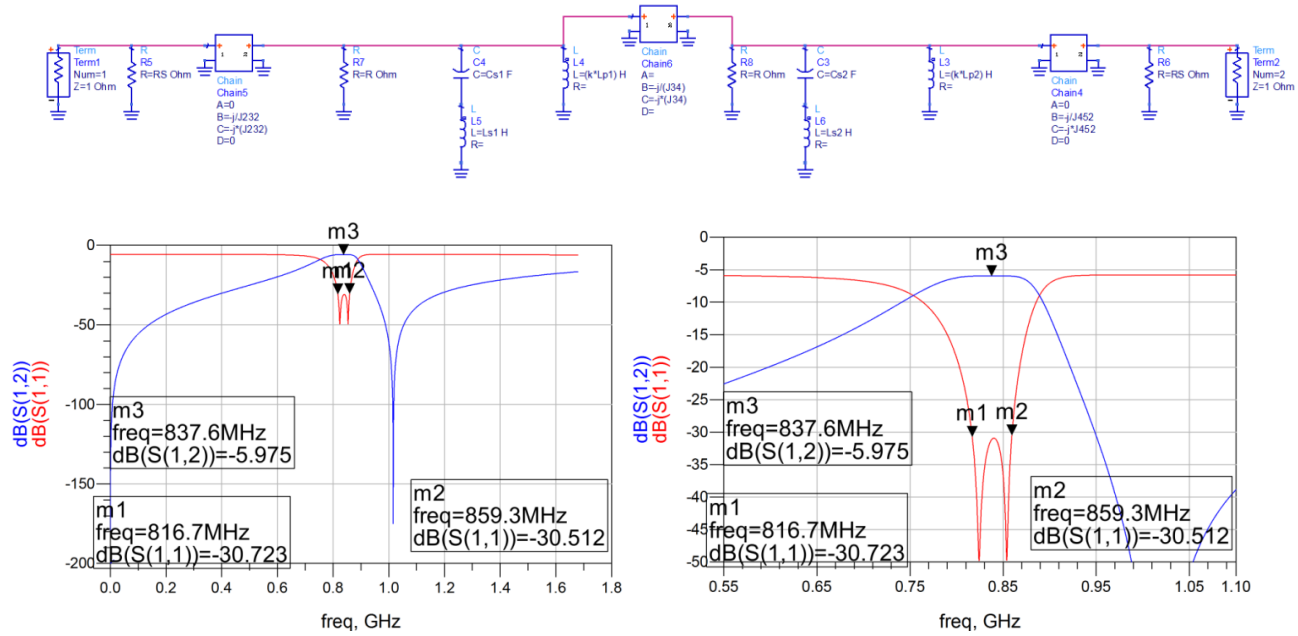

Figure 4.23. Frequency response of 2-pole lossy filter (ADS simulation)

The feasible circuit model is represented after replacing the ideal inverters with actual inductive inverters and the value of circuit elements are realizable.

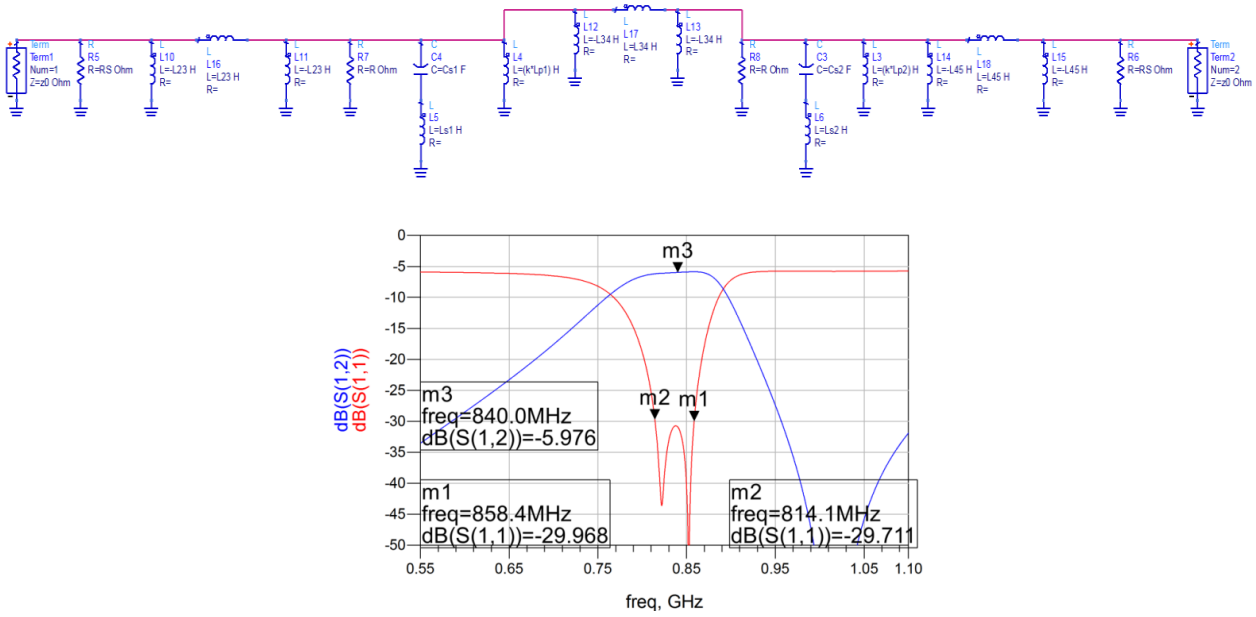

Figure 4.24. Two-pole lossy filter, top: circuit model, bottom: s-par

Table 4.6. Modified elements of 2-pole lossy filter

Element	*a*	R	Rs	Cs1	Cs2	(√a*Lp1 ‖L12‖L23)	(√a*Lp2 ‖L23‖L34)	Ls1	Ls2	L12	L23	L34
value	10	71.42 Ω	155.2 Ω	7.58 pF	7.58 pF	3.38 nH	3.38 nH	3.24 nH	3.24 nH	7 nH	4.37 nH	7 nH

Cascaded 3x2-pole filter with inductive coupling ADS simulation results is shown in Figure 4.25.

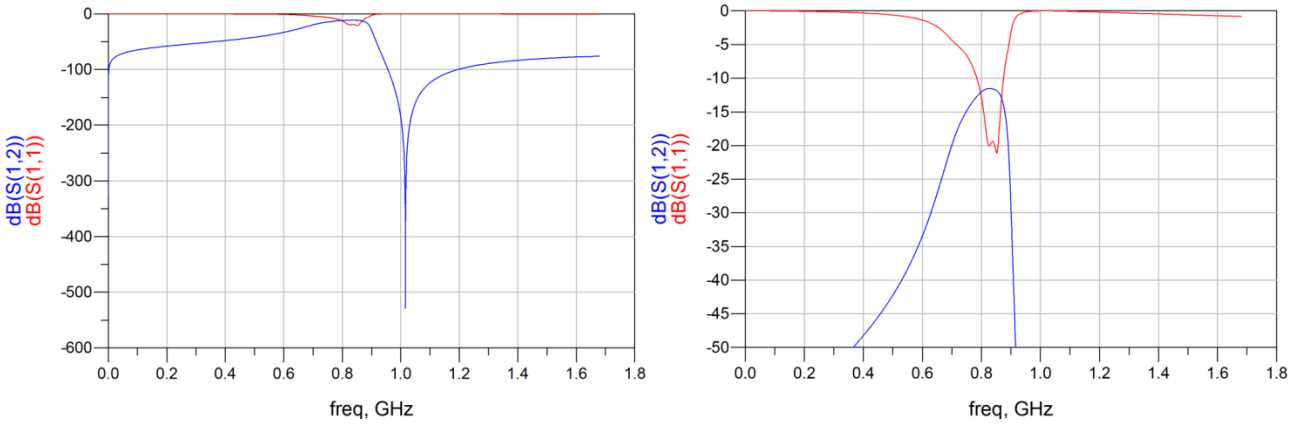

Figure 4.25. Frequency response of cascaded 2-pole filters (ADS simulation)

4.3.1 EM Design and simulation results

SONNET software V.13 is used to simulate the planar structure based on dielectric layer Rogers 6202 with the effective permittivity of 2.95 and thickness of 0.127 mm. In the first step, each element (capacitors and inductors) are simulated to obtain the correct dimensions based on Table 4.6. The geometry and EM simulation results of input and output 2-pole filters are shown in Figure 4.26 respectively.

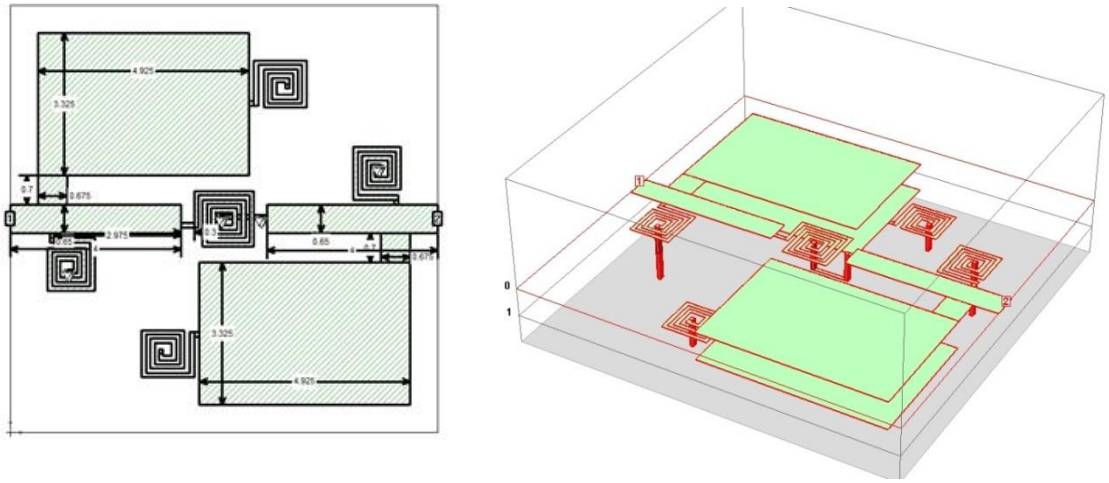

Figure 4.26. Physical layout of 2-pole filter (SONNET)

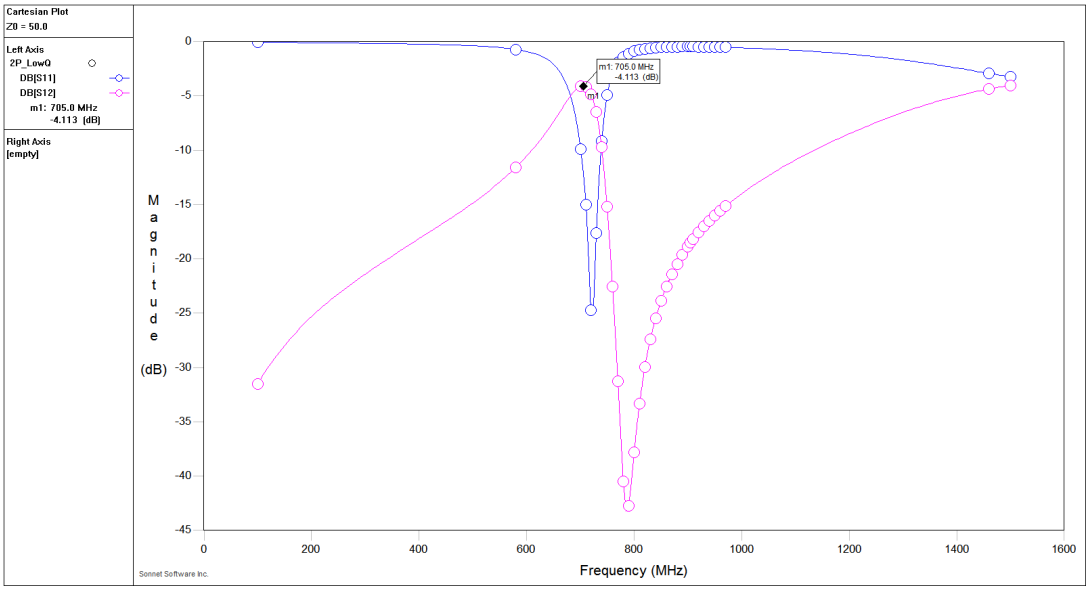

Figure 4.27. Frequency response of 2-pole filter (SONNET simulation)

A slightly frequency shift is observed in the EM simulation s-par due to the dimension of the elements connecting together which is removed by optimizing the geometry (Figure 4.28).

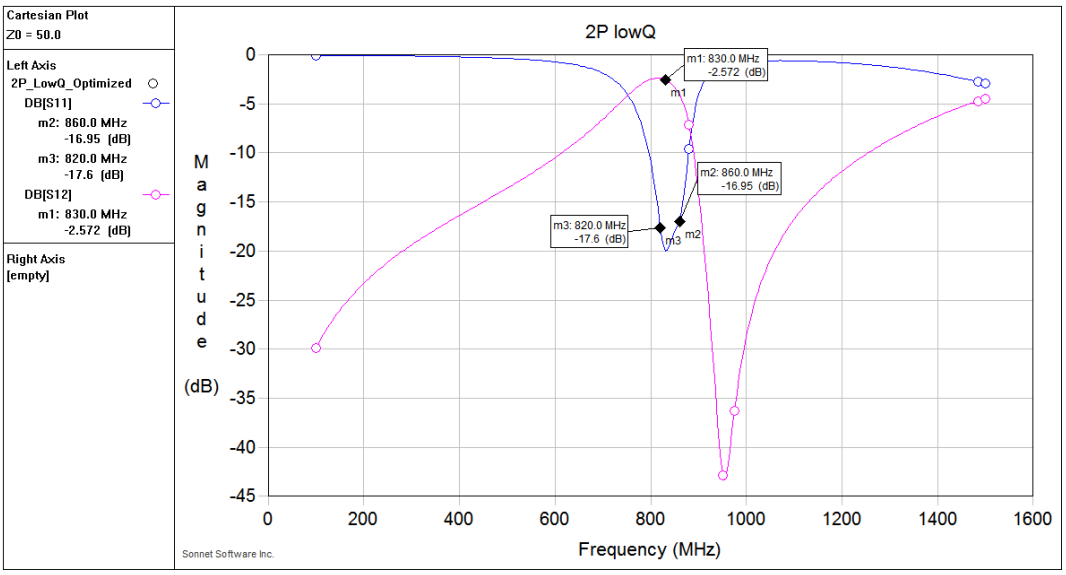

Figure 4.28. Optimized frequency response of 2-pole filter (SONNET simulation)

The input and output inductors in 2-pole lossy filter (L_p1 and L_p2) are negative and in the circuit model, they are absorbed in the input and output inductors of ideal 2-pole filters. Therefore, it is not possible to simulate the 2-pole lossy filter in EM simulator separately. However, the EM simulation of the 2-pole lossy filter (Figure 4.29) carried out without L_p1 and L_p2 has a good agreement with the circuit simulation in ADS

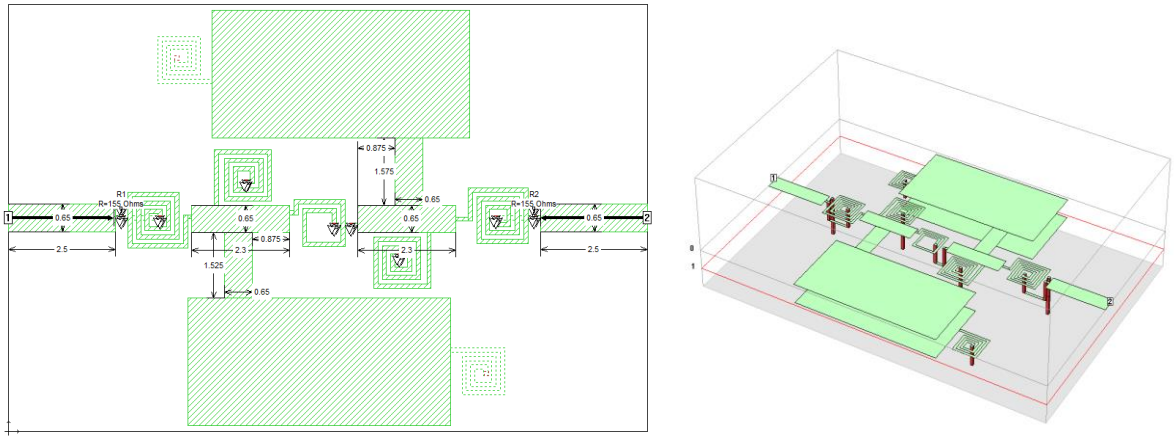

Figure 4.29. Physical layout of 2-pole lossy filters (SONNET)

Finally the cascaded 3x2-pole filter has been simulated in SONNET 13 EM simulation and the results are shown Figure 4.31.

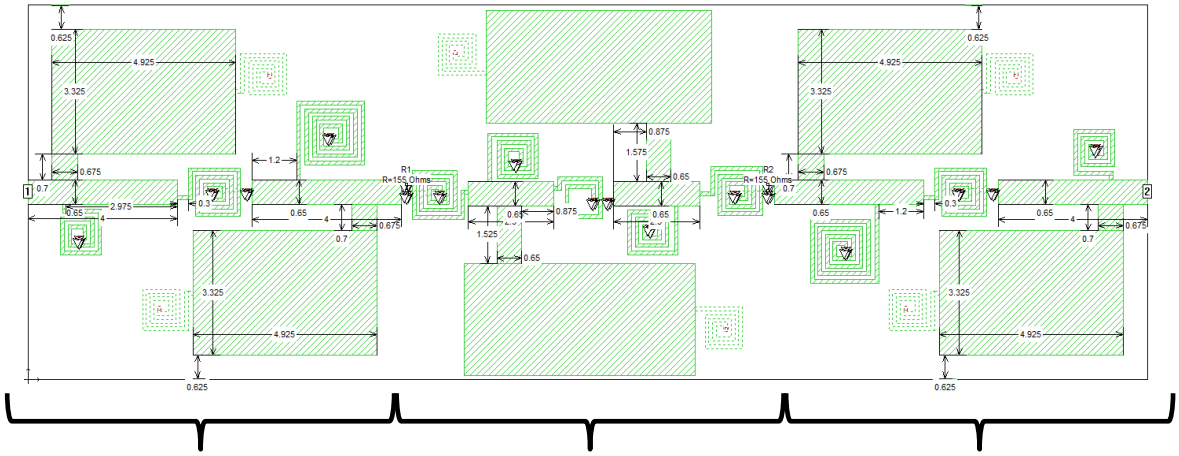

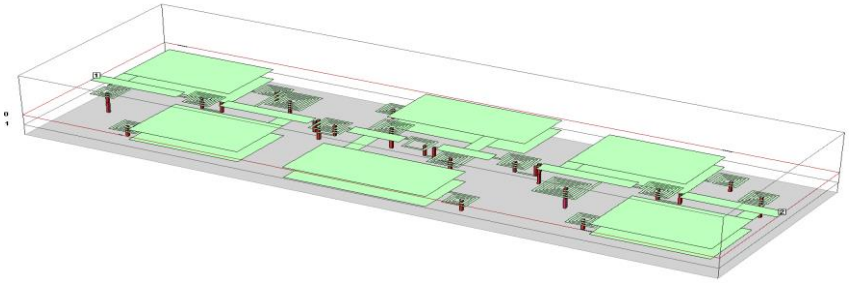

Figure 4.30. Physical layout of the cascaded 2-pole lossy filters (SONNET)

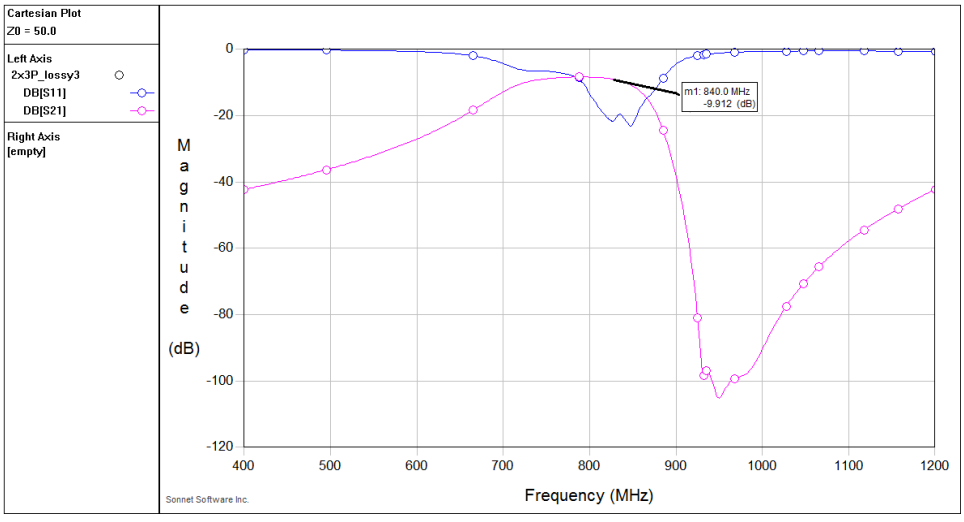

Figure 4.31. EM simulation results for 3x2-pole cascade filter (Q=30)

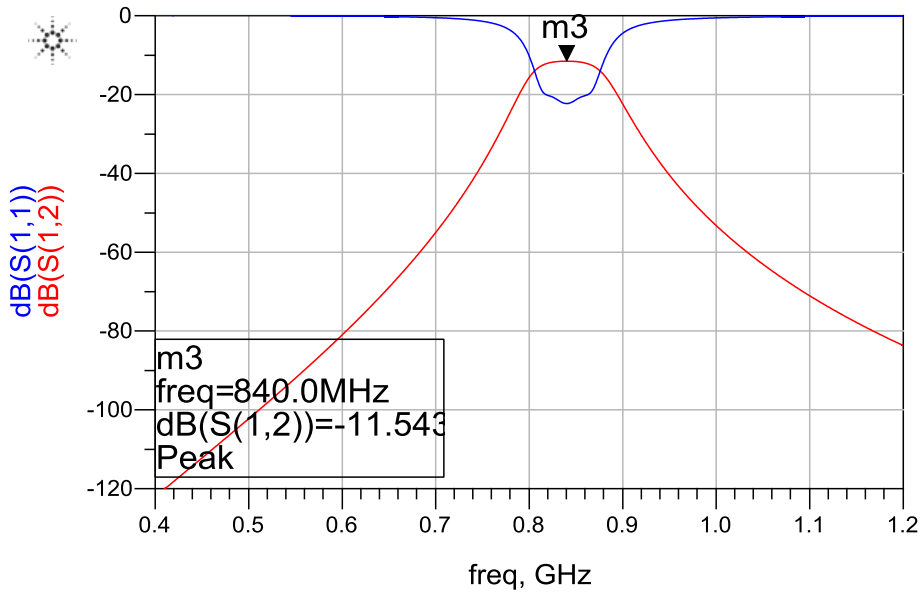

Figure 4.32. Circuit model simulation of 6-pole ideal filter with Q=30

Figure 4.32 shows the circuit simulation of a 6-pole ideal filter with Q=30 at the same center frequency of 840 MHz and same BW of 4.7%. Although manipulating the circuit introduced a transmission zero of frequency response and effected the selectivity, the insertion loss of 3x2-pole lossy filter is higher than ideal 6-pole filter about 2 dB.

Chapter 5

5.1 Summary

In the first section of this thesis, direct and transversal coupling matrix synthesis methods were discussed and the lossy coupling matrix was derived using the transversal method. However, the coupling matrix, derived based on the transversal method, was not feasible in terms of practice. Thus, in order to obtain a practical coupling matrix, some unwanted couplings were annihilated with a sequence of similarity transforms (rotations) until a more convenient form with a minimal number of couplings was obtained. A loss distribution technique (hyperbolic and trigonometric rotations) was applied to the coupling matrix to distribute the loss evenly among the resonators and to obtain equal Q factor resonators; the technique was illustrated with an example.

In the next section, a study was carried out to obtain the relation between the value of the actual quality factor and the achievable equivalent quality factor for certain amounts of fractional bandwidths of the filter. The results showed that the relation between the actual Q factor and the introduced amount of loss is not linear and varies for different FBWs. In the next part, the predistortion technique was discussed in detail, followed by an illustrative example. The results also indicated that the predistortion technique is an effective method for maintaining the selectivity and passband flatness of the filter frequency response for small loss and narrow bandwidth (e.g., FBW=1% results in Q factor around 1000). Regarding the lumped element filters, since the Q factor is about 30 to 40, the predistorted technique can be applied only to wideband filter with FBW more that 20%.

In the second part of this thesis, the lossy technique was used to design two lumped element filters. The first filter was a 4-pole Chebyshev filter with an equivalent Q of 1,000, an actual Q of 100, a 4% bandwidth, and an operating frequency of 2 GHz. The design characteristics introduced a 18dB insertion loss in addition to the 0.5dB loss associated with the equivalent Q of 1,000. The second filter formed by cascading three 2-pole filters where one of them is a lossy filter. Cascading was chosen in order to achieve close to zero dB reflection in the rejection band. The filter was designed for a center frequency of 840 MHz, an FBW of 40 MHZ bandwidth (FBW=4.7%), and a Q-factor of 30.

5.2 Future work

Since highly selective resonator filters are needed in all communication systems, future work could aim for Q factor enhancement by compensating for the effect of loss in a lossy filter design. The novelty is to combine the idea of lossy filters with active elements to increase the Q factor of some resonators in a filter while significantly reducing the Q factor in other resonators.

In loss distribution, it is possible to drastically reduce the actual Q factor of resonators at the cost of having some of them be negative. For instance, while it is possible to achieve an actual Q factor of 30 for a 3-pole Chebyshev filter with an equivalent Q of more than 1,000, the middle resonator would have a Q factor of -30. Therefore, an extension of this work could involve designing a suitable negative resistor or negative impedance convertor (NIC) to be employed in some resonators to reduce the Q factor more than conventional lossy filters. The challenges in NIC designs include noise, linearity, and dynamic range analysis in terms of input and output power. Dealing with the NIC circuit individually, the topology and realization process of NIC circuitry is an important focus of study since it is related to all of the parameters mentioned above. Moreover, the type of active element that would be employed to realize the NIC would be substantial for the same reasons.

Bibliography

[1] S. Darlington, “Synthesis of a reactance-four pole with prescribed insertion loss characteristics,” *J. Math. Phys*., vol. 18, no 1939, pp. 257-353.

[2] M. Dishal, "Design of dissipative filters producing exact amplitude frequency characteristics". *Proc. IRE*, 37, pp. 1050-1069, Sept 1949.

[3] IL M. Livingston, “Predistorted waveguide filters,” *G-MTT Irrt. Microwave Symp*., Dig., 1969, pp. 291-297.

[4] M. H. Chen and C. E. Mable, “Design of a lossy waveguide filter,” *COMSA T Tech. Rev*., vol. 5, no. 2, pp. 387-398, 1975.

[5] A. E. Williams, W G. Bush, R. R. Bonetti.; "Predistortion Techniques for Multicoupled Resonator Filters," *IEEE Transactions on Microwave Theory and Techniques*; vol. 3, No. 5, May 1985.

[6] A. E. Atia, A. E. Williams, and R. W, Newcomb, “Narrowband multiplexer- coupled cavity synthesis,” *IEEE Trans. Circuits Sys*., vol. CAS-21, pp. 649-655, Sept. 1974.

[7] Ming Yu, Senior Member, IEEE, Wai-Cheung Tang, Alastair Malarky, Van Dokas, Richard Cameron, Fellow, IEEE, and Ying Wang, “Predistortion Technique for Cross-Coupled Filters and Its Application to Satellite Communication Systems,” *IEEE Tran. on Microwave Theory and Techniques*, Vol. 51, No. 12, Dec. 2003.

[8] Ming Yu, Richard Cameron, David Smith, Van Dokas and Ying Wang, “Symmetrical Realization for Predistorted Microwave Filters,” *IEEE MTT-S International Microwave Symposium Digest*, 2005.

[9] Xiao-Ping Chen, Liang Han, and Ke Wu, Fellow, IEEE, “Synthesis and Design of Substrate Integrated Waveguide Filter Using Predistortion Technique,” *Asia-Pacific Microwave Conference*, 2007.

[10] A.M. Prabhu, V. Van, “Predistortion techniques for synthesizing coupled micro-ring filters with loss,” *Optics Communications* Volume 281, Issue 10, 15 May 2008, pp. 2760-2767.

[11] W M Fathelbabj and I C Hunter, “A predistortion technique for microwave high pass prototype filters,” IEE Colloquium on RF and Microwave Components for Communication Systems, Apr 1997.

[12] J.D. Rhodes, I.C. Hunter, “Synthesis of reflection-mode prototype network with dissipative circuit elements,” IEE Proceedings on Microwaves, Antennas and Propagation, Dec 1997.

[13] W.M. Fathelbab, I.C.Hunter, J.D.Rhodes, “Synthesis of lossy reflection-mode prototype networks with symmetrical and asymmetrical characteristics,” IEE Proceedings on Microwaves, Antennas and Propagation, Apr. 1999.

[14] Senior, B.S.; Hunter, I.C.; Rhodes, J.D. “Synthesis of lossy filters,” European Microwave Conference, 2002.

[15] Andrew C. Guyette, Ian C. Hunter, and Roger D. Pollard, “The Design of Microwave Bandpass Filters Using Resonators with Non-uniform Q”, *IEEE Transaction on Microwave Theory and Techniques*, Vol. 54, No. 11, Nov. 2006.

[16] Andrew C. Guyette, Ian C. Hunter and Roger D. Pollard, "Exact Synthesis of Microwave Filters with Non-uniform Dissipation," *IEEE/MTT-S International Microwave Symposium*, June 2007.

[17] Z. Zakaria, I. C. Hunter, and A. C. Guyette, "Design of Coaxial Resonator Filter with Non-uniform Dissipation," *IEEE MTT-S International Microwave Symposium Digest.,* June 2008.

[18] V. Miraftab and M. Yu, "Generalized lossy microwave filter coupling matrix synthesis and design using mixed technologies," *IEEE Trans. Microw. Theory Tech. ,* Vol. 56, No. 12, Dec. 2008.

[19] Navarro-Tapia, D., Sorolla, E., Otero, P., Mattes, M., "Coupling matrix synthesis of dissipative microwave filters*," IET Microwaves, Antennas and Propagation*, June 6 2011.

[20] Cameron, R. J., "Advanced coupling matrix synthesis techniques for microwave filters," IEEE Transactions on Microwave Theory and Techniques, Vol. 51, No. 1, Jan. 2003.

[21] Vahid Miraftab, Ming Yu,"Advanced coupling matrix and admittance function synthesis techniques for dissipative microwave filters," IEEE Transactions on Microwave Theory and Techniques, Vol. 57, No. 10, 2009.

[22] Cameron, R. J., "General coupling matrix synthesis methods for Chebyshev filtering functions," IEEE Trans. Microw. Theory Tech. , Vol. 47, No. 4, 433-442, Apr. 1999.

[23] H. C. Bell, "Canonical asymmetric coupled-resonator filters," IEEE Trans. Microwave Theory Tech., vol. MTT-30, pp. 1335-1340, Sept. 1982.

[24] R. J. Cameron, "Fast generation of Chebyshev filter prototypes with asymmetrically-prescribed transmission zeros," European Space Agency Journal., vol. 6, pp. 83-95, 1982.

[25] Cameron, R. J., "General coupling matrix synthesis methods for Chebyshev filtering functions," *IEEE Trans. Microw. Theory Tech*., Vol. 47, No. 4, 433-442, Apr. 1999.

[26] E. Atia, A. E. Williams, R. W. Newcomb, "Narrow-band multiple-coupled cavity synthesis", *IEEE Trans. Circuits Syst.* 21, 649-655 (1974).

[27] V. Miraftab and M. Yu, "Generalized lossy microwave filter coupling matrix synthesis and design using mixed technologies," *IEEE Trans. Microw. Theory Tech.,* Vol. 56, No. 12, Dec. 2008.

[28] Navarro Tapia, Diego; Sorolla, Eden; Otero Roth, Pablo; Mattes, Michael, "Coupling matrix synthesis of dissipative microwave filters," *IET Microwaves, Antennas and Propagation*, Vol. 5, 201.

[29] Cameron, R. J., "Advanced coupling matrix synthesis techniques for microwave filters," *IEEE Transactions on Microwave Theory and Techniques*, Vol. 51, No. 1, Jan. 2003.

[30] Vahid Miraftab, Ming Yu*,"*Advanced coupling matrix and admittance function synthesis techniques for dissipative microwave filters," *IEEE Transactions on Microwave Theory and Techniques*, Vol. 57, No. 10, 2009.

[31] M. Yu, V. Miraftab, "Shrinking Microwave Filters" IEEE Microwave Magazine, October 2005, pp. 40-54.

[32] H. C. Bell, “Canonical asymmetric coupled-resonator filters,” I*EEE Trans. Microwave Theory Tech.*, vol. MTT-30, pp. 1335-1340, Sept. 1982.

[33] J. D. Rhodes, “A low-pass prototype network for microwave linear phase filters,” IEEE Trans. Microwave Theory Tech., vol. MTT-18, pp. 290–300 June 1970.

[34] Guyette, I. Hunter, and R. Pollard, “The design of microwave bandpass filters using resonators with nonuniform,” *IEEE Trans. Microw. Theory Tech*., vol. 54, no. 11, pp. 3914–3922, Nov. 2006.

[35] R.J. Cameron, C. Kudsia, and R. Mansour, Microwave Filters for Communication Systems. Hoboken, NJ: Wiley, 2007.

[36] S. Darlington, “Synthesis of a reactance-four pole with prescribed insertion loss characteristics,” *J. Math. Phys*., vol. 18, no 1939, pp. 257-353.

[37] IL M. Livingston, “Predistorted waveguide filters: *G-MTT Irrt. Microwave Symp*., Dig., 1969, pp. 291-297.

[38] M. H. Chen and C. E. Mable, “Design of a 10SSY waveguide filter,” *COMSA T Tech. Rev*., vol. 5, no. 2, pp. 387-398, 1975.

[39] E. Williams, W G. Bush, R. R. Bonetti.; "Predistortion Techniques for Multicoupled Resonator Filters" *IEEE Transactions on Microwave Theory and Techniques*; vol. 3, No. 5, May 1985.